Boston University

OpenBU **http://open.bu.edu**

Theses & Dissertations Boston University Theses & Dissertations

2020

Topological specification of connections between prefrontal cortex and hypothalamus in rhesus monkey

https://hdl.handle.net/2144/41744

Boston University

BOSTON UNIVERSITY

SCHOOL OF MEDICINE

Thesis

TOPOLOGICAL SPECIFICATION OF CONNECTIONS BETWEEN PREFRONTAL CORTEX AND HYPOTHALAMUS IN RHESUS MONKEY

by

ANNE MARIE WELLS

B.A., William Marsh Rice University, 2016

Submitted in partial fulfillment of the

requirements for the degree of

Master of Science

2020

© 2020 by
ANNE MARIE WELLS
All rights reserved

Approved by

First Reader _____

Helen Barbas, Ph.D.
Professor of Health Sciences
Professor of Anatomy and Neurobiology

Second Reader _____

Louis Gerstenfeld, Ph.D.
Professor of Orthopaedic Surgery

DEDICATION

I dedicate this work to my mentors, family, and friends.

"It is important to realize that if certain areas of science appear to be quite mature, others are in the process of development, and yet others remain to be born."

- *Santiago Ramón y Cajal, Advice for a Young Investigator*

ACKNOWLEDGMENTS

I thank my mentor, Dr. Helen Barbas, for imparting her dedication and enthusiasm for the study of the primate brain. I thank my academic advisor, Dr. Louis Gerstenfeld, and program advisor, Dr. Gwynneth D. Offner, for their encouragement and thoughtful insight on my studies and project. I thank members of the Neural Systems Lab, including Dr. Miguel Ángel Garcia Cabezas, Dr. Basilis Zikopoulos, Dr. Mary-Kate P. Joyce, Jingyi Wang, Tara McHugh, Abigail Mark, and Jess Holz for their thoughtful advice and technical support. I thank the many professors, mentors, and students of the MAMS/GMS community at Boston University for their support in guiding me through the complexities and uncertainties of this graduate program.

I thank my wonderful family and friends for supporting my goals and ambitions, near and far, and for their patience through this process. I also thank my parents for their grit and determination, for without their example, I would not have pushed this far.

TOPOLOGICAL SPECIFICATION OF CONNECTIONS BETWEEN PREFRONTAL CORTEX AND HYPOTHALAMUS IN RHESUS MONKEY

ANNE MARIE WELLS

ABSTRACT

The hypothalamus is a subcortical brain region whose limits and constituent nuclei lack consensus. The hypothalamus has been linked to emotion and different states of stress, providing critical feedback about the internal environment to the prefrontal cortex, a region known for executive function within the cortex of humans. An understanding of the developmental origin of the hypothalamus can provide a basis for defining which limits and nuclei are ontologically hypothalamic, and which are not, as well as a framework for understanding its connectional relationship with other brain regions.

The Prosomeric Model (Rubenstein et al. 1994; Puelles and Rubenstein 2003; Nieuwenhuys and Puelles 2016; Puelles 2018) explains the embryological development of the central nervous system (CNS) shared by all vertebrates as a Bauplan. As a primary event, the early neural plate is patterned by intersecting longitudinal plates and transverse segments, forming a mosaic of progenitor units. The hypothalamus is specified by three prosomeres [hp1, hp2, and the acroterminal domain (At)] of the secondary prosencephalon with corresponding alar and basal plate parts, which develop apart from the diencephalon. Mounting evidence suggests that progenitor units within alar plate and basal plate parts of hp1 and hp2 give rise to distinct hypothalamic nuclei, which preserve their relative invariant positioning (topology) in the adult brain. Nonetheless, the

principles of the Prosomeric Model have not been applied to the hypothalamus of adult primates.

The Structural Model (Barbas 1986; Barbas and Rempel-Clower 1997) highlights the variation of laminar structure in the grey matter of the prefrontal cortex as a basis for predicting specific cortico-cortical connections. The areas of the prefrontal cortex vary along a spectrum by number of layers, laminar definition, and cellularity of those layers. The systematic laminar patterns of different areas of the prefrontal cortex seem to be associated with differential rates of development or maturation. A topographical analysis of bidirectional projections between the prefrontal cortex and the hypothalamus was previously applied using the Structural Model (Rempel-Clower and Barbas 1998). The authors found the prefrontal cortex has highly specific projections to the hypothalamus, originating mostly from limbic orbital and medial prefrontal areas, which have lower laminar definition than other prefrontal areas. In addition, the hypothalamus has relatively specific patterns of projection to the prefrontal cortex.

We previously lacked an organizing principle to examine the specific pattern of connections between the hypothalamus and prefrontal cortex in adult rhesus monkey. In the present study, hypothalamic nuclei in the rhesus monkey (*Macaca mulatta*) were parcellated using classic architectonic boundaries and stains. The topological relations of hypothalamic nuclei and adjacent hypothalamic landmarks were then analyzed with homology across rodent and primate species to trace the origin of adult hypothalamic nuclei to the alar or basal plate components of hp1 and hp2. A novel atlas of the hypothalamus of the adult rhesus monkey was generated with developmental ontologies

for each hypothalamic nucleus. This atlas was then applied to a topological analysis of the strength and pattern of connections between the hypothalamus and prefrontal cortex in the adult rhesus monkey. The result is a systematic reinterpretation of the adult hypothalamus of the rhesus monkey whose prosomeric ontology was used to study connections and neuraxial pathways linking the hypothalamus and prefrontal cortex. The convergence of the Prosomeric and Structural Models provides a framework through development to explain the structural patterns found in the adult primate cortex and hypothalamus, and the likely consequences of their disruption.

TABLE OF CONTENTS

LIST OF TABLES

LIST OF FIGURES

LIST OF ABBREVIATIONS

A6..... premotor prefrontal cortical area 6

A8.....dorsolateral prefrontal cortical area 8 (D8)

A9..... dorsolateral prefrontal cortical area 9

A10..... medial prefrontal cortical area 10

A11.....orbital prefrontal cortical area 11

A12..... orbital prefrontal cortical area 12 (O12)

A25..... medial prefrontal cortical area 25

A32..... medial prefrontal area 32

A46d/v..... dorsolateral prefrontal cortical area 46

BSA.....bovine serum albumin

BDA .....biotinylated dextran amine

ABb .....alar-basal boundary

ac .....anterior commissure

AChE..... acetylcholinesterase

ARC .....arcuate nucleus

At..... acroterminal domain

BDA .....biotinylated dextran amine

BM ..... basal nucleus of Meynert

CB .....calbindin

Cd..... caudate nucleus

CPa..... central paraventricular progenitor area

CNS.....central nervous system

CR ..... calretitin

DARPP-32 .....dopamine- and cAMP-regulated phosphoprotein M(r) 32 kDA

Dien..... diencephalon

DM .....dorsomedial nucleus

DPa..... dorsal paraventricular progenitor area

f .....fornix

FB.....fast blue

FR..... fluororuby

GP .....globus pallidus, ventral part

h..... hypophysis

hp1.....hypothalamic prosomere 1

hp1a.....hypothalamic prosomere 1, alar plate part

hp1b.....hypothalamic prosomere 1, basal plate part

hp2.....hypothalamic prosomere 2

hp2a.....hypothalamic prosomere 2, alar plate part

hp2b.....hypothalamic prosomere 2, basal plate part

HRP-WGA.....horseradish peroxidase, wheatgerm agglutinin

ic..... internal capsule

INF .....infundibulum

LA .....lateral hypothalamic area

LM.....lateral mamillary nucleus

Mb ..... mamillary bodies

MBD ..... mean bouton diameter (Feret's)

Mes ..... mesencephalon

MM ..... medial mamillary nucleus

Mp ..... mamillary progenitor area

MPall ..... medial periallocortex

mtt ..... mamillothalamic tract

oc ..... optic chiasm

Olf ..... olfactory bulb

OPall ..... orbital periallocortex

OPro ..... orbital proisocortex

ot ..... optic tract

p1 ..... diencephalic neuromere 1

p2 ..... diencephalic neuromere 2

p3 ..... diencephalic neuromere 3 (prethalamus)

Pal ..... pallium

PaM ..... paraventricular complex, magnocellular group

PaP ..... paraventricular complex, parvicellular group

PB ..... phosphate buffer

PBS ..... phosphate buffer saline

pOFC ..... posterior orbitofrontal cortex

Pef ..... perifornical nucleus

PeM.....perimamillary nucleus

PreM.....premamillary nucleus

PM.....paramamillary nucleus

PMp.....premamillary progenitor area

PRM.....preretromamillary progenitor area

Pro.....proisocortex

POA.....preoptic area

PTh.....prethalamic nuclei

PV ..... parvalbumin

Rhomb.....rhombencephalon

RM ..... retromamillary progenitor area

RPa.....rostral paraventricular nucleus

RTuD.....dorsal retrotuberal progenitor area

RTuI .....intermediate retrotuberal progenitor area

RTuV..... ventral retrotuberal progenitor area

sc .....spinal cord

SCH.....suprachiasmatic nucleus

SM..... supramamillary nucleus

SMI-32 ..... non-phosphorylated intermediate microtubule protein SMI-32

SN ..... substantia nigra reticulata

SNc.....substantia nigra compacta

SO .....supraoptic nucleus

SPa ..... subparaventricular progenitor area

SPal ..... subpallium

SPro ..... secondary prosencephalon

STN ..... subthalamic nucleus

TCA ..... area of the tuber cinereum

Tel ..... telencephalon

TM ..... tuberomamillary nucleus

TPa ..... terminal paraventricular progenitor area

TRN ..... reticular nucleus

TSPa ..... terminal subparaventricular progenitor area

Tx ..... Triton-X

TuD ..... dorsal tuberal progenitor area

TuI ..... intermediate tuberal progenitor area

TuV ..... ventral tuberal progenitor area

V ..... third ventricle

VM ..... ventromedial nucleus

VMc ..... ventromedial nucleus, core part

VMs ..... ventromedial nucleus, shell part

VP ..... ventral pallidum

VPa ..... ventral paraventricular area

WFA ..... *Wisteria fluoribunda* agglutinin

INTRODUCTION

The hypothalamus is a relatively small subcortical brain region that lacks consensus on its precise limits and the nuclei contained within it. An understanding of the developmental origin of the hypothalamus can provide a basis for defining which limits and nuclei are ontologically *hypothalamic,* and which are not. The convergence of evolution, development, and anatomy of the hypothalamus could reveal a pattern and strength of connections that exist with surrounding and relatively distant brain regions.

The hypothalamus has been linked to emotion and different states of stress, providing critical feedback about the internal environment to the prefrontal cortex, otherwise known as the region for executive function within the cortex of humans (for review Barbas 2000). While the diverse nuclei of the adult hypothalamus may be involved in simple "on or off switch" functions of neuraxial systems, conscious regulation of these neuraxes is fragile and related to both development and evolution of the central nervous system (CNS). Further, while the prefrontal cortex can select specific sensory information reflecting the external and internal states to guide behavior, it must obtain all information indirectly from other cortical and subcortical regions, like the hypothalamus. Thus, establishing the anatomical and functional organization of connections between the hypothalamus and the prefrontal cortex along a causal basis is of great importance.

Remarkably, there are two prevailing models whose convergence may point to such a causal basis: the *Prosomeric Model* (Rubenstein et al. 1994; Puelles and

Rubenstein 2003; Nieuwenhuys and Puelles 2016; Puelles 2018) for the development of the CNS, and the *Structural Model* (Barbas and Rempel-Clower 1997) for the patterns in cortico-cortical and cortico-subcortical connections. The Prosomeric and Structural Models arose independently with high predictive power, yet from distinct methodologies and perspectives. Still, both models point to events in embryological development of the CNS to explain the intrinsic structure of the adult hypothalamus and the prefrontal cortex, respectively. Thus, it proves worthwhile to consider how these models may overlap in predictions about the structure and pattern of connections between the prefrontal cortex and the hypothalamus, which are often disrupted in psychiatric and neurological diseases.

In the following sections, fundamental principles of the Prosomeric and Structural Models area outlined. The principles of these models were used as a basis for a novel analysis of the hypothalamus and its connectional relationship with the prefrontal cortex in the adult rhesus monkey.

Conflicting developmental ontologies for the central nervous system

In recent decades, two conflicting models have proposed divergent developmental ontologies for the hypothalamus and adjacent brain regions. The classical *Columnar Model* conceptualizes the diencephalon as a column intercalated between the telencephalon (rostrally) and the mesencephalon (caudally). The diencephalic column is subdivided into the epithalamus (dorsal), the thalamus (middle), and the hypothalamus (ventral). Thus, the Columnar Model defines the telencephalon as a different vesicle from the diencephalon and places it as the most rostral part of the neural tube (Herrick 1910; Kuhlenbeck 1973; Swanson 1992, 2003).

A different framework – the *Prosomeric Model* – has been proposed to explain the embryological development and evolution of the central nervous system (CNS). Appendix 1 provides a summary of terms used here to relate the key principles of the Prosomeric Model. This model is based on *genoarchitectonic* studies in embryos of vertebrate species and provides a causal basis for the naming, or ontology, of developmental components of the entire CNS (Rubenstein et al. 1994; Puelles and Rubenstein 2003; Nieuwenhuys and Puelles 2016; Puelles 2018). According to the Prosomeric Model, the progressive regionalization of the CNS begins when the early neural plate is patterned by intersecting longitudinal zones, called *plates*, and transverse segments, called *proneuromeres*. These segments are further divided into *neuromeres* with specific proneuromeric names (i.e., the *pros*omeres of the *secondary prosencephalon*). Differential gene expression induced by organizers in the early neuroepithelium specifies a mosaic of *progenitor units* with characteristic molecular profiles. After specification (primary event), these units expand radially due to histogenetic processes (secondary events) like neurogenesis, neuron migration, and neuron differentiation. The expansion of units across the neural tube varies by the duration and intensity of histogenesis, leading to differential morphogenesis (tertiary event) of CNS structures.

The Prosomeric Model proposes a *Bauplan* for the development of the neural tube that is shared by all vertebrates. Consequently, the Prosomeric Model can predict homologies of CNS regions that share the same unit of origin in the neural plate across

vertebrate species (Puelles and Ferran 2012; Puelles 2013; Nieuwenhuys and Puelles 2016).

The Prosomeric Model defines hypothalamic developmental ontology

One of the most significant changes in our understanding of the CNS brought forth by the Prosomeric Model is the reassignment of the hypothalamus apart from the diencephalon (Fig 1). The Prosomeric Model defines five transverse segments of the neural plate, or *proneuromeres*. These include, from caudal to rostral: the spinal cord (sc), the rhombencephalon (Rhomb), the mesencephalon (Mes), the diencephalon (Dien), and the secondary prosencephalon (SPro). Modern genoarchitectonic studies show that the hypothalamus develops from three *prosomeres* [hp1, hp2, and the acroterminal domain (At)] in the *secondary prosencephalon*, a different proneuromere from the diencephalon. Of note, the prosomere that gives rise to the dorsal and ventral thalamus (p2) is further separated from the hypothalamus by a *prethalamic prosomere* (p3) of the diencephalon, which gives rise to the reticular nucleus, the zona incerta, and the prethalamic nuclei.

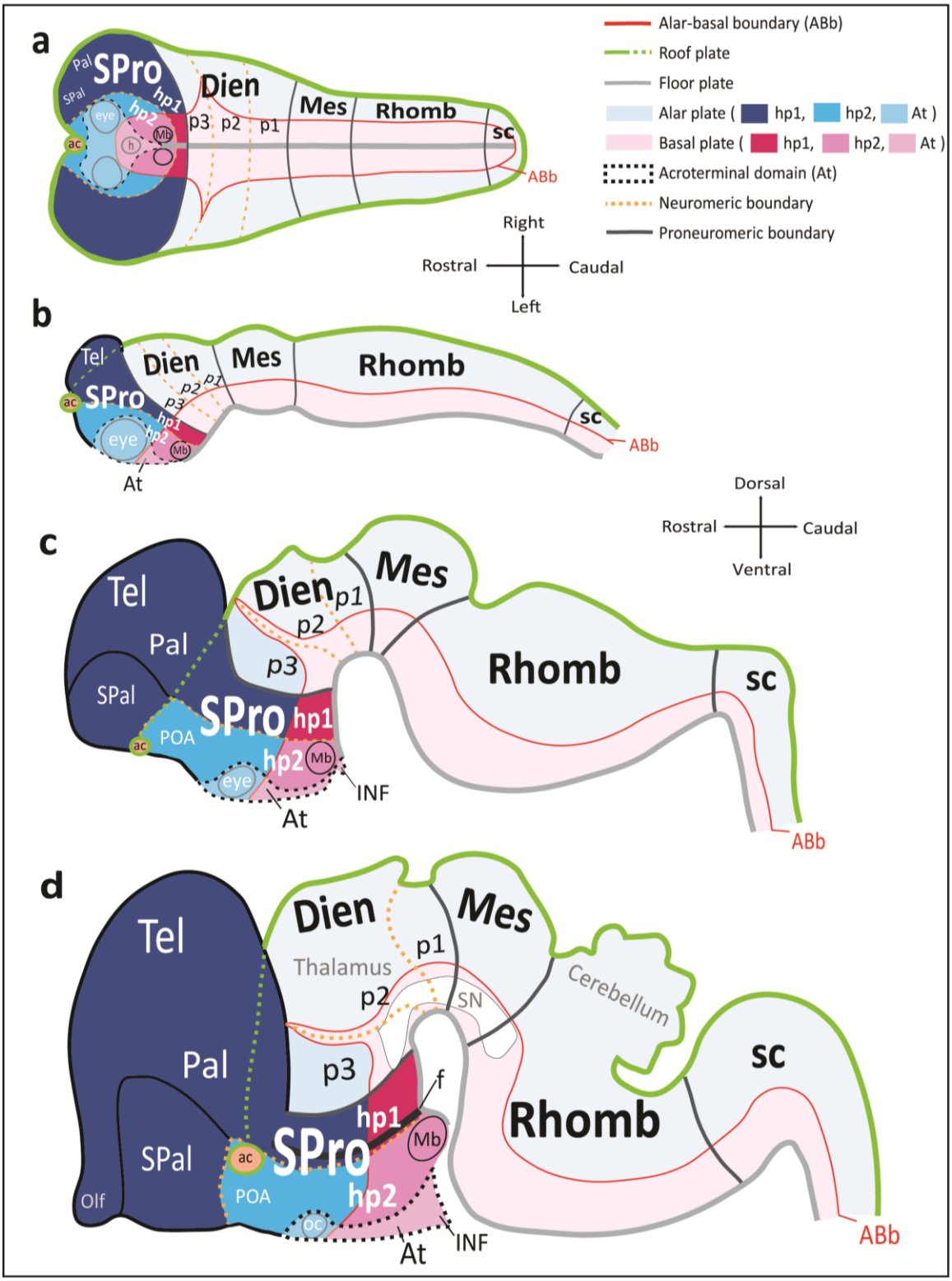
a
Pal
SPro
SPal
hp1
Dien
Mes
Rhomb
eye
hp2
p3
p2
p1
sc
ac
h
Mb
ABb
Alar-basal boundary (ABb)
Roof plate
Floor plate
Alar plate (hp1, hp2, At)
Basal plate (hp1, hp2, At)
Acroterminal domain (At)
Neuromeric boundary
Proneuromeric boundary
Right
Rostral
Caudal
Left
b
Tel
Dien
Mes
Rhomb
SPro
p1
p2
p3
hp1
hp2
eye
Mb
sc
ac
ABb
At
Dorsal
Rostral
Caudal
Ventral
c
Tel
Dien
p1
Mes
p2
p3
Pal
Rhomb
sc
SPal
SPro
hp1
POA
ac
hp2
Mb
eye
INF
At
ABb
d
Tel
Dien
Mes
Thalamus
p1
p2
SN
Cerebellum
sc
Pal
p3
f
hp1
Rhomb
Mb
SPal
ac
SPro
POA
hp2
Olf
oc
At
INF
ABb

Figure 1: Schematic of progressive regionalization of the hypothalamus according to the Prosomeric Model. (a) Dorsal view of the neural plate with intersecting of longitudinal (rostro-caudal) zones, named plates, and transverse (medio-lateral) segments named proneuromeres and neuromeres, forming a mosaic of units with unique molecular profiles. The floor plate and the roof plate are organizers whose signals pattern and specify the alar and basal plates. The roof plate encircles the entire neural plate, and the floor plate terminates rostrally just caudal to the prospective mamillary bodies (Mb). Other organizers, like the acroterminal domain (At), pattern and specify transverse segments. The alar-basal boundary (ABb) divides each neuromere into alar plate and basal plate parts. The diencephalic proneuromere (Dien; p3, p2, p1), from which the thalamus arises, lies topologically caudal to the neuromeres of the secondary prosencephalon (SPro: hp1, hp2, At). (b) Lateral view from the left of the neural tube shows progressive morphogenesis following neural plate specification into a mosaic of units. Hp1 gives rise to the telencephalon (Tel), including the pallium (Pal) and subpallium (SPal), while hp2 contributes the preoptic area (POA) to the SPal. (c) Lateral view from the left of the neural tube shows progressive morphogenesis and tertiary folding events pushing the hypothalamus to a topographical position ventral to the thalamus, as its name indicates. (d) Lateral view from the left of the neural tube shows progressive morphological expansion of brain regions by neuromere and plate of origin. Several architectonic landmarks, like the fornix (f), the optic chiasm (oc), and the anterior commissure (ac), in the adult brain are visualized as outgrowths along proneuromeric and neuromeric boundaries. The sketches of this figure were adapted from Puelles et al. 2008; Puelles et al. 2012; Puelles 2013; Puelles and Rubenstein 2015. Color code applies to all subsequent figures. See list of abbreviations for complete terms.

The early specified limits of p3 that separate the thalamus from the hypothalamus seem to function like other limits in maintaining a relative invariant positioning, or *topology*, into adulthood. Another limit, the *alar-basal boundary* (ABb), subdivides each developing hypothalamic prosomere into longitudinal *alar plate* and *basal plate* parts, forming six progenitor units in the germinal matrix of the secondary prosencephalon. Each unit is further divided into progenitor areas which give rise to subsequent hypothalamic *nuclei* and contribute portions of the telencephalon. As such, each adult hypothalamic nucleus can be traced to progenitor areas of either alar or basal plate origin within hp1, hp2, or the acroterminal domain (Puelles et al. 2008; Puelles et al. 2012;

Ferran et al. 2015; Puelles and Rubenstein 2015). According to the Prosomeric Model, the telencephalon forms as a vesicular outgrowth of the alar plate sector of hp1 with a small contribution from the alar plate of hp2 and is, therefore, not the rostral-most part of the neural tube (Rubenstein et al. 1994; Puelles and Rubenstein 2003; Puelles 2018).

The Prosomeric Model is a powerful model that predicts the development of the adult hypothalamus from specified topological divisions, or *progenitor units*, of the early neural plate during embryological development. The principles of the Prosomeric Model allow for the definition of ontologically hypothalamic limits and structures, which likely determine the structural and functional development of subsequent telencephalic brain regions, like the prefrontal cortex.

The Structural Model predicts cortico-hypothalamic connections

The prefrontal cortex may serve as a model system for characterizing the structural and regulatory pathways between the cerebral cortex and subcortical brain regions like the hypothalamus (Goldman-Rakic 1996; Barbas 2015). The *Structural Model* highlights the variation of laminar structural in the grey matter of the prefrontal cortex as a basis for predicting specific cortico-cortical and cortico-subcortical connections (Barbas and Rempel-Clower 1997) and applies to the entire cortex (reviewed in Barbas 2015; Barbas et al. 2018). As seen in Figure 2, the areas of the prefrontal cortex (Barbas and Pandya 1989) are composed of several layers (I-VI), and different areas vary along a spectrum of laminar definition and cellularity of those layers. The “limbic areas” are defined on one end of this spectrum as “agranular” or “dysgranular” cortical areas with a maximum of 3 layers and an absent or minimal layer IV. The “eulaminate areas”

lie on the opposite end of the spectrum with a more complex structure and as many as 6 layers along with an increase in prominence of layer IV.

The systematic structural patterns of different areas of the prefrontal cortex seem to be associated with differential rates of development or maturation of limbic and eulaminate prefrontal areas (Garcia-Cabezas et al. 2019). Limbic areas seem to retain some developmental features into adulthood (Barbas 1995). Specifically, it is thought that the simpler limbic areas appear earlier in development than the more complex eulaminate areas (Garcia-Cabezas et al. 2019). Further, it is possible that variation in the structure of prefrontal areas may explain a differential vulnerability to pathology in diseases like depression, schizophrenia, and Alzheimer's, amongst others (Dombrowski et al 2001; García-Cabezas et al. 2017).

Using data from neural tracers injected into areas of the prefrontal cortex, the Structural Model has reliably predicted the existence and directionality of connections between the prefrontal cortex and subcortical brain regions in the rhesus monkey (Rempel-Clower and Barbas 1998; Zikopoulos and Barbas 2006, 2012; Barbas et al. 2013). A topographical analysis of bidirectional projections between the prefrontal cortex and the hypothalamus was previously applied using the Structural Model (Rempel-Clower and Barbas 1998). The authors found that the prefrontal cortex has highly specific projections to the hypothalamus, originating mostly from limbic orbital and medial prefrontal areas. In addition, the hypothalamus has relatively specific patterns of projection to the prefrontal cortex. Projection neurons targeting orbital limbic cortices

were more prevalent in the lateral part of the hypothalamus, whereas those targeting medial limbic cortices were more prevalent in the tuberal and medial hypothalamus.

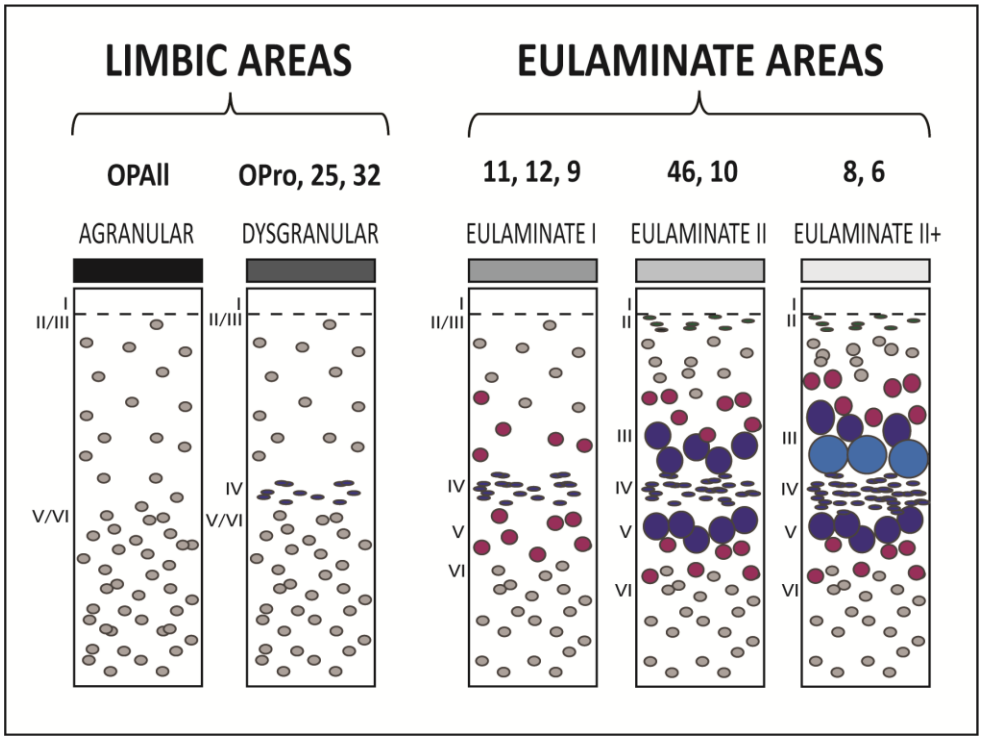

Figure 2: Laminar variation in the architectonic areas of the prefrontal cortex of rhesus monkeys according to the Structural Model. Schematic of laminar definition of each type of area of the prefrontal cortex. The Structural Model defines a spectrum of cortical types based on the natural variation in neuron density, size, and distribution. These types range from the simplest agranular structure with two discernable layers and an absent layer IV to eulaminate types with defined layers I-VI, an increasingly prominent layer IV and an increase in size of neurons found in layer III (i.e., eulaminate II+).

Testing the convergence of two disparate models

Most of our current understanding of the boundaries of the hypothalamus and its nuclei in rhesus monkeys is derived from comparative architectonic analyses of sections stained for Nissl, myelin, or acetylcholinesterase in humans, mice, and rats [e.g., Nauta and Haymaker (1969); Bleier (1984); Rempel-Clower and Barbas (1998)]. The developmental origin of hypothalamic nuclei in the adult brain has been described in atlases of chickens and mice with some comparative analyses in guinea pigs, rhesus monkeys, and humans (Puelles et al. 2012; Puelles and Rubenstein 2015; Puelles 2019; Puelles et al. 2019b). However, there is no atlas that aligns the developmental framework of the Prosomeric Model with the position and limits of the hypothalamus and its nuclei in adult primates. Further, the Prosomeric Model has not been tested in its convergence with the Structural Model on its ability to predict the pattern of connections between the hypothalamus and brain regions like the prefrontal cortex, whose development, structure, and connections likely arise from the patterning in the hypothalamus.

The Structural Model is a predictive model that has correlated the laminar variation of the cortex to the strength and patterns in cortico-cortical and cortico-subcortical connections in the rhesus monkey (reviewed in Barbas 2015; Barbas et al. 2018). The structural patterns of the prefrontal cortex likely adhere to underlying processes that unify the development of all telencephalic CNS regions, including the hypothalamus. While it follows that the reciprocal nature of connections the prefrontal cortex and the hypothalamus would be based on a common set of developmental and evolutionary progenitors, we have previously lacked an organizing principle to examine

such a relationship. The convergence of the Prosomeric and Structural Models provides the foundation for this analysis in the present study.

The result of this systematic reinterpretation of the hypothalamus in the adult rhesus monkey is an atlas with developmental ontologies for each hypothalamic nucleus, which is denoted by a uniform color scheme across all figures. This atlas will help predict connections between the hypothalamus and other CNS structures in primates and disruption in pathological states. The atlas was applied to test the convergence of two key models in predicting the pattern and strength of connections between the prefrontal cortex and the hypothalamus. The findings reveal an astonishing level of agreement between the Prosomeric and Structural Models that may allow for the neural systems that connect other brain regions to be studied on a predictive basis.

Specific aims

1. Apply the principles of the Prosomeric Model to create a topological atlas of the hypothalamus in the adult rhesus monkey with developmental ontologies.
2. Evaluate the pattern and strength of connections between most areas of the prefrontal cortex to the hypothalamus by developmental ontologies and laminar variation of the cortex.
3. Evaluate the mean diameter of axon terminals projecting from areas of prefrontal cortex to the hypothalamus to test the convergence of patterns from development and structure according to the Structural Model.

METHODS

Animal cases and surgical procedures

Sections from 35 young adult rhesus monkeys (*Macaca mulatta*) were analyzed in this study. Seven cases were used for analysis and construction of the topological atlas of the hypothalamus (Table 1), and 28 cases were used with injections of neural tracers for analysis of bidirectional connections between the prefrontal cortex and hypothalamus (Table 2). These cases were also used for other studies (Barbas et al. 1993; Rempel-Clower and Barbas 1998; Dombrowski and Barbas 1996; Zikopoulos and Barbas 2006; Ghashghaei et al. 2007; Garcia-Cabezas et al. 2017; Joyce and Barbas 2018). Detailed protocols were approved by Institutional Animal Care and Use Committees (Harvard Medical School and Boston University School of Medicine) according to NIH guidelines [DHEW Publication no. (NIH) 80-22, revised 1996, Bethesda, MD, USA].

In all cases, rhesus monkeys were given a lethal dose of anesthetic (sodium pentobarbital ~50 mg/kg, intravenous, to effect) and perfused transcardially, with 4% paraformaldehyde in either cacodylate buffer or PBS (0.1 M, pH 7.4). Brains were removed from the skull, photographed, cryoprotected in ascending sucrose solutions (10–25% in PBS 0.01 M at pH 7.4), frozen in -75°C isopentane (Fisher Scientific, Pittsburgh, PA, USA) for rapid and uniform freezing (Rosene et al. 1986), and cut in the coronal plane on a freezing microtome (AO Scientific Instruments, Reichert Technologies; Buffalo, NY, USA) at 40 or 50 µm to produce 10 matched series.

Table 1. Summary of cases and stains used for hypothalamic atlas.

Case	Myelin	SMI-32	WFA	NADPH/NOS	DARPP-32	AChE	Nissl	PV	CB	CR
AL	+				+		+			
AN		+		+			+			
AP		+					+			
AQ	+			+	+		+			
AT			+			+	+			
AX							+			+
AZ						+	+	+	+	

Assays and stains for hypothalamic atlas

To visualize nuclei and architectonic landmark features of the hypothalamus, series of sections from 7 cases were stained for Nissl, myelin, acetylcholinesterase (AChE), nicotinamide adenine dinucleotide phosphate (NADPH/NOS), *Wisteria floribunda* agglutinin (WFA), dopamine and adenosine 3'-5'monophosphate (cAMP) regulated phosphoprotein of M(r) 32kDA (DARPP-32), non-phosphorylated intermediate microtubule protein SMI-32 (SMI-32), and calcium-binding proteins parvalbumin (PV), calbindin (CB) and calretinin (CR). Assays and stains for each animal case are summarized in Table 1. Sections were stained with thionin blue for Nissl as previously described (García-Cabezas et al. 2016). Sections were stained for visualization of myelin using the Gallyas silver technique (Gallyas 1979; Zikopoulos et al. 2016). For AChE staining, the protocol of Wang and Barbas (2018) was followed. For NADPH/NOS staining, a marker for localizing nitric oxide synthase (NOS), the protocol of

Dombrowski and Barbas (1996) was followed. DARPP-32 was stained as described previously (Barbas et al. 1993). Staining for SMI-32 was done as described previously (Medalla and Barbas 2006). Staining for PV, CB, and CR calcium-binding proteins was done as described previously (Dombrowski et al. 2001).

The extracellular matrix and perineuronal nets were stained with WFA for antigen retrieval. Briefly, free-floating sections were rinsed in PBS (0.01 M, pH 7.4) and incubated in hydrogen peroxide (0.3% in PBS, Sigma-Aldrich) for 30 min. For antigen retrieval sections were incubated in sodium citrate buffer (0.01 M, pH 8.5, at 80–85 °C) for 30 min. Then, sections were rinsed in glycine (0.05 M in PBS 0.01 M at pH 7) for 1 h and pre-blocked [20% bovine serum albumin (BSA) and 0.2% Triton X-100 in PBS 0.01 M at pH 7] for 3 h followed by overnight incubation in WFA (Biotinylated *Wisteria floribunda* lectin, cat. no. B-1355, Vector Laboratories, Burlingame, CA, USA; diluted 1/200 in 20% BSA and 0.2% Triton X-100 in PBS 0.01 M at pH 7). Sections were then incubated for 1 hour in avidin–biotin horseradish peroxidase complex (AB-HRP kit; Vectastain PK-6100 ABC Elite kit, Vector Laboratories; diluted 1/100 in 0.01 M PBS), rinsed in PBS and processed for the peroxidase-catalyzed polymerization of diaminobenzidine (DAB; Vector or Zymed Laboratories Inc., South San Francisco, CA, USA; 0.05% DAB and 0.004% H_2O_2) for 2–3 min under microscopic control.

For SMI-32 staining, sections were rinsed as described for WFA and pre-blocked [10% normal goat serum (NGS), 5% BSA and 0.2% Triton X-100 in PBS 0.01 M at pH 7]. Sections were then incubated overnight with primary antibodies against SMI-32 (Sternberger Monoclonals, Lutherville, MD, USA; diluted 1/5000 in 1% NGS, 1% BSA

and 0.1% Triton X-100 in PBS 0.01 M at pH 7), rinsed in PBS and incubated for 4 h in the secondary biotinylated antibody (goat anti-mouse IgG, cat. no. BA-9200; Vector Laboratories, diluted 1/200 in PBS, 1% NGS, 1% BSA and 0.1% Triton X100). Sections were then incubated for 1 hour in avidin–biotin horseradish peroxidase complex (AB-HRP kit; Vectastain PK-6100 ABC Elite kit, Vector Laboratories; diluted 1/100 in 0.01 M PBS), rinsed in PBS and processed for the peroxidase-catalysed polymerization of diaminobenzidine (DAB; Vector or Zymed Laboratories; 0.05% DAB and 0.004% H_2O_2) for 2–3 min under microscopic control.

For DARPP-32 staining, monoclonal antibodies to purified DARPP-32 were developed (Dr. Hugh Hemmings, Laboratory of Molecular and Cellular Neuroscience, Rockefeller University; gift from Dr. Paul Greengard). To visualize neurons labeled with antibodies to DARPP-32, series of sections were washed (3 x 30 min each in 0.01 M PBS, 0.15 M NaCl at pH 7.4 followed by 10% horse serum) and then briefly washed (5 min) and placed over night at room temperature in antiserum to DARPP-32 (diluted 1 : 250 in PBS). The next day, sections were removed from primary antiserum and washed 3 times (10 min each in PBS). The sections were then processed for immunohistochemistry according to the instructions for the Vector ABC kit (Vector Labs, Burlingame, CA).

For PV, CB, and CR, antibodies that are specific for the calcium-binding proteins without cross reactivity were purchased from commercial sources (Swiss Antibodies, anti-PV #235, monoclonal; anti-CB D-28k #300, monoclonal; anti-CR #7696, polyclonal). Sections were washed (3 x 10 min each in 0.1 M PBS at pH 7.4) and placed in 6% horse serum (PV and CB) or 6% goat serum (CR) for 1 h. Sections were then

rinsed (3 x 10 min in 0.1 M PBS), placed in 0.1 M PBS solution containing antiserum for either PV (1 : 3000 dilution), CB (1 : 2000 dilution) or CR (1 : 2000 dilution) and incubated for 72 h at 4°C with gentle agitation. Sections were then rinsed (3 x 10 min each in 0.1 M PBS) and processed for immunohistochemistry according to the Vector ABC kit (Vector Labs, Burlingame, CA).

Mapping for analysis of calcium-binding protein distribution

Exhaustive plotting was used to map the distribution of calretinin-positive (CR+) neurons in representative coronal sections of the hypothalamus (Case AX) as described previously (Joyce and Barbas 2018). Briefly, a semi-automated commercial system (Neurolucida, Version 2018.1.1; Olympus BX60 bright-field microscope) was used to plot the architectonic landmarks of the limits of the hypothalamus, including the third ventricle, the optic tract, the optic chiasm, the infundibulum, and the cerebral peduncle, at 40X magnification in brightfield. Then, each CR+ labeled neuron in the hypothalamus was plotted with a red marker at 400X magnification. Each map was then compared to matched sections of the hypothalamus stained for AChE to trace the limits of hypothalamic nuclei for qualitative analysis of the distribution of CR+ neurons. No other adjustments were necessary.

Photography for hypothalamic atlas

Images of the hypothalamus were captured in sections stained for AChE (Case AZ), Nissl (Case AT), WFA (Case AT), SMI-32 (Case AP), myelin (Case AQ), PV (Case AZ), CB (Case AZ), and CR (Case AX) with an Olympus DP70 camera mounted on an

Olympus BX51 bright-field microscope at 12.5X magnification to create 2D and 3D atlases of the hypothalamus in the adult rhesus monkey and to visualize the adult hypothalamus in alternative stains. Images were captured with the same camera at 200X magnification to visualize perineuronal nets with WFA staining. Images from the same camera at 100X magnification were used to visualize neuron populations with specific calcium-binding proteins. The boundaries of hypothalamic nuclei were then traced over images of AChE stained sections using Adobe Illustrator CC software (Adobe Systems Incorporated, San José, CA, USA). The same software was used for tracing hypothalamic nuclei and assembling all figures. Minor adjustments were made to overall brightness and contrast, but images were not retouched.

For 3D reconstruction, series of images of the hypothalamus in Nissl staining were aligned using Reconstruct ™ software (version 1.1.0.0) as described (Fiala 2005). The outlines of nuclei through aligned Nissl stained sections were traced to generate 3D Boissonat structures. No other adjustments were necessary.

Table 2. Summary of cases and neural tracers used for analysis of connections.

Case	Area	Hemisphere/Tracer			Analysis[1]
		LEFT HEMI	RIGHT HEMI	HEMI NAv	
AA	A46v		HRP		Bi, RM
AB	A46d		HRP		Bi
AC	A8		HRP		Bi
AD	A8		HRP		Bi
AE	A32	HRP			Bi, RM
AF	OPro	HRP			Bi
AG	OPAll/OPro	HRP			Bi
AH	A25	HRP			Bi
AM	A11	HRP			Bi
AO	M9	HRP			Bi, RM
AY	A32		BDA		Bi, AM, BD
BC	A10	BDA			Bi, AM
BG	A32/9	BDA - A9	BDA - A32/9		Bi, AM
BH	A46d	BDA			Bi, AM
BP	A25	FB			R, RM
BQ	A25	FR			Bi, AM
BR	A25	BDA			Bi, AM, BD
MAL	A6			HRP	Bi
MAO	A6			HRP	Bi
MAR	OPro			[^{3}H]	Bi
MAV	A46v			HRP	Bi
MBH	A46v		HRP		Bi
MBJ	A11		HRP		Bi
MBY	O12		HRP		Bi
MDQ	A32			[^{3}H]	Bi
MFF	A46v			[^{3}H]	Bi
MFT	A11			[^{3}H]	Bi
MSF	A10			HRP	Bi, RM

1- Analysis Abbreviations: AM, anterograde map; BD, bouton diameter analysis; Bi, bidirectional tracer; R, retrograde tracer; RM retrograde map. For all other terms, see list of abbreviations.

Assays and stains for neural tracer analysis

Table 2 summarizes the cases, lateralization of injections sites, and neural tracers used in this study. Injections of horseradish peroxidase conjugated to wheat germ agglutinin (HRP-WGA) for visualization of neuronal cell bodies, proximal dendrites and axonal terminations; tritiated amino acids ([^{3}H]) for axonal terminations; fluorescent dyes [fast blue (FB), fluororuby (FR)] for neuronal cell bodies; and biotinylated dextran amine (BDA) for neuronal cell bodies and axonal terminations were done as described previously (Rempel-Clower and Barbas 1998; Joyce and Barbas 2018). All injections were made under guidance of microscope using a microsyringe (Hamilton, 5 µl) mounted on a microdrive. In each case, small amounts of the tracer were delivered in architectonic areas of the prefrontal cortex or in adjacent premotor areas 1.5 mm below the pial surface. The total number of cortical injection sites examined was 29. There were 8 injections into orbital prefrontal areas, 9 in medial areas, 11 in lateral prefrontal areas, and 2 in lateral premotor cortices situated adjacent to prefrontal areas.

Injections of HRP-WGA (8% dilution, 0.05–0.1 µl; Sigma, St. Louis, MO) were delivered in 17 cases. Monkeys were given an overdose of anesthetic 40-48 hours after injection, perfused, and brains were extracted and processed as described. One series from each case was treated to visualize HRP (Mesulam et al. 1980) while other series were stained for AChE or Nissl for visualization of architectonic boundaries. This tissue was mounted, dried, and counterstained in neutral red.

Injections of tritiated amino acids ([^{3}H], 0.4–1.0 µl of [^{3}H]leucine and [^{3}H]proline, specific activity 40–80 µCi) were delivered in 4 cases. Monkeys were given

a lethal dose of anesthetic and perfused with 10% formalin after 10 days. The brain was removed, photographed, and then embedded in paraffin, cut into sections of 10 µm thickness, and mounted. Sections were then processed by autoradiographic method as described (Cowan et al. 1972) and counterstained with thionin.

Injections of fluorescent dyes (3% dilution FB or FR, 2 µl; Polysciences) were delivered in 2 cases. Monkeys were deeply anesthetized after 10-14 days and perfused with 4% or 6% paraformaldehyde in 0.1 M cacodylate buffer (pH 7.4). The brain was removed, photographed, and fixed in 4% or 6% paraformaldehyde with glycerol and 2% DMSO, frozen, and cut as described. Adjacent series were saved for microscopic analysis. Series were then mounted and dried in dark storage. Series stained using FB were plotted immediately as described in the next section. Injections of BDA (equal parts 10% 10kDA BDA and 10% 2 kDA, 5 µl; Polysciences) were delivered in 5 cases. Monkeys were given an overdose of anesthetic and perfused after 18-20 days. This period varies by tracer. Brains were removed, photographed and cryoprotected in ascending concentrations of sucrose solutions (10%–25% sucrose in 0.1 M PBS, pH 7.4, with 0.05% sodium azide; Sigma-Aldrich). Brains were then frozen, cut, and mounted for mapping labeled neurons using epifluorescence as described previously (Barbas et al. 2005).

Quantification and Mapping for analysis of retrogradely labeled neurons

Figure 3 summarizes the experimental protocol for injection sites and analysis of retrograde neural tracers. Here, a retrograde tracer labels an “incoming” connection to an injection site in the prefrontal cortex from the hypothalamus and appears as a labeled

neuron in the hypothalamus. A bidirectional tracer overlaps with a retrograde tracer but may also label connections flowing in the opposite (anterograde) direction. Cases with injections of HRP-WGA, [^{3}H], FR, or FB were used to quantify labeled neurons within the boundaries of parcellated nuclei in the hypothalamus ("Bi"; Table 2).

First, the quantification of HRP-WGA and/or [^{3}H] labeled neurons in each hypothalamic nucleus was verified using data previously published (Rempel-Clower and Barbas 1998). Briefly, series of sections through the hypothalamus were examined for each case, and the number of labeled neurons was calculated through matched rostro-caudal levels sections across cases. These numbers were standardized to each case and reported as a percentage of labeled neurons found in each hypothalamic nucleus from a total number of labeled neurons in the hypothalamus. In the present study, these percentages were organized by: (1) injection site (case), according to the laminar variation of the prefrontal cortex, (2) likely prosomere of origin, and (3) likely plate of origin for each hypothalamic nucleus. The percentages were then combined within each case to show the relative share of labeled neurons positioned in nuclei that derive from each prosomere and plate of origin in the hypothalamus, as well as the adjacent diencephalic neuromere p3 and the preoptic area.

Next, exhaustive plotting was used to map the distribution of labeled neurons in representative coronal sections of the hypothalamus ("RM"; Table 2) as described previously (Joyce and Barbas 2018). Briefly, a semi-automated commercial system (Neurolucida, Version 2018.1.1; Olympus BX60 bright-field microscope) was used to plot the architectonic landmarks of the limits of the hypothalamus, including the third

ventricle, the optic tract, the optic chiasm, the infundibulum, and the cerebral peduncle, at 40X magnification in bright-field. Each labeled neuron in the hypothalamus was plotted with a marker at 400X magnification. Each map was overlaid with matched sections of the hypothalamus stained for AChE or Nissl to trace the limits of hypothalamic nuclei for qualitative analysis of the distribution of labeled neurons. Each map follows the color code in Figure 1 to denote the likely developmental origin of each nucleus. No other adjustments were necessary.

Quantification and Mapping for analysis of anterogradely labeled axons and axon terminals

Figure 3 summarizes the experimental protocol for injection sites and analysis of anterograde neural tracers. Here, an anterograde tracer labels an "outgoing" connection from the area of the injection site to the hypothalamus and appears as a labeled axon with or without boutons in the hypothalamus. Cases with injections of HRP-WGA, [^{3}H], or BDA were used to quantify labeled neurons within the boundaries of parcellated nuclei in the hypothalamus ("Bi"; Table 2). First, the quantification of HRP-WGA and/or [^{3}H] labeled axons and axon terminals in each hypothalamic nucleus was verified using data previously published (Rempel-Clower and Barbas 1998). Briefly, the density and distribution of anterograde label in the hypothalamus was evaluated using a scaled density score (+ = light label; ++ = moderate label; +++ = dense label) verified for internal consistency with an image analysis system (MetaMorph, Universal Imaging System Corp., West Chester, PA; Pearson $r = 0.94$, $p < 0.001$). Each section was analyzed for the relative density of axons and axon terminals in each hypothalamic

nucleus at 100X magnification under darkfield illumination and assigned a score. In the present study, these scores were verified and organized by: (1) injection site (case), according to the laminar variation of the prefrontal cortex, (2) likely prosomere of origin, and (3) likely plate of origin for each hypothalamic nucleus. The scores were then ordered to show the relative density of label in nuclei that derive from each prosomere and plate of origin in the hypothalamus, as well as the adjacent diencephalic neuromere p3 and the preoptic area.

Next, exhaustive plotting was used to map the distribution of labeled axons in representative coronal sections of the hypothalamus ("AM"; Table 2) as described previously (Joyce and Barbas 2018). Briefly, the same semi-automated commercial system was used to plot the architectonic landmarks of the limits of the hypothalamus, including the third ventricle, the optic tract, the optic chiasm, the infundibulum, and the cerebral peduncle, at 40X magnification in brightfield. Each labeled axon in the hypothalamus was then plotted with a marker at 400X magnification. Each teal marker followed the precise course of one labeled axon within the limits of the hypothalamus, with or without visible boutons. Each map was then overlaid with matched sections of the hypothalamus stained for AChE or Nissl to trace the limits of hypothalamic nuclei for qualitative analysis of the distribution of labeled axons. Each map follows the color code in Figure 1 to denote the likely developmental origin of each nucleus. No other adjustments were necessary.

Anterogradely labeled bouton diameter analysis in the hypothalamus

Figure 3 summarizes the experimental protocol for the analysis of anterogradely labeled axon terminals (boutons) projecting from the limbic areas (A25, A32), of the prefrontal cortex to the hypothalamus. To analyze the relative density and strength of axon terminals in each nucleus of the hypothalamus, 3 representative sections of the hypothalamus were used from 2 cases with injection sites in the limbic areas of the prefrontal cortex (A25, A32; "BD"; Table 2). Serial bright-field images were captured at 1000X magnification of a standard sample area through the thickness of each section (50 µm) of clustered BDA-labeled axons with axon terminals. Sample areas were selected within nuclei representing each of the four prosomeric quadrants of the hypothalamus (prosomere, plate; Fig 1): the lateral hypothalamic area (hp1a), the supramamillary nucleus (hp1b), the rostral paraventricular nucleus (hp2a), and the ventromedial nucleus (hp2b). For comparison, sample areas were also imaged within the preoptic area and the prethalamic nuclei of the diencephalic neuromere p3.

The serial images of each sample area were overlaid and compressed into a Z-stack image using a public domain Java image processing program (ImageJ, Version 1.46r, Research Services Branch, National Institute of Mental Health, Bethesda, Maryland, USA) as described (Abràmoff et al. 2004). Z-stack pixels were calibrated to 20 µm using Reconstruct ™ (version 1.1.0.0), and boundaries were traced exhaustively around all labeled boutons visualized in each sample area. A Feret's diameter, a measure of object size along a specified direction, was then calculated for each traced axon terminal using a macro adapted for this purpose in Reconstruct ™. The distribution and

density of axon terminals originating from either A25 or A32 was then analyzed within the sample area from each nucleus using a statistical software program (IBM® SPSS© Statistics 25, Release 25.0.0.2; 1989, 2018). The mean bouton diameter (MBD) of the sample of axon terminals from each nucleus and other descriptive statistics were then assessed from un-binned data values. Feret's diameters for each sample were then binned [0.2 µm interval (0.4-3.2 µm)] and plotted on bar charts with standardized axes for each sample. A uniform bin size was used to correct for the effects of any outliers within sample areas.

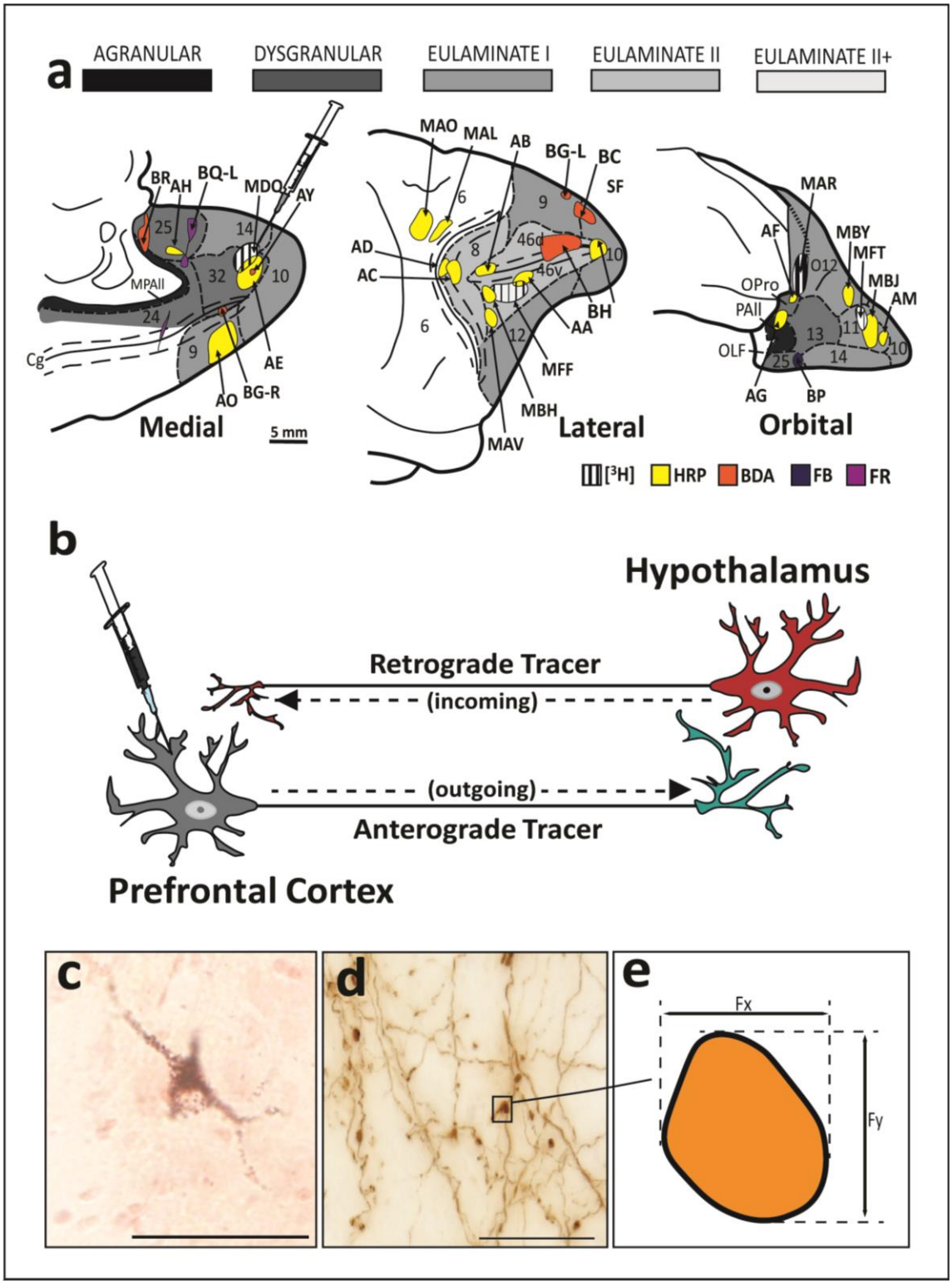
a
AGRANULAR
DYSGRANULAR
EULAMINATE I
EULAMINATE II
EULAMINATE II+
BR
AH
BQ-L
MDQ
AY
25
14
32
10
MPAll
24
9
Cg
AE
AO
BG-R
Medial
5 mm
MAO
MAL
AB
BG-L
BC
SF
6
9
AD
AC
8
46d
46v
10
BH
AA
6
12
MFF
MBH
MAV
Lateral
MAR
AF
MBY
MFT
O12
MBJ
AM
OPro
PAll
11
13
10
OLF
14
25
AG
BP
Orbital
[3H]
HRP
BDA
FB
FR
b
Hypothalamus
Retrograde Tracer
(incoming)
(outgoing)
Anterograde Tracer
Prefrontal Cortex
c
d
e
Fx
Fy

Figure 3: Summary of injection sites, neural tracer analysis, and bouton diameter analysis. (a) Summary of injection sites for neural tracers in architectonic areas of the prefrontal cortex in the adult rhesus monkey. Shading of the medial, lateral, and orbital surface of the primate cortex indicate type according to the Structural Model. Colored injection site tracings follow color code as indicated for an injection of tritiated amino acids ([^{3}H]), horse radish peroxidase (HRP), biotinylated dextran amine (BDA), fast blue (FB), and fluororuby (FR). Calibration bar (5 mm) applies to only to Fig 3a. (b) Summary schematic of neural tracer directionality with sample of labeled neurons and axon terminals analyzed. Connection directionality is analyzed relative to the injection site. A retrograde ("incoming") tracer is absorbed by an axon terminal local the injection site and carried to a distant labeled neuron. An anterograde ("outgoing") tracer is absorbed by a neuron local to the injection site and carried to a distant labeled axon and axon terminal (bouton). (c) Example HRP-WGA-labeled neuron in the supramamillary nucleus of the hypothalamus in adult rhesus monkey. Calibration bar (50 µm) applies to figure 3c at 400X magnification. (d) Example Z-stack of BDA-labeled axons and boutons in the lateral hypothalamic area. Calibration bar (20 µm) applies to figure 3d at 1000X magnification. (e) Schematic for approximate X-Y measurements taken to calculate bouton diameter using a Feret's diameter.

RESULTS

Rationale for a topological reinterpretation of the hypothalamus in adult rhesus monkeys

What makes the nuclei and anatomical landmarks of the hypothalamus *hypothalamic*? One must first acknowledge, as others have, that the classical *topography* of this brain region and its nuclei is arbitrary and, at times, problematic (Rempel-Clower and Barbas 1998; Puelles et al. 2012; Puelles 2019). For example, certain terms like "posterior area" and "dorsal area" are anatomically misleading (the majority of the "posterior area" is found dorsal to the "dorsal area" and is not in the posterior-most position of the adult hypothalamus). Further, there are many names used to describe homologous nuclei across vertebrate species, resulting in significant confusion for the study of the hypothalamus and its complex functions. Thus, until recently, it has not been possible to precisely define and study the underlying anatomical structures of the hypothalamus that contribute to its complex functions.

Before the advent of genetic and molecular studies, there was no rationale for naming of the hypothalamus and its constituent nuclei that informed structure, developmental origin and homology across species – a hypothalamic ontology. The Prosomeric Model proposes a developmental ontology for the constituent nuclei of the hypothalamus by systematic extrapolation of adult hypothalamic structures from fated embryological units based on: (1) genoarchitecture and (2) topology (Puelles and Rubenstein 2015; Puelles 2019). Topology, consistent with its use in mathematics, refers

to the invariant position of structures through continuous change. A prosomeric topology, in principle, may be related to the Japanese art of folding paper, *origami*. Beginning with a planar geometry, folds are introduced to a square piece of paper in a specific sequence and scale that results in a novel figure, like a swan or a frog. If one unfolds the origami figure, one can visualize geometric units of the paper that were shaped to contribute to its final form. As in origami, the organizers present in the early neural plate induce genetic signals that fate topological units to their final position in the adult CNS. A unique genoarchitectural profile for each neuromere, plate, and progenitor area of the neural plate provides a signature pattern for each brain region that is retained throughout secondary and tertiary morphological events in CNS development and into adult architecture. Thus, a prosomeric topology, like a developmental road map, makes it possible to identify and trace hypothalamic landmarks and nuclei to be identified and traced across a developmental sequence from the progenitor area to the final adult position.

Accordingly, what is considered as *hypothalamic* includes the adult derivatives of the three prosomeres of the secondary prosencephalon, apart from the structures derived from the telencephalic vesicle as outlined in the next section.

A brief summary of the Prosomeric Model

The main principles of the Prosomeric Model in relation to the developing hypothalamus and adjacent brain regions are briefly described here (Rubenstein et al. 1994; Puelles and Rubenstein 2003; Nieuwenhuys and Puelles 2016; Puelles 2018). The Prosomeric Model proposes a stereotyped process of regionalization (patterning or

specification) of the CNS during early development caused by gradients of signaling molecules that spread from organizers (Fig 1). The floor and roof plates pattern the neural plate along its dorso-ventral axis and specify longitudinal alar and basal plates. Other organizers pattern the neural plate along its rostro-caudal axis into transverse segments, or proneuromeres [spinal cord (sc), rhombencephalon (Rhomb), mesencephalon (Mes), diencephalon (Dien), and secondary prosencephalon (SPro)]. Each proneuromere is further patterned into several neuromeres, each composed of alar and basal plate parts. Thus, the intersection of longitudinal plates and transverse neuromeres forms a checkboard pattern of orthogonal boundaries present at the neural plate stage (Fig 1a). This pattern constitutes a fundamental Bauplan, for the development of the neural plate, which is apparently common to all vertebrates.

The Prosomeric Model divides the diencephalon into three neuromeres (p1, p2, and p3) and the secondary prosencephalon into three neuromeres (hp1, hp2, and acroterminal domain; Fig 1a - c). The alar plate part of p2 gives rise to the dorsal thalamus and the alar plate part of p3 gives rise to the reticular nucleus (TRN), the zona incerta (ZI), and prethalamic nuclei (PTh; Fig 1d). The basal parts of p2 and p3 contribute a part of the substantia nigra (SN) and other dopaminergic cell groups. Further, the prethalamic prosomere (p3) that forms a rostral boundary between the diencephalon and the secondary prosencephalon expands and creates a significant topographical and topological discontinuity between the dorsal thalamus (p2) and the caudal-most hypothalamic prosomere (hp1; Fig 1a – d). The adult hypothalamus is derived from neurogenic units within the secondary prosencephalon in the alar and basal parts of hp1,

hp2, and the acroterminal domain (Fig 1d). The alar plate part of hp1 also gives rise to most of the pallium (Pal) and subpallium (SPal) of the telencephalon (Tel), which gives rise to the entire cerebral cortex (Fig 1d). The alar plate part of hp2 also gives rise to the retina, the optic chiasm (oc), and the optic tract (ot), and contributes the preoptic area (POA) to the telencephalic subpallium (Fig 1d). The acroterminal domain functions as an organizer and gives rise to structures of the prospective neurohypophyseal portal system, including the infundibulum (INF) and neurohypophysis (h). The rostral-most termination of the roof plate is the prospective anterior commissure (ac), which lies topographically dorsal to the POA at the end of development (Fig 1a - d).

Topologically, the hypothalamus is rostral to p3 and ventral to the telencephalon. Note that at the end of morphogenesis, the hypothalamus lies below (i.e., ventral) to the thalamus in the topographical relation denoted by its name (Fig 1d). This positioning is maintained through adulthood and represents a 90-degree angle change from the early patterned units of the hypothalamus in the neural plate. It follows that a prosomeric ontology applied to the hypothalamus would emphasize naming structures and limits by the relative invariant positioning (topology) of the structures and nuclei patterned during the early neural plate stage. Thus, what classical studies refer to as “ventral” or “dorsal” according to topography are better classified as “rostral” or “caudal” in topological terms within the Prosomeric Model. For this atlas, more time has been allowed for consensus on axial nomenclature, and the atlas instead follows the example of classical studies (Nauta and Haymaker 1969; Bleier 1984; Rempel-Clower and Barbas 1998) to refer to

the relative topographical location of hypothalamic landmarks and nuclei in adult rhesus monkeys.

The color code in Figure 1 is used across all figures for consistency to denote the likely developmental origin of hypothalamic nuclei and boundaries in adult rhesus monkeys. The adult hypothalamic derivatives of the alar plate are traced in solid blue lines, and derivatives of the basal plate in solid pink lines. Adult derivatives from hp1 are shown in dark shades of pink and blue and those of hp2 are shown in lighter shades. Adult derivatives of p3 are traced in yellow perforated lines.

Architectonic parcellation and developmental ontology of hypothalamic nuclei in rhesus monkeys

The parcellation of classic hypothalamic nuclei in adult rhesus monkeys was based on images of matched coronal brain sections stained with Nissl and AChE. The boundaries of hypothalamic nuclei were further visualized using additional stains (Table 1). The latter stains confirmed some architectonic boundaries of adult hypothalamic nuclei or landmarks that were already well-defined in Nissl and AChE stained sections. The hypothalamus of the adult rhesus monkey was divided into three topographic regions ("Caudal", "Tuberal and Medial", and "Rostral") following comparative architectonic analyses in mice, rats, and humans (Rempel-Clower and Barbas 1998). In these three hypothalamic regions, 18 hypothalamic nuclei whose architectonic features are comparable across primate and rodent species were traced, as described previously (Rempel-Clower and Barbas 1998; Puelles et al. 2012). Table 3 summarizes the parcellation of these 18 nuclei into each region. Of note, the subthalamic nucleus (STN)

was included in this analysis because modern genoarchitectonic studies have shown that it is a distinct nucleus of the adult hypothalamus (Puelles et al. 2012). Further, the posterior, dorsal, and anterior hypothalamic areas and the preoptic area were excluded from this analysis because the same studies have shown that they are not part of the hypothalamus proper. Specifically, the anterior hypothalamic area was absorbed into the preoptic area (POA), which is considered one of four CNS regions derived from the telencephalic subpallium – a secondary derivative of the alar plate of hp2. The posterior and dorsal hypothalamic areas were reassigned as prethalamic nuclei (PTh) because they originate from p3 (Puelles et al. 2012).

Table 3. Topographic regions of the rhesus monkey hypothalamus and their constituent nuclei.

Region	Nucleus	Abbrev
Caudal	lateral mamillary nucleus	LM
	medial mamillary nucleus	MM
	paramamillary nucleus	PM
	perimamillary nucleus	PeM
	subthalamic nucleus	STN
	supramamillary nucleus	SM
Tuberal and Medial	area of the tuber cinereum	TCA
	arcuate nucleus	ARC
	dorsomedial nucleus	DM
	perifornical nucleus	Pef
	premamillary nucleus	PreM
	tuberomamillary nucleus	TM
	ventromedial nucleus (core and shell)	VMc/VMs
Rostral	lateral hypothalamic area	LA
	paraventricular nucleus (magnocellular/parvicellular groups)	PaM/PaP
	rostral paraventricular nucleus	RPa
	suprachiasmatic nucleus	SCH
	supraoptic nucleus	SO

The classical structure, limits, and nuclei of the adult hypothalamus of rhesus monkeys were then reinterpreted using a prosomeric ontology. The assumed developmental origin of hypothalamic structures is represented using the same color scheme throughout the figures. The analysis of the likely developmental origin by progenitor prosomere (hp1, hp2) and plate of origin (alar, basal plates) of 18 parcellated nuclei in the hypothalamus of adult rhesus monkeys is based on homology of the adult mouse in Table 4 (Puelles et al. 2012; Puelles et al. 2019b).

Table 4. Comparison of nomenclature of hypothalamic nuclei in the mouse and rhesus monkey.

hp1					
Alar Plate			**Basal Plate**		
Progenitor Area (mouse)	Adult Derivative (mouse)	Adult Homologue (rhesus)	Progenitor Area (mouse)	Adult Derivative (mouse)	Adult Homologue (rhesus)
CPa	prereticular lateral hypothalamic area	LA	RTuI	peduncular dorsomedial n. (?)	DM
	pre-eminential lateral hypothalamic area			ventrobasal perifornical n.	Pef
	peduncular supraoptic n.*			tubermamillary n. (?)	TM
	paraventricular n. (magnocellular)	PaM	RTuV	hypothalamic ventricular organ*	
VPa	paraventricular n. (parvicellular)	PaP	PRM	posterior hypothalamic n.*	
SPa	ventral entopeduncular n.*		RM	paramamillary n.	PM
	subparaventricular n.*			supramamillary n.	SM
				perimamillary n.	PeM
				subthalamic n.	STN
hp2					
Alar Plate			**Basal Plate**		
Progenitor Area (mouse)	Adult Derivative (mouse)	Adult Homologue (rhesus)	Progenitor Area (mouse)	Adult Derivative (mouse)	Adult Homologue (rhesus)
TPa	rostral paraventricular n.	RPa	TuD	anterobasal area	TCA
	terminal supraoptic n.	SO		ventromedial n. (shell)* (?)	VMs
	optic ventricular recess		TuI	median eminence	
	entrance of optic nerve			neurohypophyseal diverticule	
TSPa	anterior hypothalamic n.*			arcuate n.	ARC
	optic chiasm			terminal dorsomedial n.	DM
	optic tract			ventromedial n. (core) (?)	VMc
	suprachiasmatic n.	SCH	TuV	tuberomamillary n. (?)	TM
				ventral tuberal area*	
				hypothalamic ventricular organ*	
			PMp	dorsal premamillary n.	PreM
			Mp	lateral mamillary n.	LM
				medial mamillary n.	MM

(*) Molecularly defined nucleus in adult mice without clear definition in stained sections used in this study of the rhesus monkey.
(?) Nucleus of basal plate origin with mixed progenitor and migratory pattern from hp1 and hp2 proposed by the prosomeric model (Puelles et al. 2012). Ontological analysis of progenitor area and adult derivatives in mouse were adapted from the same authors.

Topological analysis of hypothalamic boundaries in adult rhesus monkeys

To test this developmental ontology, the topology of architectonic landmarks of the secondary prosencephalon and the diencephalon was analyzed in relation to adult hypothalamic nuclei. The Prosomeric Model provides a framework to help explain the development of the entire CNS following a topology, or fated position, which can be traced from the early neural plate to adult positioning. Topological relationships of regions of the CNS persist through development into adulthood with homology in many architectonic landmarks (Rubenstein et al. 1994; Puelles and Rubenstein 2003; Puelles and Ferran 2012; Puelles et al. 2012; Nieuwenhuys and Puelles 2016; Puelles 2018). Thus, homology was assumed and extrapolated to rhesus monkeys by topological relations of landmarks that appear in early neuroepithelial stages of developing mice. These landmarks retained a similar relative topographical positioning in relation to hypothalamic nuclei in monkeys as seen in adult mice.

In the caudal hypothalamus, the following anatomical landmarks were: the mamillary bodies (Mb), the subthalamic nucleus (STN), and the diencephalic prosomere p3 which contains the reticular nucleus (TRN), the prethalamic nuclei (PTh), the zona incerta (ZI), part of the substantia nigra (SN) and the internal capsule (ic), whose fibers course through and meet the fibers of the cerebral peduncle (cp) but originate in the telencephalon. In the tuberal and medial hypothalamus, the optic tract (ot), the internal capsule (ic), and p3 derivatives (the PTh, the ZI, and the TRN) were selected. For the rostral hypothalamus, the anterior commissure (ac), the preoptic area (POA), p3

derivatives (the PTh, the ZI, and the TRN), the optic tract (ot) and optic chiasm (oc), and the internal capsule (ic) were selected.

First, the adult derivatives of p3 and the other selected landmarks were identified and traced (Fig 4-7). Interneuromeric boundaries were then delineated as follows: between adjacent neuromeres of the diencephalon and secondary prosencephalon (p3-hp1); between hypothalamic prosomeres (hp1, hp2); between the topologically rostral-most hypothalamic prosomere and the acroterminal domain (hp2-At); between the hypothalamic part of the rostral-most hypothalamic prosomere and the preoptic area (hp2-POA); and an intrahypothalamic boundary between the alar and basal plates (ABb).

First, the interneuromeric boundary between adult derivatives of p3 and hp1 was assessed (p3-hp1). An interneuromeric boundary was traced between the derivatives of two sequential diencephalic neuromeres (p2, p3) that are found topologically caudal to the derivatives of hp1 (Fig 4a- 7f). The p2-p3 boundary is shown from the limits of the caudal hypothalamus and intersects rostrally with the anterior commissure (ac; Fig 7c – f). The boundaries along derivatives of p3 (the TRN, the ZI, and the PTh) medially to the third ventricle were traced (V; Fig 4a – 7f). The fibers of the internal capsule (ic) terminate in the cerebral peduncle (cp) and the basal plate part of p3 that contains components of the substantia nigra (SN; Fig 4e – h). The topographically ventral boundary of p3 derivatives is continuous with the dorsal limits of both hp1b derived nuclei (Fig 4a – 6b) and hp1a derived nuclei (Fig 6a – 7d). Of note, a clear neuromeric band of derivatives of p3 was visualized using the alternative stain *Wisteria floribunda* agglutinin (WFA), which further clarified the p3-hp1 boundary, as described below.

Then, an interneuromeric boundary between adult derivatives of hp1 and hp2 (hp1-hp2) was analyzed. While an hp1-hp2 boundary is not readily visualized using AChE and Nissl staining, there is a potential hp1-hp2 boundary using WFA (see next section). Additionally, the fornix (f) courses almost exclusively through hp1 close to the hp1-hp2 boundary (Fig 4-7). A branch of the fornix diverges rostrally from the basal plate part of hp1 into the MM in hp2 (Fig 4). From the MM to the rostral hypothalamus, the fornix progressively rises among hp1 derivatives and exits the hypothalamus dorsal to the anterior commissure (ac; Fig 7). Thus, according to prosomeric topology, nuclei in the adult hypothalamus that are dorsal to the fornix are likely derived from hp1 while those ventral to the fornix are likely derived from hp2.

Next, the boundary between the adult derivatives of hp2 and the acroterminal domain (hp2-At) was analyzed. The infundibulum (INF), an adult remnant of the acroterminal domain, lines the ventral border of the adult derivatives of hp2b (Fig 5c – 6d). As the infundibulum recedes moving rostrally, the emergence of the optic tract (ot), another derivative of the acroterminal domain, signals a progressive transition from basal plate to alar plate derivatives of hp2 (Fig 6a – f).

Then, the rostral boundary between adult derivatives of hp2 and the preoptic area (hp2-POA) was analyzed. The optic tract (ot) contacts both alar and basal plate nuclei of hp2 before terminating at the optic chiasm (oc). Where the optic tract meets the optic chiasm, the POA emerges medially between the likely adult derivatives of hp2a (Fig 7c – d). Thus, the POA contacts the rostral terminus of hp2a and expands dorsally and rostrally to meet the anterior commissure (ac; Fig 7e – f).

Neither intrahypothalamic nor adjacent landmarks were found in the adult rhesus monkey that clearly delineate a boundary between the alar and basal plates (ABb) through the derivatives of the secondary prosencephalon. Only the infundibulum and the optic tract differentially line the likely adult hypothalamic derivatives of the alar and basal parts of hp2. Figure 4 shows a progressive but gradual caudo-rostral transition between nuclei likely derived from the basal plate to those likely derived from the alar plate. Further, there are no adult hypothalamic nuclei with a mixed migratory pattern across the alar and basal plates according to genoarchitectonic studies (Puelles et al. 2012; Ferran et al. 2015). Thus, while the alar-basal boundary cannot be visualized in adult primates with available methods, the relative invariant position (topology) of derivatives of the alar and basal plate is retained.

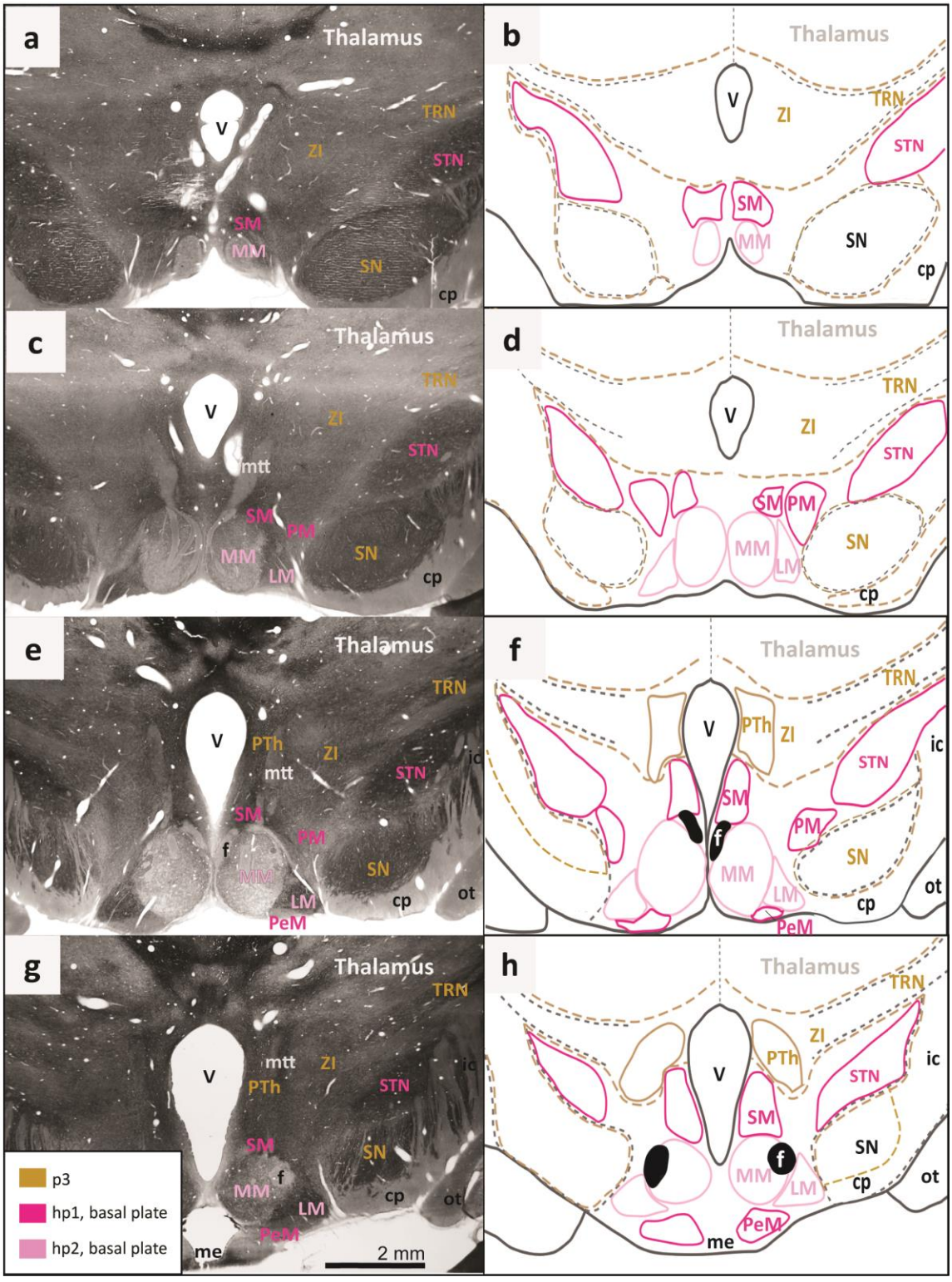
a
Thalamus
V
TRN
ZI
STN
SM
MM
SN
cp
b
Thalamus
V
ZI
TRN
STN
SM
MM
SN
cp
c
Thalamus
V
TRN
ZI
STN
mtt
SM
PM
MM
LM
SN
cp
d
Thalamus
V
TRN
ZI
STN
SM
PM
MM
LM
SN
cp
e
Thalamus
V
PTh
ZI
TRN
mtt
STN
ic
SM
PM
f
MM
SN
LM
cp
ot
PeM
f
Thalamus
V
PTh
ZI
TRN
STN
ic
SM
f
PM
SN
MM
LM
cp
ot
PeM
g
Thalamus
TRN
V
mtt
ZI
ic
PTh
STN
SM
SN
f
MM
LM
cp
ot
PeM
me
2 mm
p3
hp1, basal plate
hp2, basal plate
h
Thalamus
TRN
ZI
V
PTh
STN
ic
SM
f
SN
MM
LM
cp
ot
PeM
me

Figure 4: Architectonic boundaries of the caudal hypothalamus in the adult rhesus monkey show likely developmental origin of anatomical landmarks and hypothalamic nuclei. (a, c, e, g) Photomicrographs of coronal sections through the hypothalamus of an adult rhesus monkey stained for AChE; (b, d, f, h) maps of traced architectonic boundaries. Sections are ordered sequentially from caudal (a, b) to rostral (g, h). All nuclei of the caudal hypothalamus are likely of basal plate origin. The SM, the PM, the STN, and the PeM are likely derived from hp1 while the MM and the LM likely arise from hp2. Calibration bar (2 mm) in g applies to a, c, e, and g. For color code see Figure 1. See list of abbreviations for complete terms.

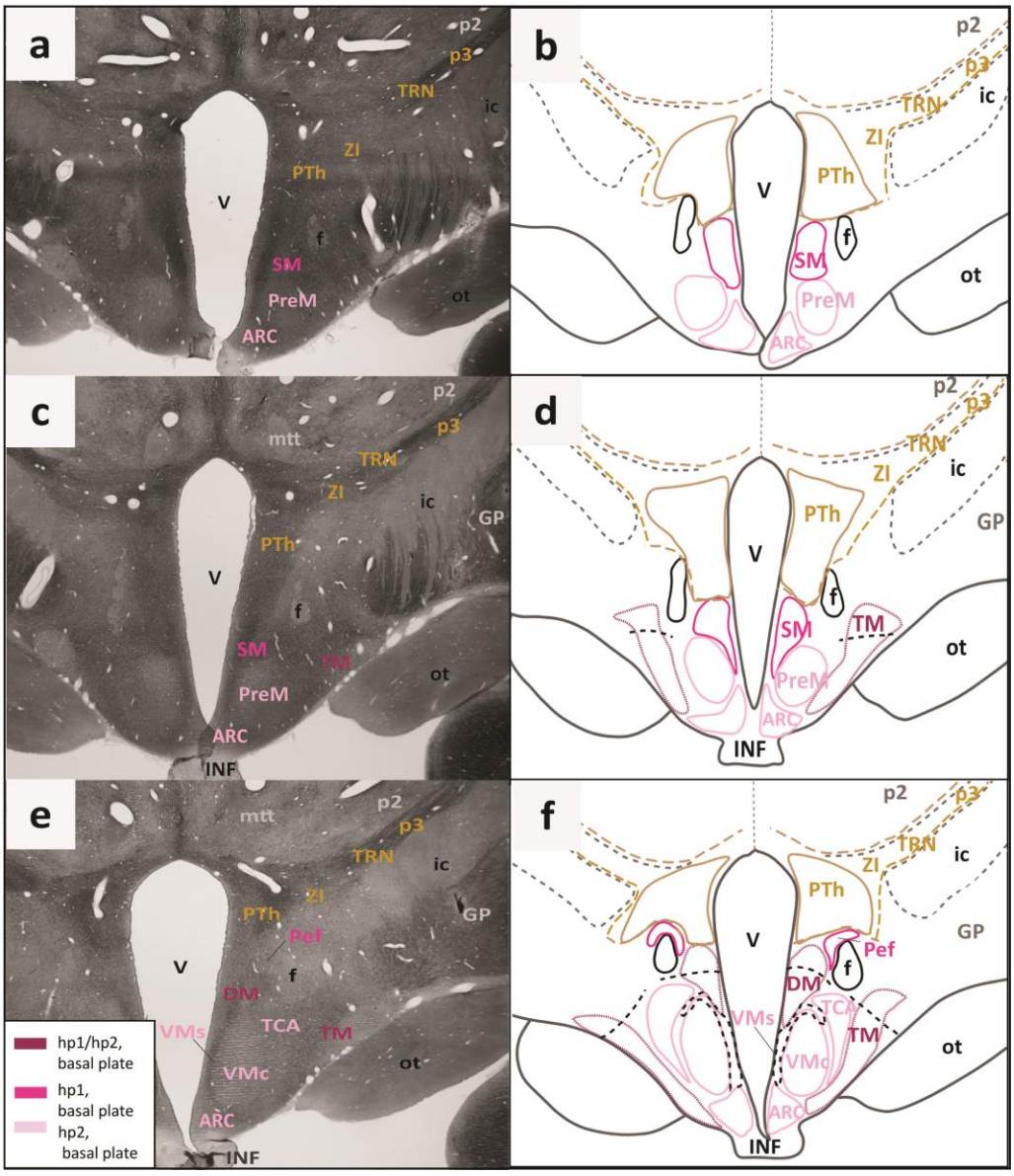

Figure 5: Architectonic boundaries of the tuberal and medial hypothalamus in the adult rhesus monkey show likely developmental origin of anatomical landmarks and hypothalamic nuclei. (a, c, e) Photomicrographs of coronal sections through the hypothalamus of an adult rhesus monkey stained for AChE; (b, d, f) maps of traced architectonic boundaries. Sections are ordered sequentially from caudal (a, b) to rostral (e, f). All nuclei of the tuberal and medial hypothalamus are of basal plate origin. The SM and the Pef are likely derived from hp1 while the PreM, the Arc, the TCA, and the VMc likely arise from hp2. The DM and the TM are thought to be derived from the basal plate parts of both from hp1 and hp2 (maroon). Proposed boundaries dividing the DM and the TM into likely hp1 or hp2 parts are also shown. Calibration bar (2 mm) in e applies to a, c, and e. For color code see Figure 1. See list of abbreviations for complete terms.

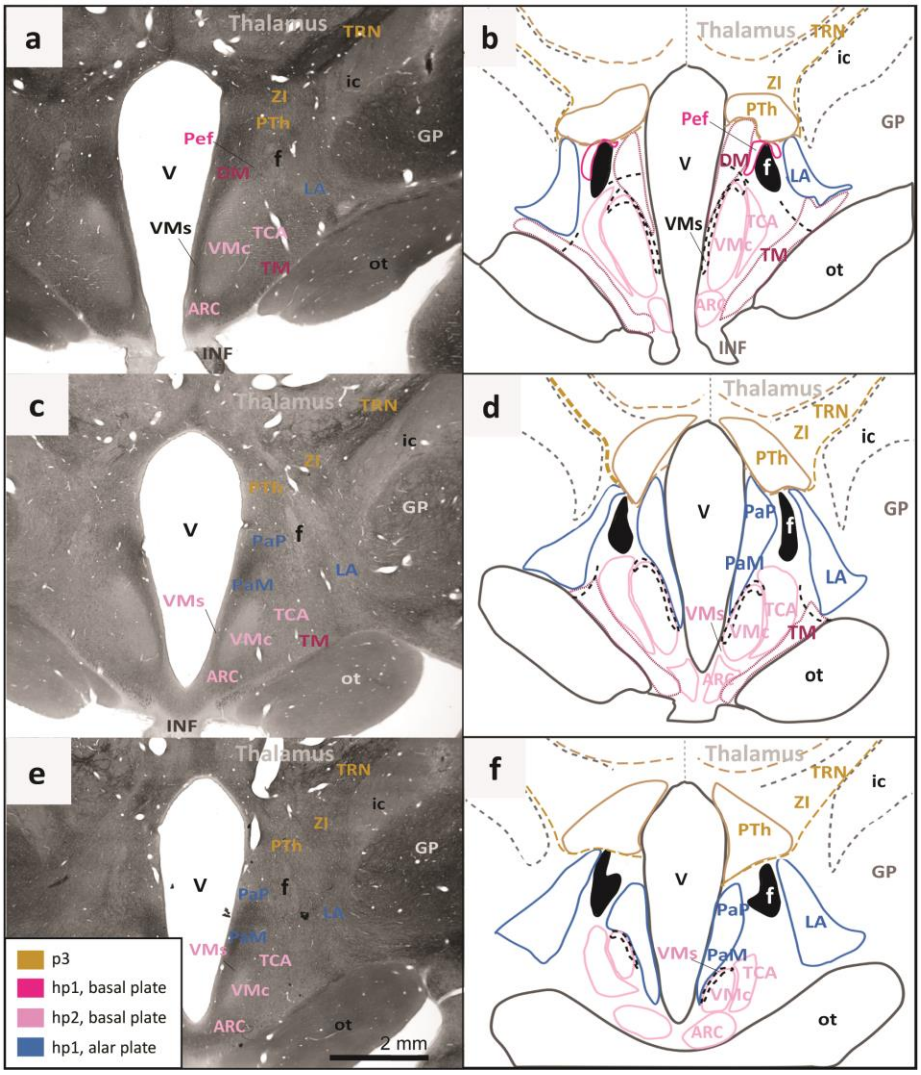

Figure 6: Continuation of the architectonic boundaries of the tuberal and medial hypothalamus in the adult rhesus monkey show likely developmental origin of anatomical landmarks and hypothalamic nuclei. (a, c, e) Photomicrographs of coronal sections through the hypothalamus of an adult rhesus monkey stained for AChE; (b, d, f) maps of traced architectonic boundaries. Sections are ordered sequentially from caudal (a, b) to rostral (e, f). All nuclei of the tuberal and medial hypothalamus are of basal plate origin. All nuclei of the rostral hypothalamus are of alar plate origin. The Pef is the rostral-most nucleus of the basal plate part of hp1. The Arc, the TCA, and the VMc arise from the basal plate part of hp2. The DM and the TM are thought to be derived from basal plate parts of both hp1 and hp2 (maroon). Proposed architectonic boundary of the VMs lines the VMc medially and course dorsally to meet the DM. The LA, the PaM, and the PaP are likely derived from the alar plate part of hp1. Calibration bar (2 mm) in e applies to a, c, and e. For color code see Figure 1. See list of abbreviations for complete terms.

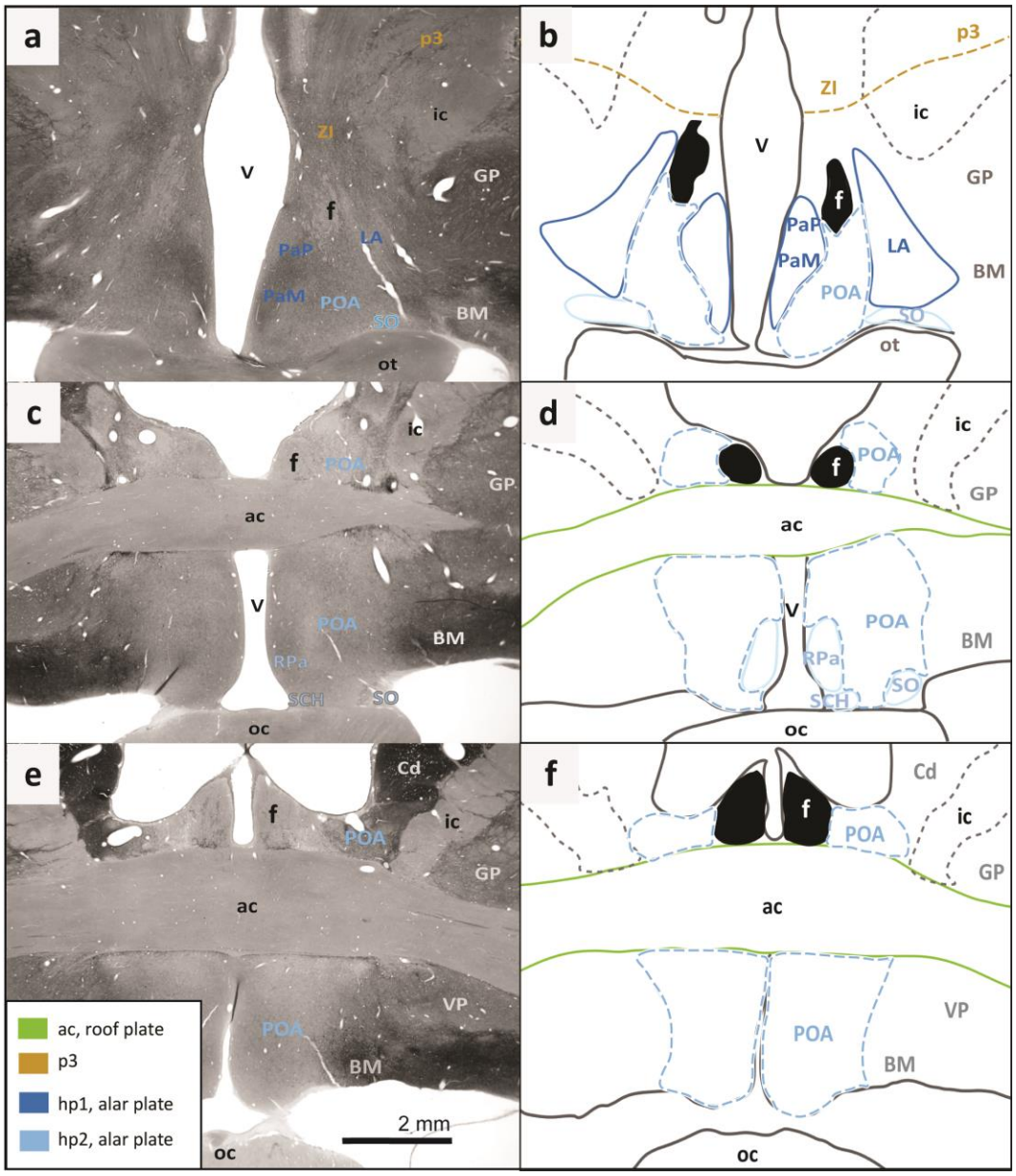

Figure 7: Architectonic boundaries of the rostral hypothalamus in the adult rhesus monkey show likely developmental origin of anatomical landmarks and hypothalamic nuclei. (a, c, e) Photomicrographs of coronal sections through the hypothalamus of an adult rhesus monkey stained for AChE; (b, d, f) maps of traced architectonic boundaries. Sections are ordered sequentially from caudal (a, b) to rostral (e, f). All nuclei of the rostral hypothalamus are of alar plate origin. The LA, the PaM, and the PaP are derived from hp1 while the RPa, the SO, and the SCH arise from hp2. The POA is excluded from the hypothalamus in the adult rhesus monkey according to (Puelles et al. 2012). Calibration bar (2 mm) in e applies to a, c, and e. For color code see Figure 1. See list of abbreviations for complete terms.

Analysis of alternative stains for resolution of hypothalamic boundaries

In addition to AChE and Nissl, coronal brain sections were stained and analyzed to demonstrate architectonic properties of the adult hypothalamus and its constituent nuclei. These stains included Gallyas silver stain to visualize myelin, nicotinamide adenine dinucleotide phosphate (NADPH/Nos) for a subclass of interneurons, *Wisteria floribunda* agglutinin (WFA) for extracellular matrix and perineuronal nets, dopamine- and cyclic-AMP-regulated phosphoprotein of molecular weight 32,000 (DARPP-32), and non-phosphorylated intermediate neurofilament protein SMI-32. Figure 8 shows representative sections of the three topographic hypothalamic regions with these stains with matched sections in AChE and traced maps demonstrating architectonic limits of nuclei by prosomere and plate of origin. The same color code in Figure 6 is used as in Figures 4-7.

Some of the alternative stains confirmed the limits of more prominent nuclei, such as the subthalamic nucleus (STN) or suprachiasmatic nucleus (SCH), that are also readily visualized in AChE and Nissl stains. Of note, this study affirms the previous observation that the hypothalamus is largely devoid of myelin was confirmed (Nauta and Haymaker 1969), but a list of other common stains seem to leave the hypothalamus entirely untouched yet consistently show major fiber tracts and/or surrounding subcortical structures. The nuclei of the hypothalamus could not be visualized for myelin, NADPH/Nos, DARPP-32, or SMI-32 staining patterns. Regarding structures proximal to hypothalamic nuclei, the prominent capsule of myelin that surrounds the medial mamillary nucleus (MM) and the subthalamic nucleus (STN) was visualized to a similar

extent. Major fiber tracts, such as the optic tract and the fornix, which course through or around the hypothalamus were visualized in all the alternative stains. The appearance of these fiber tracts in each stain was comparable to their appearance in AChE and Nissl. However, the architectonic properties of adult hypothalamic nuclei were not clearly elucidated using these staining techniques, demanding alternative methods of study.

Of note, the extracellular matrix and perineuronal nets was visualized for many medium and large neurons that fell within the boundaries of several adult hypothalamic nuclei derived from the alar and basal plate parts of hp1 (WFA; Fig 8j-l). These included the magnocellular group of the paraventricular complex (PaM; Fig 8m), the lateral hypothalamic area (LA; Fig 8n), the subthalamic (STN; Fig 8r) perimamillary (PeM; Fig 8p) and supramamillary nuclei (SM; Fig 8q). A clear neuromeric boundary was visualized between the derivatives of the basal plate parts of p3 and hp1, and a second boundary between the derivatives of the basal plate parts of hp1 and hp2 with WFA staining (Fig 8l). In contrast, there were many large neurons within the boundaries of the arcuate nucleus (ARC; Fig 8o), which is thought to be a derivative of the basal plate part of hp2. This was the only nucleus derived from hp2 with perineuronal net staining that clearly framed the soma of neurons as well as primary dendrites. This population of stained neurons in the ARC extended ventrally into the median eminence but were not found within the limits of the ventromedial nucleus (VM).

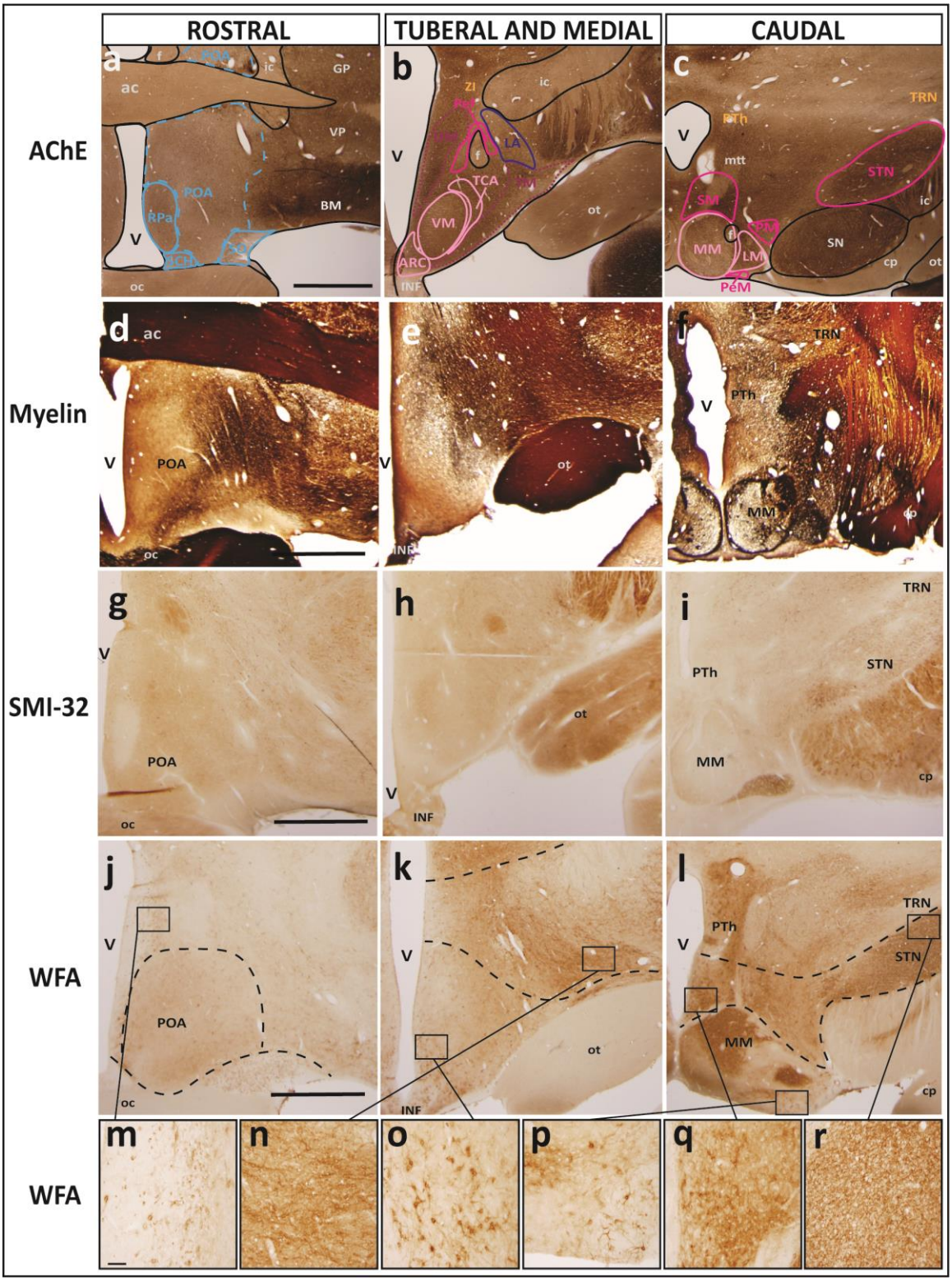
ROSTRAL
TUBERAL AND MEDIAL
CAUDAL
AChE
Myelin
SMI-32
WFA
WFA
a
b
c
d
e
f
g
h
i
j
k
l
m
n
o
p
q
r
ac
GP
ic
VP
POA
BM
RPa
V
oc
ZI
LA
TCA
VM
ot
ARC
INF
TRN
PTh
mtt
STN
SM
PM
MM
LM
SN
cp
PéM
INF

Figure 8: Representative sections of each topographic region of the adult hypothalamus visualized with distinct stains. (a-c) Traced maps of hypothalamic nuclei by prosomere and plate of origin from representative sections from each of the three topographical regions of the hypothalamus of rhesus monkey visualized with acetylcholinesterase (AChE; Case AZ). Matched sections were alternatively stained for: (d-f) myelin (Case AQ); (g-i) SMI-32 (Case AP); (j-l) WFA (Case AT). Of interest, WFA was the only alternative stain that clarified interneuromeric boundaries between p3, hp1 and hp2 (drawn in dashed lines). Medium and large neurons were visualized with WFA in the: (m) magnocellular group of the paraventricular complex (PaM); (n) lateral hypothalamic area (LA); (o) arcuate nucleus (ARC); (p) perimamillary nucleus (PeM); (q) supramamillary nucleus (SM); (r) subthalamic nucleus (STN). Calibration bar (2mm) in sections a, d, g, and j apply to all sections within corresponding rows at low magnification. Calibration bar (50 µm) in section m applies to all sections m-r at higher magnification. For color code in traced maps see Figure 1. See list of abbreviations for complete terms.

Analysis of calcium-binding proteins for resolution of hypothalamic boundaries

An analysis was performed on sections stained for parvalbumin (PV), calbindin (CB), and calretinin (CR) to visualize the distribution of hypothalamic neurons with different calcium-binding proteins. These calcium-binding proteins have previously been used label subclasses of interneurons in the prefrontal cortex of the rhesus monkey (Dombrowski et al. 2001) but also excitatory projection neurons in the dorsal thalamus (Jones 2007). Figure 9 shows representative sections of each of the three topographic regions of the hypothalamus stained for neurons with calcium-binding proteins and a traced map of nuclei by prosomere and plate of origin over sections stained with AChE for visual comparison.

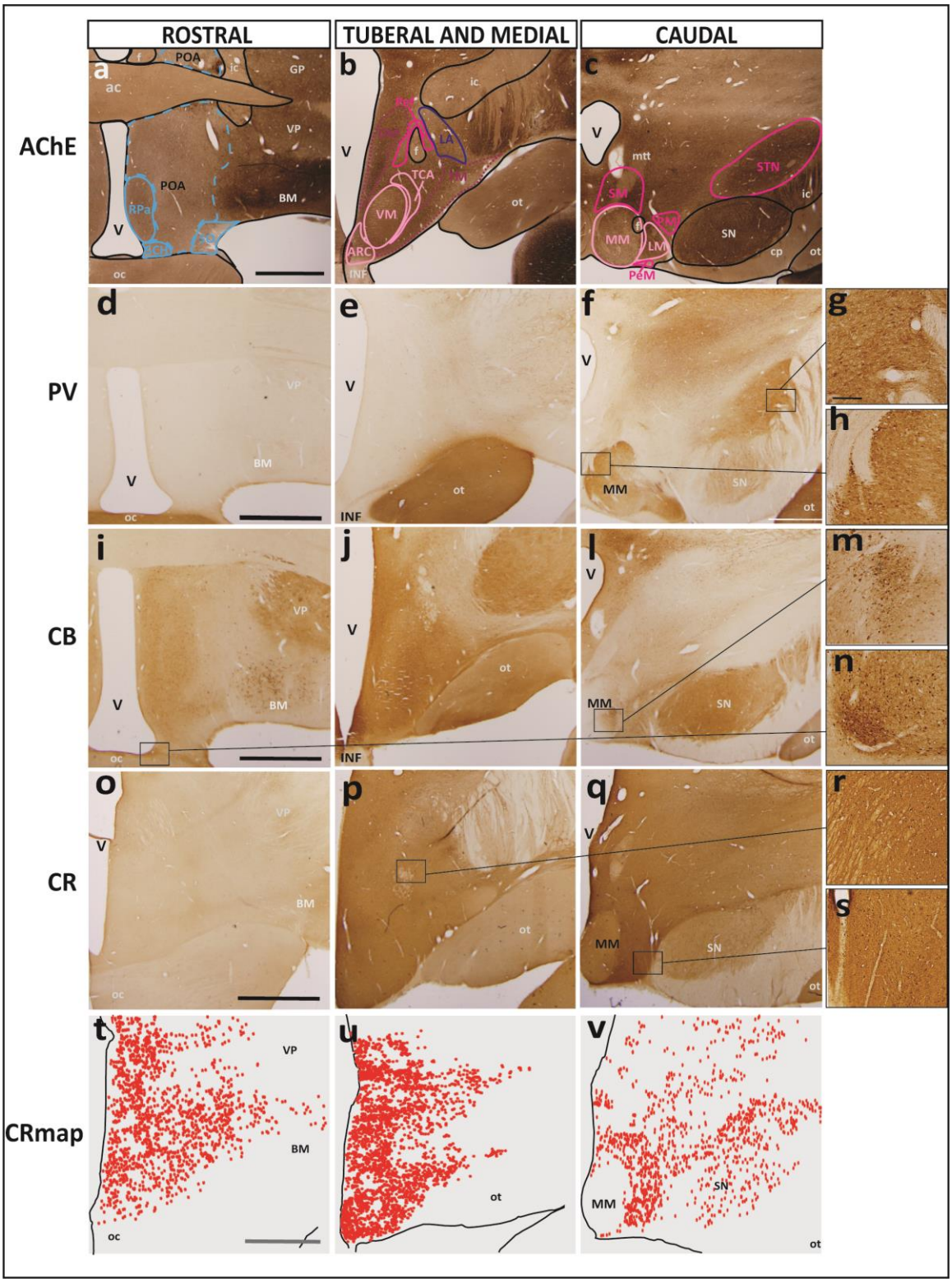
ROSTRAL
TUBERAL AND MEDIAL
CAUDAL
AChE
PV
CB
CR
CRmap
a
b
c
d
e
f
g
h
i
j
l
m
n
o
p
q
r
s
t
u
v
POA
GP
ac
ic
VP
BM
RPa
V
oc
ot
Pal
LA
TCA
VM
ARC
INF
mtt
STN
SM
PM
MM
LM
SN
cp
PéM
MM
SN

Figure 9: Representative sections of each topographic region of the adult hypothalamus visualized with AChE or stains for calcium-binding proteins. (a-c) Traced maps of hypothalamic nuclei by prosomere and plate of origin from representative sections from each of the three topographical regions of the hypothalamus of rhesus monkey in acetylcholinesterase (AChE; Case AZ). Representative sections from each topographical region of the hypothalamus of adult rhesus monkey alternatively stained for the calcium-binding proteins: (d-f) parvalbumin (PV; Case AZ); (i-l) calbindin (CB; Case AZ); (o-q) calretinin (CR; Case AX). (t-v) Maps of exhaustive plotting of CR neurons (CRmap) in representative sections show the distribution and relative density of CR when compared to PV and CB in the hypothalamus. Large PV+ neurons were found in the (g) STN and (h) MM. In stark contrast, large CB+ neurons were only found in the (m) MM and (n) SCH. (r, s) Small CR+ neurons were only found dispersed between hypothalamic nuclei with a semi-uniform distribution. Calibration bar (2mm) in sections a, d, i, o, and t apply to all sections within corresponding rows at low magnification. Calibration bar (200 μm) in g applies to sections g, h, m, n, r, and s at higher magnification. For color code in traced maps see Figure 1. See list of abbreviations for complete terms.

The distribution of parvalbumin-positive (PV+) and calbindin-positive (CB+) neurons was sparse compared to the distribution of calretinin-positive (CR+) neurons in the adult hypothalamus. A few (< 5) PV+ neurons were found in the medial mamillary nucleus (MM; Fig 9h) near the origin of the mamillothalamic tract (mtt) as well as in the lateral part of the subthalamic nucleus (STN; Fig 9g). No other PV+ neurons were found in the hypothalamus proper, and PV only gave a visual contrast (without specifically staining neurons) to the optic tract (ot) and some portions of p3, including the reticular nucleus (TRN). In stark contrast, and without specifically staining neurons, calbindin (CB) seemed to localize in structures in a way that mirrored that of PV. Sparse collections of CB+ neurons were found within several hypothalamic nuclei, including the medial mamillary (MM; Fig 9m), lateral mamillary (LM), suprachiasmatic (SCH; Fig 9i), and arcuate (ARC) nuclei and the lateral hypothalamic area (LA). Small CB+ neurons

were also found sporadically distributed in the areas between all nuclei and within the preoptic area (POA).

On the other hand, PV+ and CB+ neurons were far outnumbered by CR+ neurons (Fig 9o-q). Although CR+ neurons were much smaller than both PV+ and CB+ neurons, the density of the CR+ neurons rendered the quantity of PV+ and CB+ nearly obsolete given the same sample area. Thus, images of stained sections were used as well as exhaustive mapping to visualize the distribution of calretinin-positive (CR+) neurons in the adult hypothalamus (Fig 9t-v). The distribution of CR+ neurons in the adult hypothalamus was extensive, forming a diffuse matrix of small neurons found both within and between the limits of nearly all hypothalamic nuclei (Fig 9t-v). The labeling used did not differentiate if these neurons were also PV+ and/or CB+ neurons. By qualitative comparison, it is unlikely that CR+ neurons are also PV+ neurons due to the stark difference in appearance of stained sections, but it is plausible that small CB+ neurons may also be CR+ as the two cases had some overlap in stained neuron distribution. There was a noted absence of CR+ neurons in the medial mamillary (MM; Fig 9v), supraoptic (SO; Fig 9t) and suprachiasmatic (SCH; Fig 9t) nuclei, which are all derivatives of hp2.

Reconstruction of adult hypothalamic nuclei in 3D

For a novel view of the developmental ontology of the adult hypothalamus, aligned tracings of each hypothalamic nucleus along with the fornix, the anterior commissure, the POA, and the PTh from Nissl images were reconstructed in 3D (Fig 10 – 11). The colors used in Figures 8 and 9 are used across all figures. This reconstruction of

the adult hypothalamus provided a visual summary of the ontology and topology of each hypothalamic nucleus in its adult positioning. The 3D model demonstrated the spatial relations between nuclei of different hypothalamic prosomeres and plates of origin while illustrating the principles of the Prosomeric Model. Further, the topological relations of the adult hypothalamus as seen in 3D helped to visualize the hp2-POA boundary in greater resolution. The boundaries of the PTh and the course of the fornix were further visualized as landmarks related to nuclei derived from the alar and basal plate parts of hp1 (Fig 10). The 3D reconstruction of the hypothalamus complements the 2D images and maps to understand the spatial relations of adult hypothalamic nuclei by prosomere and plate of origin.

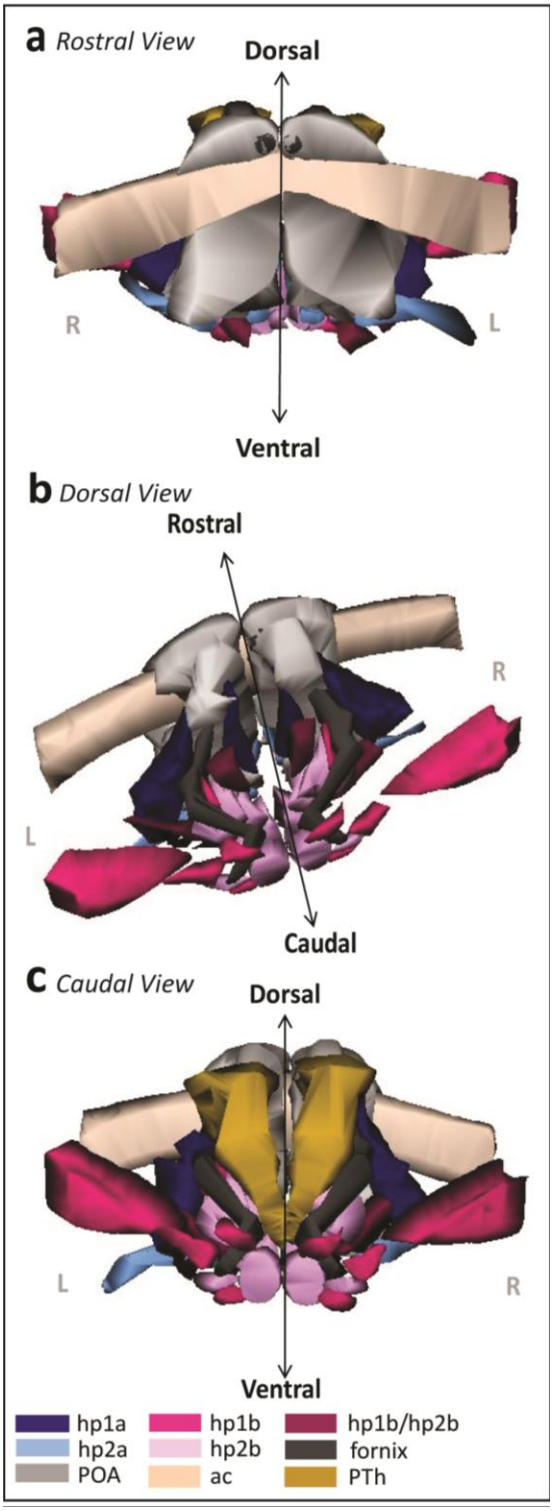

Figure 10: 3D reconstruction of the hypothalamus of the adult rhesus monkey shows developmental origin of anatomical landmarks and nuclei. (a) Rostral view of the adult hypothalamus bound by the anterior commissure (ac) and preoptic area (POA). (b) Oblique-dorsal view looking down into the third ventricle with the anterior commissure, the POA, and the relative spatial positions of alar and basal plate derivatives of hp1 and hp2 nuclei. The fornix (f) courses exclusively through alar and basal plate parts of hp1 until it diverges caudally into the MM. (c) Caudal view of the hypothalamus including prethalamic nuclei (PTh) of the diencephalon. The proposed boundaries of the VMs are not shown as it could not be visualized in any stain used in our analysis. For color code see Figure 1. See list of abbreviations for complete terms.

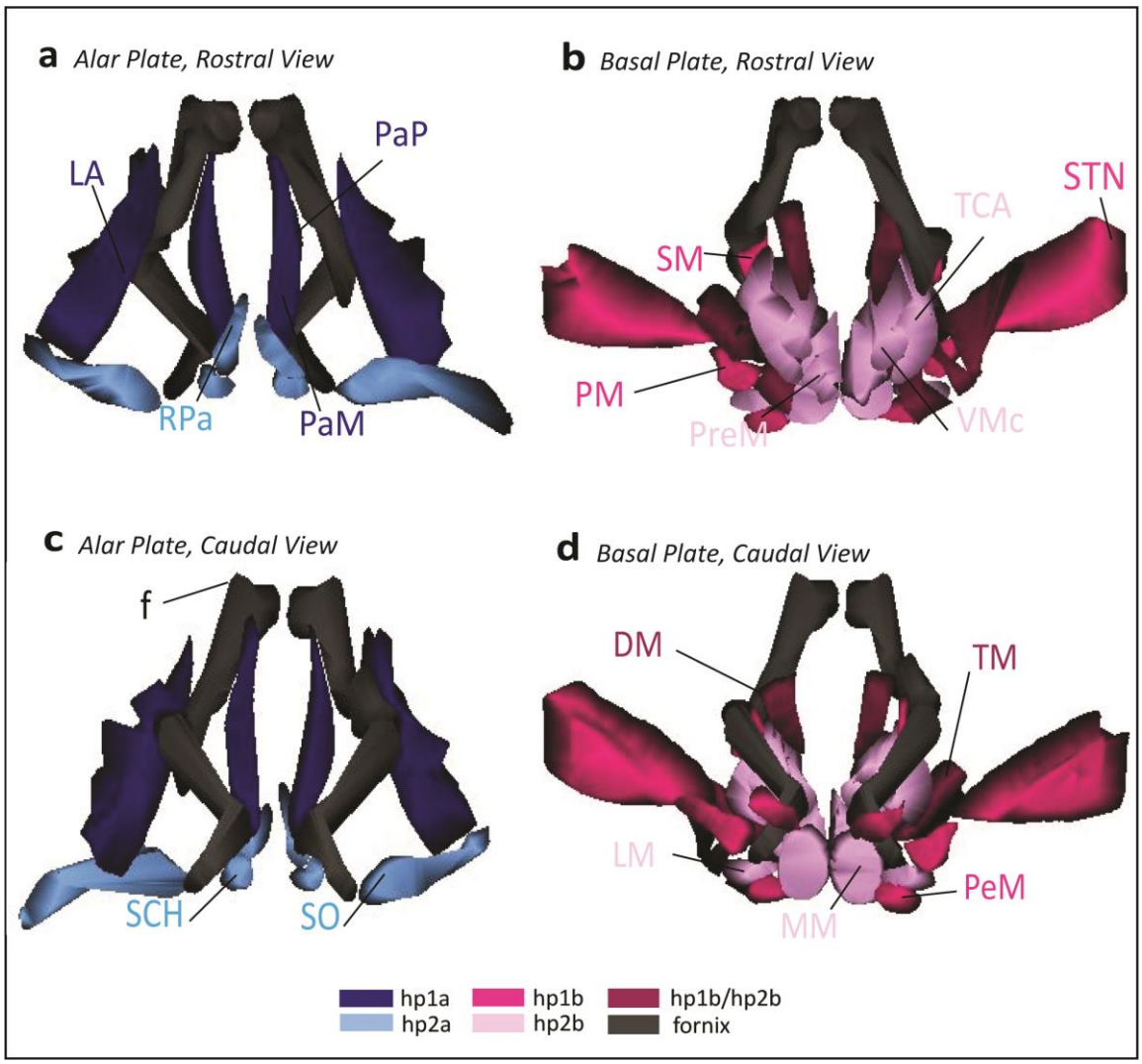

Figure 11: 3D reconstruction of the hypothalamus of the adult rhesus monkey shows developmental origin of nuclei in relation to the fornix. (a, b) Rostral view of adult hypothalamic nuclei derived from alar (a) and basal (b) plate parts of hp1 and hp2 in the rhesus monkey. (c, d) Caudal view of adult hypothalamic nuclei derived from alar (c) and basal (d) plate parts of hp1 and hp2. The proposed boundary of the VMs is not shown as it could not be visualized in any stain used in our analysis. The fornix (f) courses exclusively through alar and basal plate parts of hp1 until it diverges caudally into the MM. For color code see Figure 1. See list of abbreviations for complete terms.

Quantitative topological analysis of projections from hypothalamus to prefrontal cortex

The topological parcellation of hypothalamic nuclei in adult rhesus monkeys was used to reinterpret the distribution of projection neurons from the hypothalamus to all areas of the prefrontal cortex in the adult rhesus monkey. First, sections of the hypothalamus were reassessed for the distribution of retrogradely labeled neurons present within 16 of the 18 parcellated nuclei of the hypothalamus. The distribution, previously examined as a percent of ipsilateral retrogradely labeled neurons for injection sites with HRP-WGA, was described using the Structural Model as a basis for interpreting a pattern of bidirectional connections between each area of the prefrontal cortex and the diverse nuclei of the hypothalamus (Rempel-Clower and Barbas 1998). These data were adapted to this study with the advantage of a developmental basis for ordering the nuclei of the hypothalamus. Importantly, the dorsomedial nucleus (DM) and the tuberomamillary nucleus (TM) were excluded from these data (see explanation below) and included the subthalamic (STN) and premamillary (PreM) nuclei because they were not included at the time of the previous study. Table 5 shows the percent of ipsilateral retrogradely labeled neurons in each case examined sorted by area of injection in the prefrontal cortex, laminar type (Agranular, Dysgranular, Eulaminate I, Eulaminate II, Eulaminate II+), prosomere (hp1, hp2) and plate (alar, basal) of origin.

Table 5. Percent† ipsilateral retrogradely labeled neurons from hypothalamic nuclei to prefrontal cortex by likely prosomere and plate of origin.

		Agranular	Dysgranular					Eulaminate I				
Prosomere	Plate	PAII/Pro	Pro		25	32		11			O12	M9
Case*		AG	MAR	AF	AH	MDQ	AE	MBJ	AM	MFT	MBY	AO
p3	basal	11		25	51		32	28	25		40	13
hp1	alar	15		15	**23**		20	19	22		21	**39**
	basal	**62**		**40**	16		**27**	**34**	**40**		**30**	27
hp2	alar											
	basal	2		2			1				<1	
POA	alar			2			1					3
Total # Neurons		62		48	62		543	251	68		194	94

		Eulaminate II						Eulaminate II+		Premotor	
Prosomere	Plate	V46				D10	D46	D8		6	
Case		MAV	MBH	AA	MFF	SF	AB	AC	AD	MAL	MAO
p3	basal	26	31	27		23	33	40	25	24	
hp1	alar	27	27	3		32	17	9	32	15	**62**
	basal	**39**	**36**	**54**		**33**	**25**	**29**	**33**	**41**	19
hp2	alar										
	basal	2	1								
POA	alar										
Total # Neurons		86	106	37		181	12	92	84	51	27

*Cases are listed in grey.

† Number in each column corresponds to the percentage of retrogradely labeled neurons (HRP-WGA) in the hypothalamus that project to the designated injection site in the prefrontal cortex. Data adapted from (Rempel-Clower and Barbas 1998).

In the present study, several key findings of the previous authors (Rempel-Clower and Barbas 1998) were affirmed. First, the highest shares of neurons were found in nuclei implicated in autonomic functions, as in the lateral hypothalamic area, and extending into several nuclei the caudal hypothalamic region. Labeled neurons were found in nuclei of all three classically defined regions of the hypothalamus that projected to all types of areas of the prefrontal cortex. However, the laminar variation of the cortex does not fully explain the distribution of these labeled neurons in the hypothalamus, as the projections to the prefrontal cortex originating in the hypothalamus do not seem to vary by laminar definition in an obvious way. Rather, all cortical types seemed to receive a significant share of projections if the nuclei of the hypothalamus are parcellated by arbitrary regions according to classical studies. Yet, not all nuclei contained labeled neurons, as would be expected if there were no correlation between nucleus of origin and laminar type of the cortex. Thus, the hypothalamus required an alternative organizational scheme to clarify this discrepancy.

To further analyze this pattern, the percent of neurons found within each nucleus in each case was combined based on the likely developmental origin of each nucleus by prosomere and plate of origin according to the Prosomeric Model. The prethalamic nuclei of p3 and the preoptic area, a derivative of the hp2 alar plate contribution to the subpallium, were separated from the percent published for nuclei derived from the alar and basal plate of hp1 and hp2. Further, data previously collected from the dorsomedial nucleus (DM) and the tuberomamillary nucleus (TM) were excluded from this anlaysis. According to the Prosomeric Model, these nuclei have mixed prosomeric origin, and the

share of neurons contributed from each prosomere could not be distinguished, an issue outside of the scope of this study. The hypothalamic quadrant in each case (hp1a, hp1, hp2a, hp2b) with the highest combined percentage of projection neurons to each area of the prefrontal cortex is bolded (Table 5).

When the percent retrogradely labeled neurons in each case was ordered according both the Structural Model and the Prosomeric Model, a clear pattern of projections emerged. Retrogradely labeled neurons were found almost exclusively within the boundaries of all hypothalamic nuclei derived from the alar and basal plate portion of hp1. Nuclei likely derived from the basal plate portion of hp1 held the predominant share of these neurons. These retrogradely labeled neurons projected to areas of all laminar types of the prefrontal cortex, from the simplest Agranular types to the most complex Eulaminate II+. There was no significant difference between the distribution of projections from these hypothalamic nuclei to the limbic- (Agranular/Dysgranular) or eulaminate-type areas of the prefrontal cortex when analyzed as a combined percentage. Apart from nuclei derived from the hp1 prosomere, the prethalamic nuclei of p3 held the highest percent of retrogradely labeled neurons and projected to all areas of the prefrontal cortex.

Of note, there were almost no labeled neurons found within nuclei derived from the alar or basal plate parts of hp2, and the preoptic area was equally devoid of labeled neurons. Further, the subthalamic nucleus (STN) was the only hypothalamic nucleus likely derived from the basal plate part of hp1 without labeled neurons. The

magnocellular and parvicellular groups of the paraventricular nucleus (PaM/PaP) derived from hp1 alar plate presented in the same way.

Mapping projection neurons from hypothalamus to prefrontal cortex by topology

To visualize the pattern of projection neurons from hypothalamus to different areas of the prefrontal cortex by topology, maps of exhaustive plotting of retrogradely labeled neurons were constructed (Fig 12). Three representative sections (rostral, tuberal/medial, caudal) of the hypothalamus were selected from each of 4 cases that received injections of HRP-WGA from cases used previously (Cases AA, AE, AO, MSF; Rempel-Clower and Barbas 1998) as well as 1 new case with FB (Case BP) injection ("RM"; Table 2). Maps of labeled neurons in hypothalamic nuclei were made from sections of 5 cases with injection sites representing areas of the prefrontal cortex of different cortical types: A25 (Agranular/Dysgranular), A32 (Dysgranular), A9 (Eulaminate I), A10 (Eulaminate I), and A46 (Eulaminate II). Labeled were exhaustively plotted using a marker. Each nucleus of the hypothalamus was then traced over these maps following the color code for likely developmental origin as in Figure 1. An arbitrary boundary was drawn in a dashed line to denote the likely interneuromeric boundaries between the derivatives of p2-p3, p3-hp1, and hp1-hp2.

The maps of retrogradely labeled neurons provided a qualitative supplement to the percentages in Table 6. Each map consistently demonstrated a tendency for projection neurons to each area analyzed to be situated within hypothalamic nuclei derived from the alar and basal plate parts of hp1 or from the diencephalic neuromere p3. The lateral hypothalamic area (LA; Fig 12a, d, h, m) from the alar plate portion of hp1and the

prethalamic nuclei (PTh; Fig 12f, i, o) from p3 showed the strongest clustering of labeled neurons projecting to limbic areas (A25, A32) and eulaminate areas (A10). On the other hand, the paraventricular complex (PaM/PaP; Fig 12a, m) and the subthalamic nucleus (STN; Fig 12c, f, i, l, o) represent two of the largest nuclei of the hypothalamus, but they contained no labeled neurons. Further, nuclei derived from the alar and basal plate part of hp2 were also devoid of labeled neurons. The only exception was the area of the tuber cinereum (TCA; Fig 12b, e, h), which contained 2-3 labeled neurons projecting to limbic areas A25 and A 32 as well as eulaminate area A9. Thus, the topologically based interneuromeric boundaries overlaid on each map seemed to be predictive of projection neuron distribution in the hypothalamus of the adult rhesus monkey.

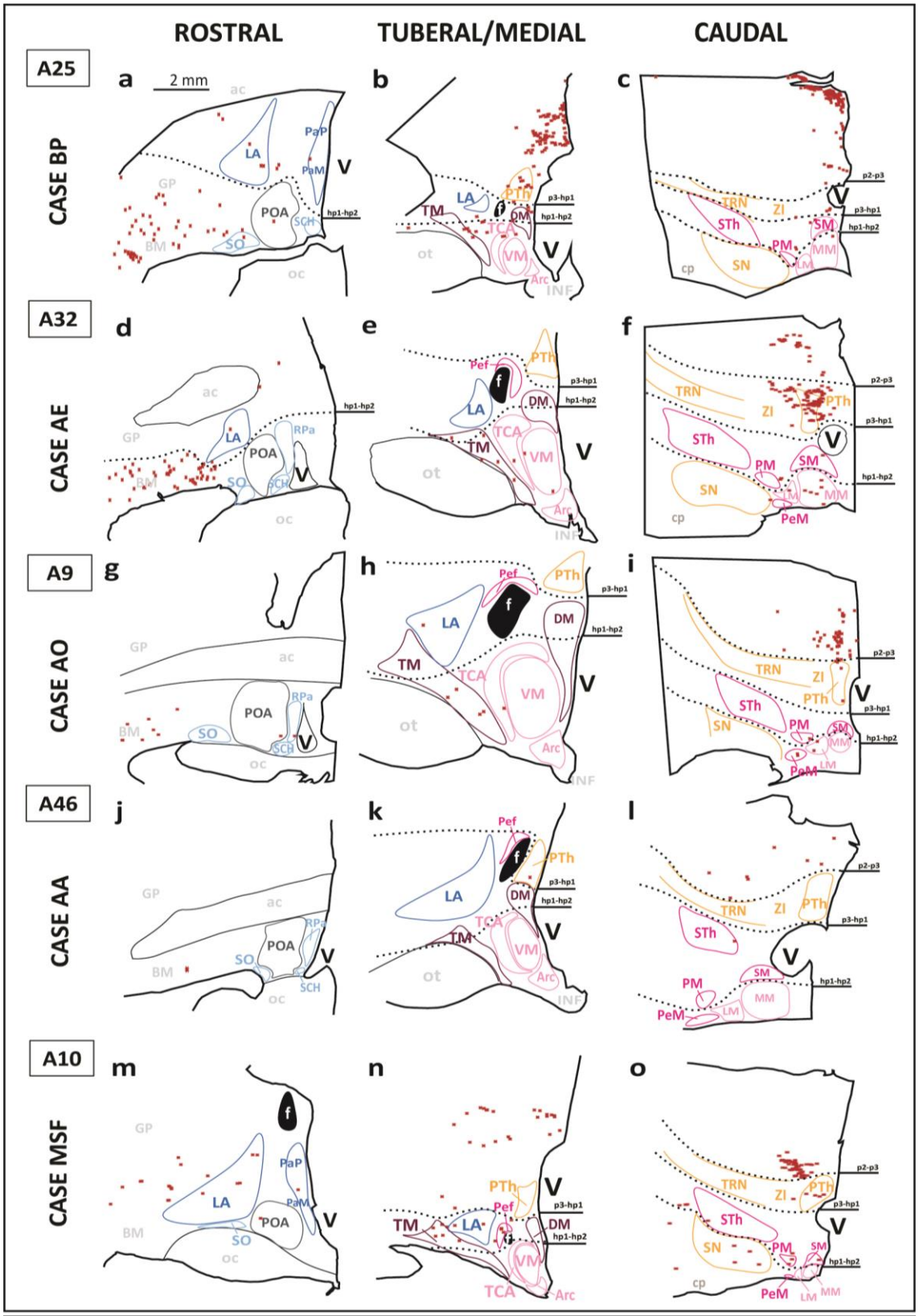
ROSTRAL
TUBERAL/MEDIAL
CAUDAL
A25
CASE BP
A32
CASE AE
A9
CASE AO
A46
CASE AA
A10
CASE MSF
a
b
c
d
e
f
g
h
i
j
k
l
m
n
o
2 mm
ac
GP
BM
oc
ot
cp
INF
LA
PaP
PaM
POA
SCH
SO
RPa
V
f
Pef
PTh
DM
TM
TCA
VM
Arc
TRN
ZI
STh
SN
PM
SM
MM
LM
PeM
p2-p3
p3-hp1
hp1-hp2

Figure 12: Maps of retrogradely labeled neurons in the hypothalamus from limbic and eulaminate areas of the prefrontal cortex in rhesus monkey. Maps of representative coronal sections through the rostral, tuberal/medial, and caudal regions of the hypothalamus of the adult rhesus monkey. Plotted neurons originating in the hypothalamus project to (a-c) A25, (d-f) A32, (g-i) A9, (j-l) A46, and (m-o) A10 of the prefrontal cortex demonstrate clustering patterns within topological boundaries of the derivatives of p2, p3, and hp1 while derivatives of hp2 are largely absent of projection neurons to any area of the prefrontal cortex. Calibration bar (2 mm) applies to all maps a-o. Projection neurons are labeled in red. Architectonic landmarks for hypothalamic boundaries are in light grey. For color code of hypothalamic nuclei see Figure 1. See list of abbreviations for complete terms.

Topological analysis of projections from prefrontal cortex to hypothalamus

The topological parcellation of hypothalamic nuclei in adult rhesus monkeys was used to reinterpret the distribution of labeled projections from all areas of the prefrontal cortex to the hypothalamus in the adult rhesus monkey. First, sections of the hypothalamus were reassessed for the density of ipsilateral anterogradely labeled axons and axon terminals (boutons) present within 16 of the 18 parcellated nuclei of the hypothalamus. The distribution, previously examined using a qualitative scale (+ = light label, ++ = moderate label, +++ = dense label) for injection sites with HRP-WGA and [^{3}H]-tritriated amino acids, was described using the Structural Model as a basis for interpreting a pattern of bidirectional connections between each area of the prefrontal cortex and the diverse nuclei of the hypothalamus (Rempel-Clower and Barbas 1998). These data were adapted to this study with the advantage of a developmental basis for ordering the nuclei of the hypothalamus. Importantly, the dorsomedial nucleus (DM) and the tuberomamillary nucleus (TM) were excluded from these data (see explanation above), and the subthalamic (STN) and premamillary (PreM) nuclei, not included at the

time of the previous study, were added. Table 6 shows the density of ipsilateral anterogradely labeled axons in each case examined sorted by area of injection in the prefrontal cortex and laminar type (Agranular, Dysgranular, Eulaminate I, Eulaminate II, Eulaminate II+).

The present study again affirmed several key findings by the previous authors (Rempel-Clower and Barbas 1998). First, dense anterograde label was found throughout the hypothalamus and within hypothalamic nuclei. The densest label was found in the nucleus most strongly implicated in autonomic functions, the lateral hypothalamic area, and extending into several nuclei in the posterior hypothalamic region. Labeled axons were found in nuclei of all three classically defined regions of the hypothalamus that projected to all types of areas of the prefrontal cortex. Additionally, the projections from the prefrontal cortex originating in the hypothalamus seemed to vary by laminar definition. Projections originating in the limbic areas (Agranular/Dysgranular type) of the prefrontal cortex were moderate to dense, while projections from eulaminate areas were light to absent in the hypothalamus. Still, not all nuclei contained the same relative density of labeled axons from either limbic or eulaminate areas of the prefrontal cortex, as would be expected if there were no correlation between laminar type of the cortex and each nucleus. Thus, the hypothalamus required an alternative organizational scheme to clarify this point.

Table 6. Density† of ipsilateral anterogradely labeled axons to prefrontal cortex to hypothalamic nuclei by likely prosomere and plate of origin.

			Agranular	Dysgranular					Eulaminate I				
Prosomere			PAII/Pro	Pro		25	32		11			O12	M9
Case*	Plate	Nucleus	AG	MAR	AF	AH	MDQ	AE	MBJ	AM	MFT	MBY	AO
p3	basal	PA		(++)	(++)	(+)	(+)	(+++)	(+)	(+)	(+)	(++)	
		DA		(++)	(++)	(++)	(+)	(+++)	(++)	(++)	(++)	(++)	
hp1	alar	LA	**(+)**	**(+++)**	**(+++)**	**(++)**	**(+)**	**(+++)**	**(++)**	**(++)**	**(++)**	**(++)**	
		PaP											
		PaM											
	basal	Pef		**(++)**	**(++)**	**(+)**	**(+)**	**(+++)**	**(+)**	**(+)**	**(+)**	**(+)**	
		SM	**(+)**	**(++)**	**(+++)**	**(+)**	**(+)**	**(++)**	**(+)**	**(+)**	**(+)**	**(++)**	
		PeM											
		PM	**(++)**	**(++)**	**(+++)**	**(+)**	**(+)**	**(++)**	**(++)**	**(+)**	**(+)**	**(++)**	
		STN	**(+)**		**(++)**	**(+)**		**(+++)**		**(++)**	**(+)**	**(+)**	
hp2	alar	SCH											
		RPa											
		SO											
	basal	TCA											
		ARC											
		PreM											
		VM											
		LM		**(+)**	**(++)**			**(++)**		**(+)**		**(+)**	
		MM			**(++)**			**(++)**		**(++)**		**(+)**	
POA	alar	AA				(+)		(++)	(+)	(+)	(+)	(+)	

			Eulaminate II						Eulaminate II+		Premotor	
Prosomere			V46				D10	D46	D8		6	
Case	Plate	Nucleus	MAV	MBH	AA	MFF	SF	AB	AC	AD	MAL	MAO
p3	basal	PA	(+)				(+)		(+)			
		DA	(+)	(+)			(+)				(+)	
hp1	alar	LA	**(+)**	**(+)**			**(+)**		**(+)**		**(+)**	
		PaP										
		PaM										
	basal	Pef					**(+)**		**(+)**			
		SM	**(+)**				**(+)**					
		PeM										
		PM	**(+)**				**(+)**					
		STN					**(+)**					
hp2	alar	SCH										
		RPa										
		SO										
	basal	TCA										
		ARC										
		PreM										
		VM										
		LM	**(+)**						**(+)**		**(+)**	
		MM							**(+)**			
POA	alar	AA									(+)	

*Cases are listed in grey.

† Number in each column corresponds to the density of anterogradely labeled neurons (HRP-WGA) in the hypothalamus that project from the designated injection site in the prefrontal cortex to the hypothalamus. Data adapted from (Rempel-Clower and Barbas 1998).

To further analyze this pattern, the scored densities of labeled axons found within each nucleus was ordered by case based on the likely developmental origin of each nucleus by prosomere and plate of origin according to the Prosomeric Model. Further, the prethalamic nuclei (PTh) of p3 and the anterior hypothalamic area (AA) of the preoptic area (POA), a derivative of the hp2 alar plate contribution to the subpallium, were separated from the data previously collected for nuclei derived from the alar and basal plate of hp1 and hp2. Further, data from the dorsomedial nucleus (DM) and the tuberomamillary nucleus (TM) were excluded as these nuclei have mixed prosomeric origin, and the share of labeled axons projecting to each prosomere could not be determined. The data for each nucleus derived from hypothalamic quadrants (hp1a, hp1, hp2a, hp2b) with labeled axons were bolded for clarity (Table 6).

A topological parcellation of projections from the prefrontal cortex to hypothalamic nuclei revealed a clear pattern. As with retrogradely labeled neurons, anterogradely labeled axons were found almost exclusively within the boundaries of all hypothalamic nuclei derived from the alar and basal plate portion of hp1. Nuclei likely derived from the basal plate portion of hp1 held the predominant share of labeled axons. These projections originated predominantly from limbic areas (Agranular/Dysgranular) of the prefrontal cortex with a graded decrease in density in from Eulaminate I to Eulaminate II+ areas. Apart from nuclei derived from the hp1 prosomere, the prethalamic nuclei (PTh) of p3 held the highest density of anterogradely labeled axons. Of note, the subthalamic nucleus (STN) received light to moderate projections predominantly from

the limbic areas (Agranular/Dysgranular), a stark contrast from the lack of retrogradely labeled neurons.

Of note, there were negligible anterogradely labeled axons found within nuclei derived from the alar or basal plate parts of hp2, and anterior hypothalamic area (AA) within the preoptic area (POA) was absent of label. The magnocellular and parvicellular groups of the paraventricular nucleus (PaM/PaP) derived from hp1 alar plate presented in the same way.

Mapping labeled axons from prefrontal cortex to hypothalamus by topology

To visualize the pattern of projections from the prefrontal cortex to the nuclei of the hypothalamus by topology, maps were constructed using exhaustive plotting to visualize anterogradely labeled axons (Fig 13). Three representative sections (rostral, tuberal/medial, caudal) of the hypothalamus from each of 6 new cases that received injections of BDA [Cases BC, BG (left and right injections), BH, BR, AY] as well as 1 new case with FR (Case BQ) injection ("AM"; Table 2). Maps of labeled axons with or without axon terminals (boutons) in the hypothalamus were made from sections of 5 cases with injection sites representing areas of the prefrontal cortex of different cortical types: A25 (Agranular/Dysgranular), A32 (Dysgranular), A9 (Eulaminate I), A10 (Eulaminate I), and A46 (Eulaminate II). Maps for two cases [BQ, BG (right injection)] are not included in Figure 13 as they were like other cases for projections from limbic areas. The course of each labeled axon was plotted using a line representing each axon, but not necessarily the thickness of each axon. Each nucleus of the hypothalamus was traced over these maps and follow the color code for likely developmental origin as in

Figure 1. An arbitrary boundary was drawn in a dashed line to denote the likely interneuromeric boundaries between the derivatives of p2-p3, p3-hp1, and hp1-hp2.

The maps of anterogradely labeled neurons provided a qualitative supplement to the percentages in Table 7. Each map consistently demonstrated a strong bias for labeled axons projecting from the limbic areas (A25, A32) to nearly all nuclei of the hypothalamus. There was a clear contrast, rather than a graded change, between the density of projections originating from limbic areas (Fig 13a-f) and eulaminate areas (Fig 13g-o) of the prefrontal cortex. Further, projections from the limbic areas tended to cluster among hypothalamic nuclei derived from the alar and basal plate parts of hp1 or from the diencephalic neuromere p3. The lateral hypothalamic area (LA; Fig 13a, m) from the alar plate portion of hp1and the prethalamic nuclei (PTh; Fig 13c, f, i, l o) of p3 showed the highest density of labeled axons projecting from limbic areas A25 and A32. In particular, the axons coursed towards, but abstained from crossing, the arbitrary interneuromeric boundaries between p3-hp1 and hp1-hp2 traced in each map. On the other hand, projections from all areas of the prefrontal cortex coursed around the nuclei of the paraventricular complex (PaP/PaM; Fig 13a), a derivative of the alar plate part of hp1, as well as the supraoptic (SO), suprachiasmatic (SCH), and rostral paraventricular (RPa) nuclei, all derivatives of the alar plate part of hp2 (Fig 13a, d, g, j, m).

The pattern of projections strictly adhered to the topological boundaries drawn between prosomeres. There was a diffuse pattern of axons with axon terminals among the derivatives of p3 and hp1, and there was paucity of axons below the hp1-hp2 boundary. The exception to this rule was the ventromedial nucleus (VM; Fig 13 b, e), which

received projections from both A25 (ventrally; Fig 13b) and A32 (dorsally; Fig 13e) within its limits. Thus, the topologically based interneuromeric boundaries overlaid on each map seemed to be predictive of projection neuron distribution in the hypothalamus of the adult rhesus monkey.

By comparison, there were no projections from eulaminate-type areas of the prefrontal cortex to the any nucleus of the hypothalamus (Fig 13g-o). Of the labeled axons present, there were no labeled axon terminals (boutons), indicating that these axons were likely passing through rather than projecting to the hypothalamus. Further, nuclei derived from the alar and basal plate part of hp2 were also devoid of projections from the prefrontal cortex of any laminar type.

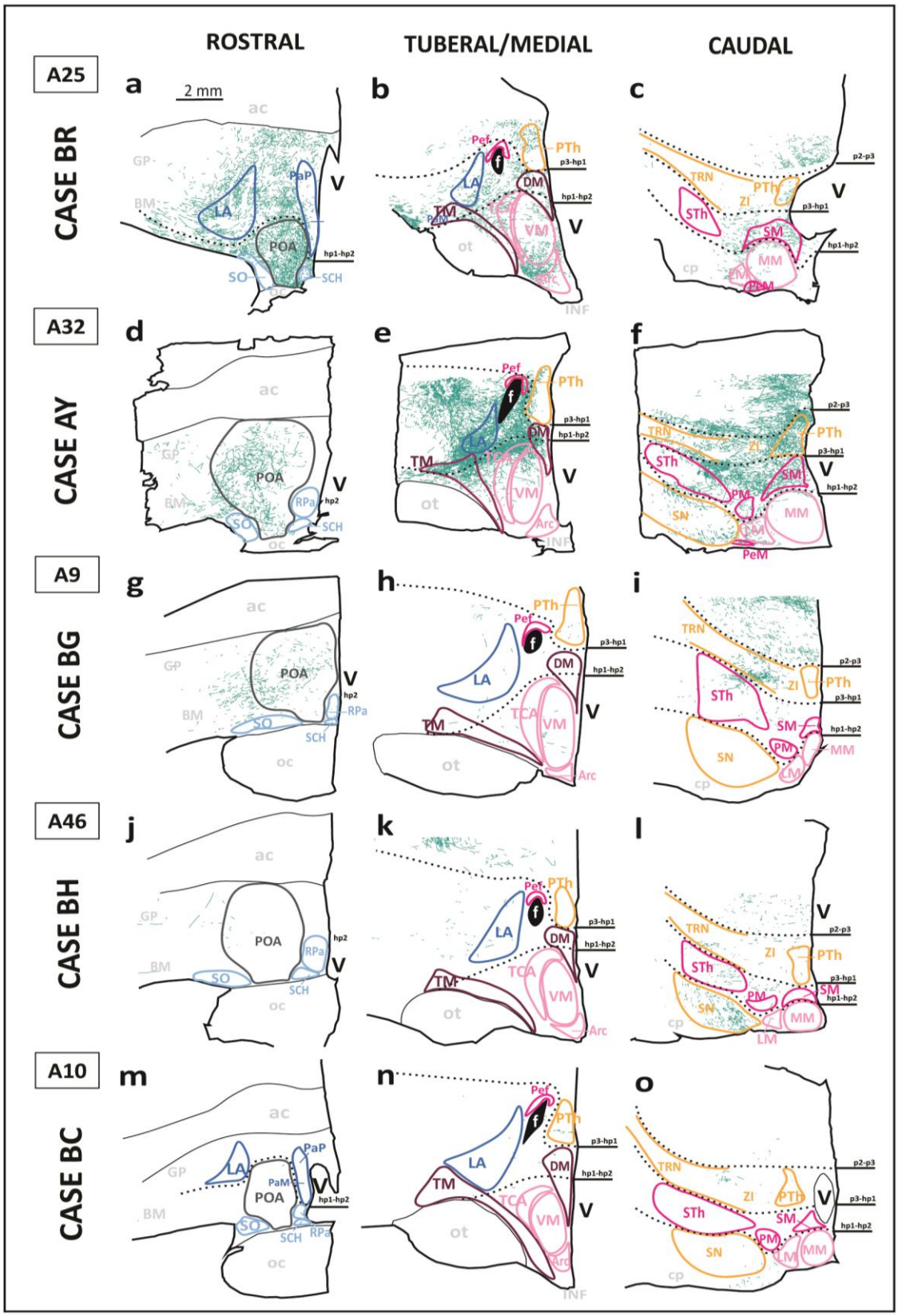
ROSTRAL
TUBERAL/MEDIAL
CAUDAL
A25
CASE BR
A32
CASE AY
A9
CASE BG
A46
CASE BH
A10
CASE BC
a
b
c
d
e
f
g
h
i
j
k
l
m
n
o
2 mm
ac
GP
BM
LA
PaP
POA
V
hp1-hp2
SO
SCH
oc
Pef
PTh
p3-hp1
DM
TM
PaM
VM
ot
TC
INF
p2-p3
TRN
ZI
STh
SM
MM
cp
PM
PeM
RPa
hp2
TCA
Arc
SN
LM

Figure 13: Maps of anterogradely labeled axons in the hypothalamus from limbic and eulaminate areas of the prefrontal cortex in rhesus monkey. Maps of representative coronal sections through the rostral, tuberal/medial, and caudal regions of the hypothalamus of the adult rhesus monkey. Plotted axons originating in the prefrontal cortex project from (a-c) A25, (d-f) A32, (g-i) A9, (j-l) A46, and (m-o) A10 of the prefrontal cortex demonstrate clustering patterns within topological boundaries of the derivatives of p2, p3, and hp1. There is also a strident difference between the density of projections from limbic areas (A25, A32) when compared to eulaminate areas (A9, A46, A10) to all parts of the hypothalamus. Calibration bar (2 mm) applies to all maps a-o. Projection axons are labeled in teal. Architectonic landmarks for hypothalamic boundaries are in light grey. For color code of hypothalamic nuclei see Figure 1. See list of abbreviations for complete terms.

Bouton diameter analysis of projections from limbic areas to hypothalamus

The analysis of anterogradely labeled axons from the prefrontal cortex to the hypothalamus revealed that projections from the limbic areas (A25, A32) were in significant density compared to projections from eulaminate areas (A46, A10, A9). Further, projections from the limbic areas were the only projections to indicate synaptic activity by the presence of labeled axon terminals (boutons). Thus, sample areas of boutons from representative nuclei of each hypothalamic prosomere and plate of origin were analyzed to determine the relative strength of connections from the limbic areas terminating in the hypothalamus. Sampled areas were selected from the lateral hypothalamic area (LA; hp1a), the supramamillary nucleus (SM; hp1b), the rostral paraventricular nucleus (RPa; hp2a), the ventromedial nucleus (VM; hp2b), the preoptic area (POA; SPal), and the zona incerta (ZI; p3) as projections to the prethalamic nuclei of p3 were too dense for bouton analysis.

Briefly, images were captured through the thickness of the section representative sections of the hypothalamus from two cases with injctions into A25 (Case BR) and A32

(Case AY). One sample area for each nucleus was selected from each case and captured a series of images at 1000X magnification at bright-field using an oil-immersion lens, rendering approximately 25-30 images per sample area. These images were overlaid and condensed into a single Z-stack image, and the limits of the boutons visible within each sample area were then manually traced. A Feret's diameter was calculated for each bouton, representing the longest distance across a traced area from a perimeter-based macro designed for this purpose (Reconstruct ™). The number (N) of boutons and the mean bouton diameter (MBD) for each sample was determined, and an Independent T-Test of Means was conducted to determine if there was a statistically significant difference between the MBD of boutons from projections originating in A25 and A32. The bouton Feret's diameter was operationalized as an indicator of the relative synaptic strength of connections, with a larger bouton diameter representing a stronger connection.

Table 7 provides a summary of descriptive statistics analyzed to determine the relative strength of connections from limbic areas of the prefrontal cortex to the representative nuclei of each hypothalamic quadrant. Several quantitative measures were calculated to provide a basis for comparison between nuclei from different prosomeres and plate of origin. The number (N) of labeled boutons from A25 or A32 in each sample area within a given nucleus was determined. There were significantly more labeled boutons present in any sample originating from A25 when compared to samples of projections from A32. Further, the mean bouton diameter (MBD) of labeled boutons from each sample was greater in projections from A25 than A32 for most sampled nuclei [LA ($p < 0.007$); SM ($p < 0.005$); RPa ($p < 0.00003$); POA ($p < 0.00002$)].

There were two exceptions found to this pattern. One of these was the ventromedial nucleus (VM), for which there was no statistically significant difference between MBD for projections from A25 and A32 [VM ($p \geq 0.292$)]. Another was the zona incerta (ZI), a likely derivative of p3, for which the MBD was greater for boutons projecting from A32 than A25 [ZI ($p < 0.000001$)].

Table 7. Summary of descriptive statistics for bouton analysis.

Origin	Nucleus	N (A25)	N (A32)	MBD (A25)	MBD (A32)	Mean Difference†	CI (95%)	p
hp1a	LA	1517	667	1.03	0.98	0.06	[0.01, 0.10]	< 0.007
hp1b	SM	416	506	0.94	0.86	0.08	[0.02, 0.13]	< 0.005
hp2a	RPa	2324	133	0.91	0.77	0.14	[0.08, 0.21]	< 0.00003
hp2b	VM*	99	186	1.17	1.10	0.07	[-0.06, 0.20]	≥ 0.292
p3	ZI**	1049	528	0.80	1.00	-0.20	[-0.24, -0.16]	< 0.000001
SPal	POA	1866	512	0.86	0.79	0.07	[0.04, 0.11]	< 0.00002

† Mean difference was calculated from a 2-tailed Independent T-Test of means between MBD of A25 and A32.
* There was no significant difference between projection strength from A25 and A32 to VM.
** ZI received a stronger projection to derivatives of p3 from A32 than A25.

The Feret's diameter of boutons was further analyzed using qualitative measures. Briefly, Feret's diameters from each sample were binned into standardized ranges (0.2 μm increment) and plotted to visualize the relative density and size of boutons present on the axons projecting from A25 or A32 to distinct derivatives of the hypothalamus. Figure 14 shows the Z-stack images of each sample analyzed as well as an adjacent bar chart with the total number of boutons analyzed and the distribution of Feret's diameters for all boutons.

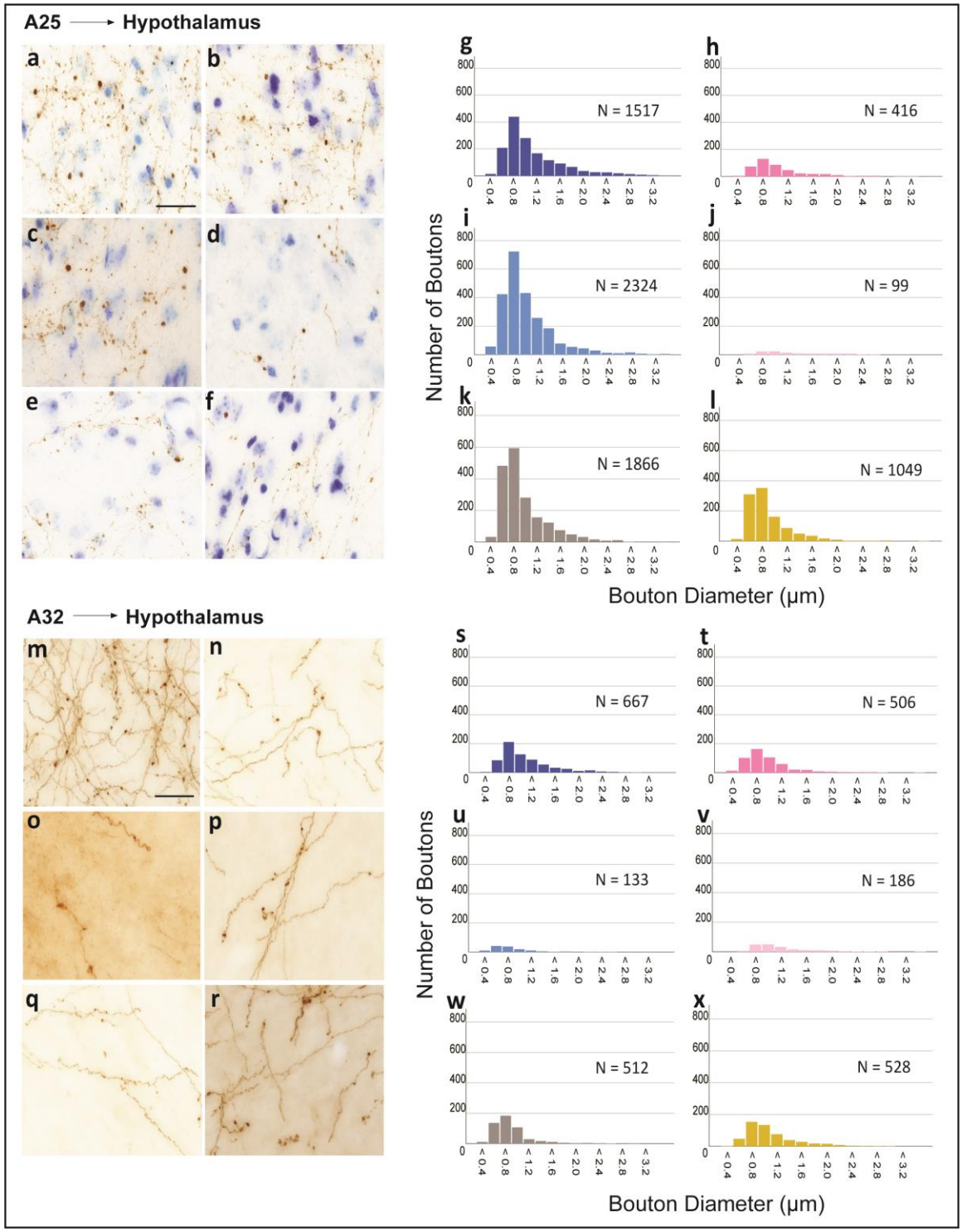
A25 → Hypothalamus
a
b
c
d
e
f
g
h
i
j
k
l
N = 1517
N = 416
N = 2324
N = 99
N = 1866
N = 1049
Number of Boutons
Bouton Diameter (μm)
A32 → Hypothalamus
m
n
o
p
q
r
s
t
u
v
w
x
N = 667
N = 506
N = 133
N = 186
N = 512
N = 528
Number of Boutons
Bouton Diameter (μm)

Figure 14: Bouton diameter analysis shows significant difference in quantity and strength of connections from A25 and A32 to hypothalamic nuclei. (a-f) Z-stack images of sample areas of BDA-labeled boutons (Case BR) in hypothalamic nuclei from projections originating in A25 of the prefrontal cortex [(a) LA, (b) SM, (c), RPa, (d) VM, (e) POA, (f) ZI]. Calibration bar in a (20 µm) applies to a-f. (g-l) Corresponding bar plots of Feret's diameters for labeled boutons in each hypothalamic nucleus [(g) LA, (h) SM, (i), RPa, (j) VM, (k) POA, (l) ZI]. (m-r) Z-stack images of sample areas of BDA-labeled boutons (Case AY) in hypothalamic nuclei from projections originating in A32 of the prefrontal cortex [(m) LA, (n) SM, (o), RPa, (p) VM, (q) POA, (r) ZI]. Calibration bar in a (20 µm) applies to m-r. (s-x) Corresponding bar plots of Feret's diameters for labeled boutons in each hypothalamic nucleus [(s) LA, (t) SM, (u), RPa, (v) VM, (w) POA, (x) ZI]. For bar plots, the x-axis represents the bin range for bouton diameter (µm) and the y-axis represents the quantity of bouton diameters within each range. For color code of bar plots, see Figure 1.

The distribution of bouton diameters was uniform across all nuclei and right skewed (mean > mode), with a typical median around bouton diameters less than 0.8 µm (Fig 14). The density of labeled boutons originating in A25 (Fig 14g-l) was significantly greater than those originating in A32 (Fig 14s-x) apart from the exceptions previously described. Further, projections from A25 were biased to terminate within the limits of the derivatives of the alar and basal parts of hp1, but only the alar plate part of hp2 (Fig 14g-i). In contrast, projections from A32 did not show such strident preference, with only a marginal bias towards the derivatives of hp1 (Fig 14s, t). There was a relative paucity of labeled boutons in derivative of the basal plate part of hp2 from both A25 (Fig 14j) and A32 (Fig 14v). The density of boutons from both A25 and A32 to the POA (Fig 14k, w) and the ZI (Fig 14l, x) were comparable to projections to the derivatives of hp1 in each case.

DISCUSSION

The Prosomeric Model provides a novel framework that explains the patterning and development of the central nervous system as a Bauplan across vertebrates (Rubenstein et al. 1994; Puelles and Rubenstein 2003; Puelles 2018; Nieuwenhuys and Puelles 2016). The principles of the Prosomeric Model were applied to a topological analysis of architectonic landmarks to trace adult hypothalamic nuclei to their likely developmental origin in rhesus monkeys, as summarized in Figure 15. This analysis relied on tracing distinct hypothalamic nuclei to their respective progenitor plate and neuromere of origin by assuming homology across species, and was guided by prominent homologous architectural landmarks (Puelles et al. 2012). This analysis rendered a visual summary of likely adult hypothalamic derivatives in a 2D and 3D atlas, which was then used to analyze the connections between the hypothalamus and its supposed immediate successor in neurodevelopment, the prefrontal cortex.

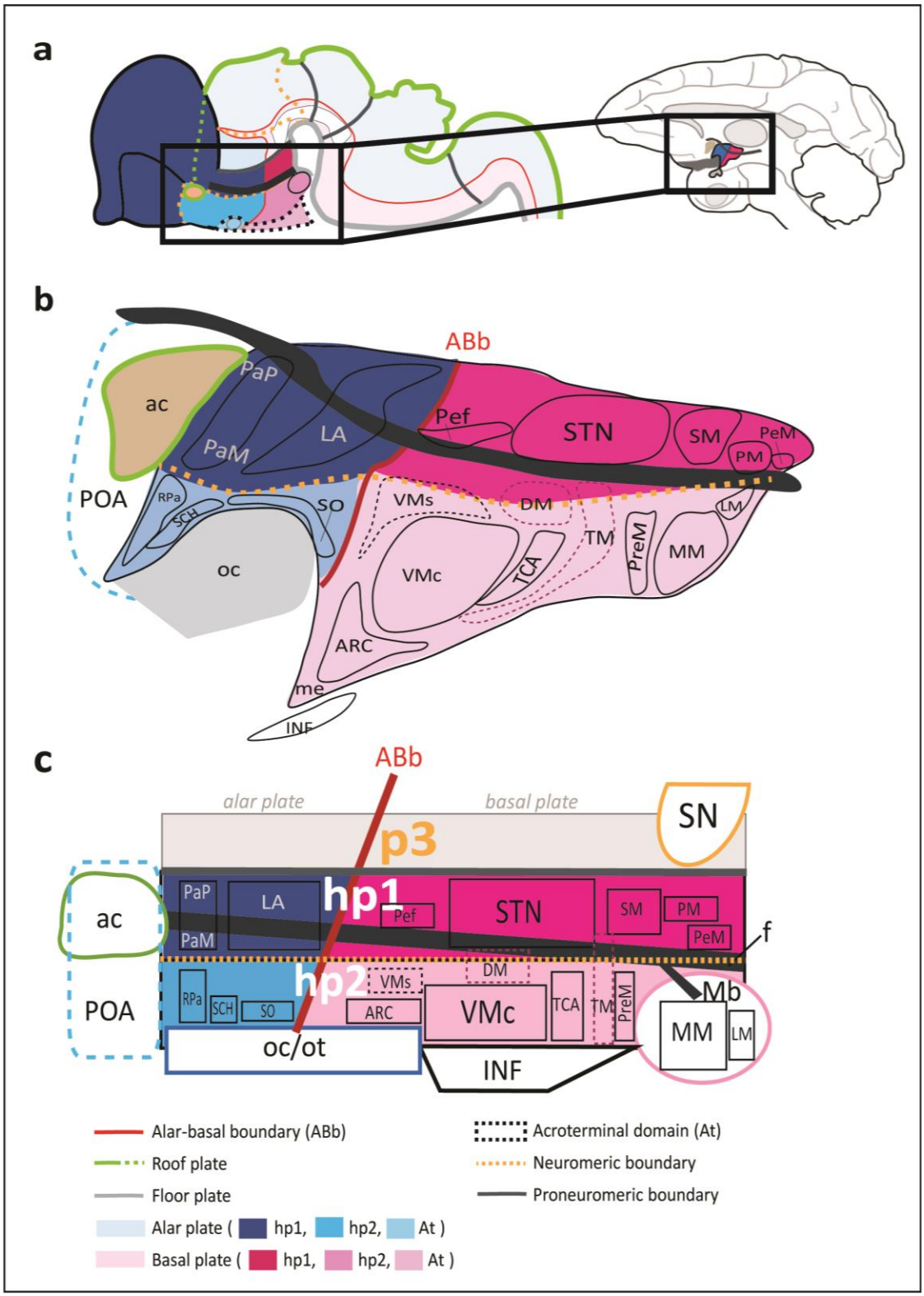
a
b
ABb
PaP
ac
LA
Pef
STN
SM
PeM
PM
PaM
POA
RPa
SCH
SO
VMs
DM
LM
TM
PreM
MM
oc
VMc
TCA
ARC
me
INF
c
ABb
alar plate
basal plate
SN
p3
hp1
PaP
LA
Pef
STN
SM
PM
PeM
f
ac
PaM
hp2
VMs
DM
RPa
SCH
SO
ARC
VMc
TCA
TM
PreM
Mb
POA
oc/ot
MM
LM
INF
Alar-basal boundary (ABb)
Acroterminal domain (At)
Roof plate
Neuromeric boundary
Floor plate
Proneuromeric boundary
Alar plate (hp1, hp2, At)
Basal plate (hp1, hp2, At)

Figure 15: Schematic summary of architectonic boundaries and hypothalamic nuclei in the adult rhesus monkey by likely prosomere and plate of origin. (a) Developmental origin of adult hypothalamic nuclei in the rhesus monkey as predicted by the Prosomeric Model (Puelles et al. 2012; Puelles and Rubenstein 2015). Architectonic boundaries of the adult hypothalamus in the rhesus monkey are illustrated by relative invariant position (topology) in relation to each hypothalamic prosomere (hp1, hp2, acroterminal domain) and plate of origin (alar and basal plate). Theoretical boundaries of adult hypothalamic nuclei are traced over their likely prosomere(s) and plate of origin. (b) Sketch of architectonic landmarks and nuclear boundaries of the adult hypothalamus in rhesus monkeys with corresponding developmental origin as predicted by the prosomeric model. (c) Technical schematic of architectonic landmarks and nuclear parcellation of the hypothalamus in the adult rhesus monkey by developmental origin. Proposed boundaries with uncertain boundaries or mixed migratory patterns from both hp1 and hp2 are shown in a dashed line. For color code see Figure 1. See list of abbreviations for complete terms.

Prosomeric topology differs from classical topography

The analysis of prosomeric topology of the hypothalamus resulted in key differences with some aspects of classical parcellations in the rhesus monkey [e.g., Nauta and Haymaker (1969)]. First, some nuclei included in our atlas were not included in the hypothalamus traditionally (Puelles et al. 2012; Puelles and Rubenstein 2015; Ferran et al. 2015). For example, the subthalamic nucleus (STN) was classically defined as a component of the ventral thalamus in the rhesus monkey (Whittier and Mettler 1949), but new genetic and molecular data have ascribed this nucleus to the hypothalamus (Puelles et al. 2012). Its “wing” positioning and connections with the basal ganglia suggest it may have a distinct functional role from other basal plate nuclei of hp1 (Hashimoto et al. 2003; Puelles et al. 2012; Haynes and Haber 2013). Similarly, the “anterior hypothalamic area” was reassigned to the preoptic area (POA) in accord with the Prosomeric Model (Puelles et al. 2012), and by its separation from the hypothalamus in rhesus monkeys (Bleier 1984; Rempel-Clower and Barbas 1998). The exclusion of the POA from the

hypothalamus proper is further supported by molecular data for inclusion instead with the telencephalic subpallium (Puelles and Rubenstein 2015; Puelles et al. 2016).

On the other hand, the classical parcellation in mice and primates of dorsal and rostral boundaries of the adult hypothalamus was blurred by three classically defined "areas" (Bleier 1984; Rempel-Clower and Barbas 1998; Puelles et al. 2012). Nauta included the dorsal and posterior areas to the hypothalamus to give topographical meaning to a space between a gross dorsal boundary, the *hypothalamic sulcus*, and prominent nuclei of the tuberal and medial hypothalamus (Nauta and Haymaker 1969). With recent genetic and molecular data, the dorsal and posterior hypothalamic areas are now regarded as "prethalamic nuclei" (PTh) derived from neuromere p3 (Puelles et al. 2012). As shown here, the stain WFA established a more refined dorsal boundary between p3 and the nuclei of the alar and basal parts of hp1 in adult rhesus monkeys. Some PTh neurons likely contribute to the thalamic dopaminergic system with other p3 derived structures in rhesus monkeys (Sánchez-González et al. 2005; García-Cabezas et al. 2009). The reassignment of the PTh to p3 may thus connect topological and physiological evidence to distinguish adult diencephalic derivatives from hypothalamo-telencephalic derivatives.

A topological analysis of the structure and limits of the hypothalamus in adult rhesus monkeys required necessary considerations for what is considered ontologically "hypothalamic". The inclusion or reassignment of conventional hypothalamic nuclei into by developmental topology may elucidate organizing principles for their involvement in diverse neural circuits.

Some tuberal and medial hypothalamic nuclei have complex developmental origins

The tuberomamillary nucleus (TM), the core and shell parts of the ventromedial nucleus (VMc/VMs), and the dorsomedial nucleus (DM) presented non-trivial challenges to tracing topological boundaries. Developmental evidence in mice has shown complex migratory patterns from progenitor sites to the adult positioning for these three nuclei (Puelles et al. 2012). Architectonic descriptions of the TM in humans, rats, and rhesus monkeys contain discrepancies when defining one or more nuclear substructures, suggesting that the TM may exist as a complex (Rempel-Clower and Barbas 1998).

Similarly, at least three distinct nuclei likely make up the VMc while a fourth forms the VMs in mice (Puelles et al. 2012; Puelles and Rubenstein 2015). While the architectonic boundary of the VMc is prominent in adult rhesus monkeys, a VMs was not visualized with architectonic methods but relied on topological boundaries based on its likely homologue in adult mice. However, it is possible that in primates the VMs follows a different migratory pattern than the VMc or is even absorbed within the boundaries of VMc (Puelles et al. 2012). Similarly, recent genoarchitectural data suggest that the DM is also a nuclear complex from basal hp1 and hp2 (Puelles et al. 2012). Here, topological boundaries were proposed for the VMs, the DM, and the TM with hp1-hp2 boundaries, but boundaries for constituent nuclei of the VMc could not be visualized. Further, the VMs could not be visualized for any subsequent analyses.

Thus, nuclei with complex migratory pathways require further study using to confirm the existence of subpopulations of neurons in the adult rhesus monkey. A

genoarchitectural study of the ventromedial, dorsomedial and tuberomamillary nuclei may allow for a refined parcellation of these nuclei based on their development.

Alternative stains may indicate plasticity in adult hypothalamus

The architecture of prominent hypothalamic nuclei in monkeys was previously studied with a variety of stains [reviewed in (Rempel-Clower and Barbas 1998)]. The addition of stains beyond AChE and Nissl provided little additional assistance in our hypothalamic parcellation (Fig 8-9). Besides the noted exception of WFA, calretinin (CR) broadly stained small neurons within and between hypothalamic nuclei. The relative paucity of label in the hypothalamus with other markers stands in contrast to the surrounding non-hypothalamic structures and tracts, including the globus pallidus, ventral pallidum, thalamus, or reticular nucleus.

The relative lack of staining of the hypothalamus may highlight similarities between the adult hypothalamus and the developing brain for plasticity over a lifetime (Ramón y Cajal 1904a, b; Nauta and Haymaker 1969). The hypothalamus lacks architectonic characteristics traditionally understood to reflect the structural stability seen in other brain regions (Garcia-Cabezas et al. 2019; Garcia-Cabezas et al. 2017; De Luca and Papa 2017, 2016), including WFA (Mueller et al. 2016; Bozzelli et al. 2018), SMI-32 (Louis et al. 2012), and myelin (Garcia-Cabezas et al. 2019; Nauta and Haymaker 1969). The paucity of myelin in the hypothalamus suggests retained plasticity throughout life, as suggested by the distribution of markers associated with the plasticity-stability continuum in the prefrontal cortex (Garcia-Cabezas et al. 2017). This pattern was first described by Cajal by recently born cats and rats (Ramón y Cajal 1904b, p. 696, 715-753), who

hypothesized that the relative paucity of myelinated axons in the postnatal hypothalamus, likely meant that the structure and connections of the hypothalamus were in flux much later than the surrounding myelinated brain regions. This study provided the adult corollary to Cajal's hypothesis, demonstrating that the hypothalamus is also largely devoid of myelin in adult rhesus monkeys.

There are significant indicators of continued plasticity of the hypothalamus in adult rhesus monkeys that may impact state-dependent dynamics of hypothalamic function. Both classical and modern lines of evidence call for further study the plastic properties of both inter- and intra-hypothalamic signaling, and how the structural properties of the hypothalamus might be altered by changes in homeostatic dynamics to facilitate changes in signaling.

Anatomic hypothalamic pathways vary by systematic variation of the prefrontal cortex

Can the Structural Model provide a causal and topologically consistent explanation for patterns in adult neural circuitry of the primate hypothalamus? Pathways that connect the hypothalamus with the prefrontal cortex are associated with high cognitive functions including working memory and emotional regulation (Schwartz and Goldman-Rakic 1990; Barbas 1993; van Eerdenburg and Rakic 1994; Barbas 2007; Barbas et al. 2018). A systematic relationship in the connections between prefrontal cortices and the hypothalamus has been previously described that is in accord with a Structural Model, which relates cortical connections to the graded laminar architecture of the cortex (Barbas and Rempel-Clower 1997; Rempel-Clower and Barbas 1998). The

phylogenetically ancient limbic prefrontal cortical areas have the densest and uniquely bidirectional connections with the hypothalamus. This study demonstrated that the limbic areas have considerable strength in connections with hypothalamic nuclei with relatively large boutons, a proposed indicator of synaptic strength (Meyer et al. 2014; Xie et al. 2017; Rollenhagen et al 2018; Santuy et al. 2018). In contrast, the relatively complex eulaminate areas, which are uniquely complex in primates, lack direct pathways to the hypothalamus (García-cabezas et al. 2019). Further, projections from limbic area 25 are significantly denser and stronger when compared to those from limbic area 32, suggesting a graded pattern in the strength and pattern of cortico-hypothalamic projections based on subtle differences in laminar definition. The sparse axons that originate in the eulaminate areas simply pass through the hypothalamus, as there was no evidence of synapses or any other structural capacity for communication stemming from these projections. Thus, the pattern and strength of hypothalamic projections varies systematically from the least differentiated limbic areas to the most laminated (eulaminate) areas.

The Structural Model has been traced to the development and evolution of the neocortex (Dombrowski et al. 2001; Barbas and García-Cabezas 2016; García-Cabezas et al. 2019; Garcia-Cabezas and Zikopoulos 2019; Barbas 2015). This evidence provides a clear — and previously unsuspected — convergence of the Prosomeric Model and the Structural Model to predict that the specificity of cortico-hypothalamic connections has a common developmental sequence that likely begins with the specification of the

hypothalamus. This study is the first to contribute evidence demonstrating the inter-predictive power of the Prosomeric Model and the Structural Model (Fig 16).

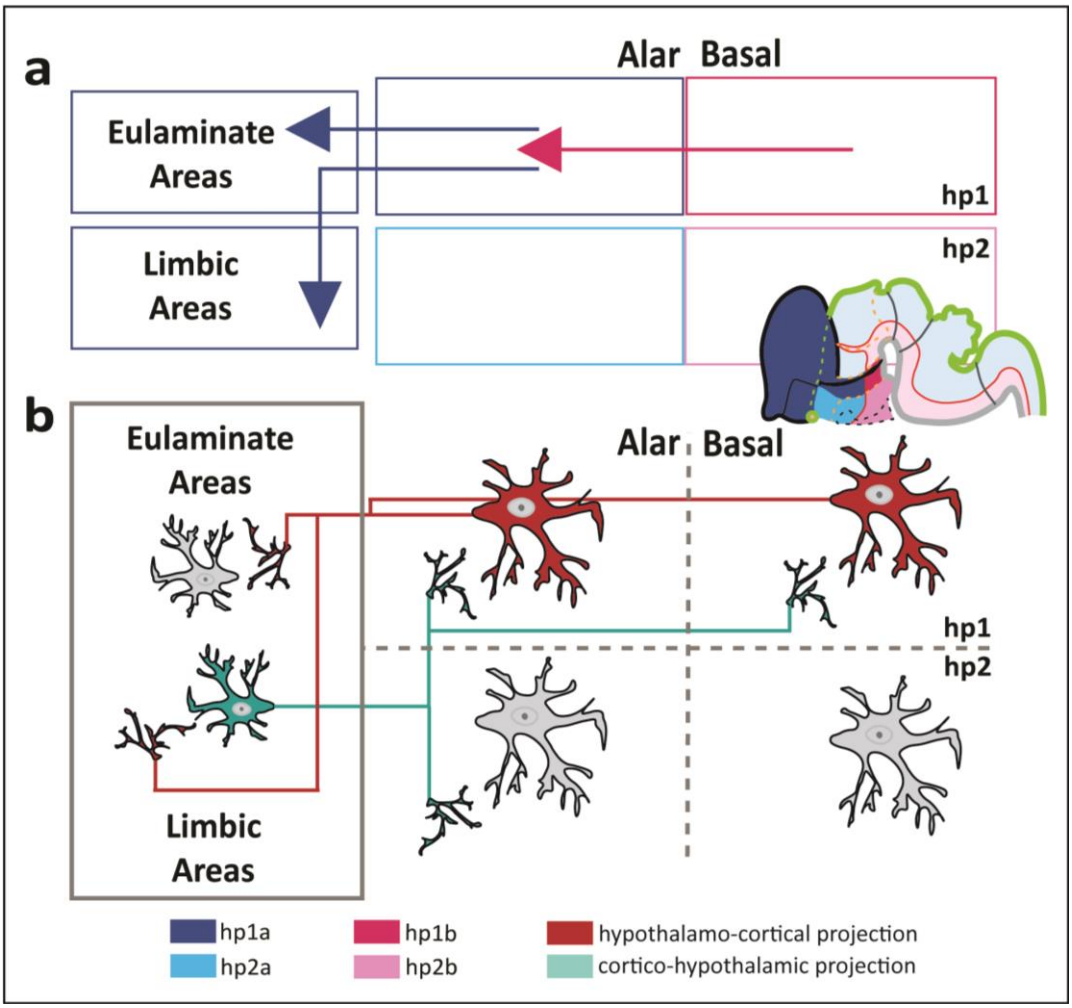

Figure 16: Convergence of the Prosomeric Model and the Structural Model links developmental, anatomical, and functional pathways between hypothalamus and prefrontal cortex. (a) Technical schematic of developmental pathway of the hypothalamus (hp1, hp2, alar, basal) and the two major cortical types of the prefrontal cortex. (b) Technical schematic of the anatomical pathways driving functional compartmentalization of the derivatives of the hypothalamus and involvement of the prefrontal cortex in those pathways.

Derivatives of hp1 have bidirectional connections with limbic prefrontal cortex

A topological analysis of the connections between the prefrontal cortex and the hypothalamus in adult rhesus monkeys revealed an underlying principle: brain regions that share a common or close progenitor unit of the early neuroepithelium share significant structural and functional pathways in the adult brain. The Prosomeric Model positions the prefrontal cortex as one of the derivatives of the pallium contributed by the derivatives of the alar plate portion of hp1 in mammals (Rubenstein et al. 1994; Puelles and Rubenstein 2003; Puelles 2018; Nieuwenhuys and Puelles 2016). The present study demonstrated strong, bidirectional connections between the largest derivative of the alar plate part of hp1 in primates, the lateral hypothalamic area (LA), and the limbic areas of the prefrontal cortex. The LA projects to both limbic and eulaminate areas of the prefrontal cortex and receives projections from both area types with some bias from limbic areas. Thus, brain regions that are topologically proximal in early development develop common structural pathways and remain connected in the adult. The LA seems to have a central role in propagating autonomic responses to a variety of external stimuli directly from the prefrontal cortex to the hypothalamus, and from there to the brainstem and spinal cord (Barbas et al. 2003).

On the other hand, the paraventricular complex (PaP/PaM), the only other likely alar plate part of hp1 in rhesus monkey, lacked connections with all areas of the prefrontal cortex analyzed here. Periventricular cells from the alar plate part of hp1 (paraventricular complex) and hp2 (rostral paraventricular nucleus) origin seem to have an exclusive role in detecting pH changes in cerebrospinal fluid for respiratory and

metabolic regulation (Williams et al. 2007; Jalalvand et al. 2018). Thus, on a structural level, pathways for neuroautonomic signaling depend heavily on a shared developmental pathway, but this may be modified as a tertiary event by the patterned development of vasculature (Puelles 2019; Puelles et al. 2019b). These later events may allow for the integration of the ventricular system with orexigenic (Filby and Gross 1983; Van Vugt et al 2006), sympathetic (Ishikawa et al 1976), and reproductive signals (Michael and Rees 1982; Van Vugt et al 2006) in the adult hypothalamus that also contribute to homeostatic autonomic functions like heart rate and respiration.

Derivatives of the basal plate part of hp1 project to both limbic and eulaminate areas of the prefrontal cortex but receive fewer projections from the limbic areas than the derivatives of the alar plate. Importantly, the subthalamic nucleus (STN), does not project to the prefrontal cortex and only receives projections from the limbic areas. This may be explained by a complex migratory pattern of this nucleus apart from the other nuclei derived from the basal plate part of hp1 (Puelles et al. 2012). Thus, as a tertiary event, the STN may become more closely positioned and integrated into dopamine signaling with the basal ganglia network (Shimo and Wichmann 2009; Galvan et al 2014; Min et al 2016) despite a distinct developmental origin.

A topological analysis of the hypothalamus revealed a unique pattern of bidirectional connections between the likely derivatives of hp1 and the areas of the prefrontal cortex. With little exception, the common developmental origin of the nuclei derived from hp1 and the pallial telencephalon provides a rationale for the existence of these connections and their exclusive patterning.

Derivatives of hp2 lack connections with the limbic prefrontal cortex

By topology, the present study demonstrated the inverse of the first principle: brain regions that arise from more distant progenitor units should not share significant structural or functional pathways in the adult brain. According to the Prosomeric Model, only the preoptic area (POA) is contributed to the subpallium of the telencephalic vesicle as a derivative of the alar plate portion of hp2 (Rubenstein et al. 1994; Puelles and Rubenstein 2003; Puelles 2018; Nieuwenhuys and Puelles 2016). Of interest, this study advanced the hypothesis of a topological parcellation of the anterior hypothalamic area (AA) as with the POA and apart from the hypothalamus. The POA, a likely secondary derivative of the alar plate portion of hp2 and one of four bands contributed to the subpallial telencephalon, has close ties with the prefrontal cortex with bidirectional connections with the limbic areas of the prefrontal cortex much like the derivatives of hp1. Otherwise, the derivatives of the alar and basal plate portions of hp2, which become the largest and most complex portions of the adult hypothalamus, seem to be largely self-contained (Puelles et al. 2012). The hypothalamic derivatives of the alar and basal plate parts of hp2 neither project to nor receive significant projections from the limbic and eulaminate areas of the prefrontal cortex investigated here. Rather, the sparse label found in the vicinity of hp2-derived nuclei seem to simply pass through and course to other unknown terminations. Thus, it may be hypothesized that the derivatives of the alar and basal parts of hp2 only share considerable intrahypothalamic pathways caused by topological proximity during development.

A prosomeric topology correlates the compartmentalization of neuroendocrine function of the hypothalamus apart from the influence of prefrontal cortex. All the likely adult hypothalamic derivatives of the alar and basal plate parts of hp2 seem to have diverse and significant roles in neuroendocrine signaling in rhesus monkeys (Appendix 2). Further, there seem to be differences of involvement between the derivatives of the alar and basal plate portions of hp2. The likely derivatives of the alar plate part of hp2 seem to share a role in dopamine (Shimo and Wichmann 2009) and neuropeptide Y (Finn et al 1998; Thind et al 1993; Van Vugt et al 2006) signaling for orexigenic and some reproductive signaling. In contrast, the likely derivatives of the basal plate part of hp2 contribute to every known hypothalamus-mediated neuraxial pathway for endocrine homeostasis. These include responses to satiety via leptin (Finn et al 1986; Van Vugt et al 2006), prolactin (Quadri et al 1977), other stress and metabolic indicators like somatostatin and growth hormone (Filby and Gross 1983), and reproductive signaling (Pfaff et al 1976; Quadri et al 1977; Michael and Rees 1982; Garris et al 1983; Thind et al 1993). While intrahypothalamic structural pathways and signaling mechanisms have yet to be elucidated, the exclusive proximity of the arcuate nucleus (ARC) and the core part of the ventromedial nucleus (VMc) to the infundibulum (INF) is likely indicative of a common structural pathway for hypothalamo-pituitary signaling in adult rhesus monkeys and reflect the internal state.

A topological analysis clarifies important structural and functional patterns in the compartmentalization of the hypothalamus. The relative isolation of the derivatives of hp2 from cortical centers of executive functioning may retain a protective evolutionary

benefit for the major centers for homeostatic regulation from the necessity of conscious regulation. On the other hand, the relative paucity of connections between the neuroendocrine portion of the hypothalamus and the prefrontal cortex requires closer examination of any intrahypothalamic connections that allow for relay of information about the internal state to modify higher functions of the cortex.

Patterning of normal and pathological prosencephalon development

For over a century, the *Columnar Model* was assumed to reflect the development of the diencephalon and hypothalamus. The Columnar Model positioned the hypothalamus as the ventral-most part of the diencephalon and placed the telencephalon as the rostral-most vesicle of the neural tube [Herrick (1910); Kuhlenbeck (1973); reviewed in Puelles and Rubenstein (2015); Puelles (2019)]. Mounting genoarchitectonic evidence strongly supports a new paradigm of CNS development, where progressive regionalization positions the hypothalamus as the antecedent to all pallial and subpallial structures (Puelles et al. 2012; Puelles and Rubenstein 2015). The reassignment of the hypothalamus from the diencephalon to the secondary prosencephalon is centered around a change in the axial terminus of the early neural plate that respects the curve of the cephalic flexure (Puelles et al. 1987). Accordingly, the new axial terminus, termed the acroterminal domain, is the rostral-most prosomere of the secondary prosencephalon (Puelles et al. 2012; Puelles and Rubenstein 2015). Thus, the Prosomeric Model shows that development of pallial and subpallial structures that contribute to the telencephalon are patterned exclusively by the prosomeres of the secondary prosencephalon, i.e., the hypothalamus (Puelles 2019; Puelles and Rubenstein 2015; Puelles et al. 2019a).

What happens when chromosomal aberrations or teratogenic factors disrupt the patterning of the secondary prosencephalon early in human development? *Prosencephalic malformations* accompany disruptions to the developmental sequence of the mediolateral patterning of the rostral neural plate (Simon et al. 2000; Solomon et al. 2010; Puelles et al. 2012; ten Donkelaar et al. 2014). A specific subset of malformations known as *holoprosencephaly* describes a spectrum of interhemispheric cleavage malformations of the forebrain ranging from impaired to complete absence of cleavage. The etiology of holoprosencephaly can be traced in part to specific abnormalities in the *Shh* (sonic hedgehog) signaling pathway in the early tissues of the rostral neural plate [reviewed in Hong and Krauss (2018); (Andreu-Cervera et al. 2019)]. Consequently, there are massive patterning defects in the hypothalamus and later-appearing structures, including the telencephalon, the eyes, the infundibulum, and the neurohypophysis portion of the pituitary gland. The secondary prosencephalon and its derivatives are thus severely impacted by early genetic aberrations in holoprosencephaly while diencephalic derivatives like the thalamus remain largely unaffected (Puelles et al. 2012; ten Donkelaar et al. 2014; Simon et al. 2000).

The Prosomeric Model thus explains several aspects of both normal and abnormal patterning of CNS development in ways that the Columnar Model cannot (Puelles et al. 2012; Nieuwenhuys and Puelles 2016; Puelles and Rubenstein 2015). Given this key developmental finding, this study advances the principles of the Prosomeric Model to examine the relationship of the adult hypothalamus with other regions of the CNS. A better understanding of neurogenesis and neural patterning of the hypothalamus may

allow for new strategies to unify the etiology of diseases involving hypothalamic circuits (Radad et al. 2017). The hypothalamus is implicated in neurodegenerative diseases like Alzheimer's and Parkinson's (Goldman-Rakic 1987a, 1987b; Ishii and Iadecola 2015; Radad et al. 2017). Symptoms include sleep, metabolic, and non-cognitive abnormalities like neuroendocrine function as potential driver pathologies (Ishii and Iadecola 2015; Radad et al. 2017; Van Erum et al. 2018). Neuraxial pathways from the hypothalamus to the pituitary and adrenal glands also play central roles in dysregulated stress signaling seen in depression, anxiety, and migraine headaches (Min et al. 2014; Myers et al. 2014; Bao and Swaab 2019; Johnson et al. 2019; Kandasamy et al. 2019; Chen et al. 2019). Recent studies in metabolic and hormonal regulation by the hypothalamus seem to support this idea (Grove et al. 2003; Myers et al. 2014; Ishii and Iadecola 2015).

These pathologies may represent disruptions to critical regulatory centers for neuraxial pathways of a common developmental origin. A prosomeric topology for hypothalamic nuclei thus appears to predict and explain the roles of hypothalamic nuclei in both normal and pathological signaling pathways.

CONCLUSION

A modern understanding of the complex structure and connections of the hypothalamus may be elucidated by study of its systematic development. At the nexus of embryological and adult findings likely exists the essence of what makes the adult hypothalamus truly "hypothalamic" and thus integral to structural and neuraxial pathways. A topological analysis of the structure and limits of the hypothalamus lends clarity and uniformity to the way we study the hypothalamus across vertebrates and its complex involvement in diverse neural systems.

The topological atlas of the hypothalamus in rhesus monkey will serve as a valuable tool to study cortico-subcortical pathways involving the hypothalamus and its intricate connectivity with other areas of the CNS. In the present study, this atlas pointed to the convergence of two independent models, the Prosomeric and the Structural Models by revealing striking patterns in the connections between the prefrontal cortex and hypothalamus. Future studies may expand on these findings to investigate patterns in the inhibitory and excitatory character of neuronal populations of the hypothalamus and prefrontal cortex based on development and persistent genoarchitecture. Further, we need a closer analysis of the projections between the prefrontal cortex and hypothalamus by layers: from which layers do neurons from the prefrontal cortex project to the hypothalamus, and vice versa? An understanding of the connections between the prefrontal cortex and the hypothalamus is needed to strengthen the predictive power of

both models for their role in cortico-hypothalamic networks from the circuit to the synapse.

Using the Prosomeric Model to analyze physiological and pathological pathways may yield clarity and consistency of hypothalamic structure-function relationships. A topological analysis provided an organizational scheme to understand the compartmentalization of neuroautonomic function to the derivatives of hp1 and neuroendocrine function to the derivatives of hp2. These findings demand future study of the underlying mechanisms and organizers during embryological development that regulate this division of neuraxial involvement. Further, evaluating patterns in adult pathologies by their impact on prosomeric hypothalamic derivatives may reveal an etiology of these diseases based on changes that may occur at a common time in development that affect networks of anatomic and functional connections. Thus, this study advances the hypothesis that the convergence of the Prosomeric Model and the Structural Model is of great significance to our understanding of the hypothalamus, its structure, function, and involvement in dysfunction. At the nexus of these two models exists a unified theory for the central nervous system and pave the way for the next century research to the benefit of medical science.

APPENDIX

Appendix 1: Definitions of main concepts, theories and principles used in the text.

Main concepts

Bauplan a body plan common to all members of the same phylum or subphylum of animals

Genoarchitecture the pattern and sequence of genetic expression that specifies progenitor units and emergent structures of each neuromere and plate of origin during embryological development; applies to both embryos and adults

Proneuromere a transverse (caudo-rostral) segment of the early neural plate typically composed of two or more *neuromeres* specified by the neural tube

Neuromere a transverse unit of the early neural plate specified by caudo-rostral patterning of the neural tube; several neuromeres contribute to a *proneuromere*; in the secondary prosencephalon, these are called *prosomeres*

Plate a longitudinal division of the early neural plate specified by the dorso-ventral patterning of the neural tube (i.e. *roof*, *floor*, *alar*, and *basal plates*)

Progenitor unit a subdivision of the early neural plate patterned by the intersection of longitudinal plates and transverse segments with a characteristic molecular profile

Diencephalon the proneuromere composed of three neuromeres (p1, p2, p3) between the mesencephalon and the secondary prosencephalon that gives rise to adult brain structures such as the dorsal thalamus and the reticular nucleus

Secondary prosencephalon the rostral-most proneuromere of the early neural plate composed of three *prosomeres* (hp1, hp2, At) that gives rise to the entire hypothalamus, the infundibulum, the neurohypophysis, the optic tract, the retina and the telencephalic vesicle

Telencephalon the rostral vesicle of the alar plate part of the secondary prosencephalon (hp1, hp2) that gives rise to the entire cerebral cortex

Nucleus a collection of neuronal cell bodies in the adult hypothalamus typically derived from a common *progenitor unit*

Theories and principles

Columnar Model a classical model assumed for the development of the diencephalon and telencephalon; positions the telencephalon as the rostral-most termination of the neural plate and includes the hypothalamus in the diencephalon with the epithalamus and the thalamus (Herrick 1910; Kuhlenbeck 1973; Swanson 1992, 2003)

Prosomeric Model a predictive model that explains the development of the entire central nervous system; positions the hypothalamus apart from the diencephalon and within the secondary prosencephalon, the

rostral-most termination of the neural plate which expands to give rise to the telencephalic vesicle (Puelles and Rubenstein 2003; Rubenstein et al. 1994; Puelles 2018; Nieuwenhuys and Puelles 2016)

Structural Model a predictive model that relates the pattern and strength of cortico-cortical connections to the graded variation in laminar definition of cortical areas (Barbas and Rempel-Clower 1997; Rempel-Clower and Barbas 1998)

Topography the study of the arrangement of the natural physical features of an area

Topology the study of the relative invariant position and spatial relations of areas unaffected by continuous processes of change

Appendix 2: Neuroendocrine function of the hypothalamus in rhesus monkey.

Prosomere	Plate	Nucleus	Neurotransmitter[1]	Behavior	Ref[2]
hp1	alar	PaP/PaM	CART	orexigenic; reward	V
			NPY	reproductive signaling	T; V
			DHT	reproductive signaling	MR
			SS	GI regulation	F
hp2	alar	SO	NPY	orexigenic	T; V
hp2	basal	TCA	NPY	reproductive signaling	T
		Arc	CART, LEPTIN, OB-R, POMC	orexigenic, adiposity, reward, reproductive signaling	V; Fn
			NPY	reproductive signaling	T; Fn; V
			E2-binding	reproductive signaling	P
			Prolactin	reproductive signaling	Q
			DHT	reproductive signaling	MR
			SS	GI regulation	F
			E2/ProG-concentrating	reproductive signaling	Gr
			GHRH	metabolism	L
		VM	LEPTIN, OB-R	orexigenic, adiposity	V
			E2-binding	reproductive signaling	P
			Prolactin	reproductive signaling	Q
			DHT	reproductive signaling	MR
			SS	GI regulation	F
			E2/ProG-concentrating	reproductive signaling	Gr
			GHRH	metabolism	L
		MM	V1a	arginine vasopressin signaling	Y
hp1/hp2	basal	DM	DHT	reproductive signaling	MR
			E2/ProG-concentrating	reproductive signaling	Gr
			NPY	reproductive signaling	T

1 – Neurotransmitter Abbreviations: CART, cocaine-amphetamine-regulating transcript; DHT, dihydrotestosterone; E2, estradiol (estrogen); GHRH, growth hormone releasing hormone; GnRH, gonadotropin releasing hormone; NPY, neuropeptide Y; OB-R, lectin receptor; PGE1, prostaglandin E1; POMC, pro-opiomelanocortin; ProG, progesterone; SS, somatostatin; V1a, arginine vasopressin receptor 1a

2 – Reference Abbreviations: F, Filby and Gross 1983; Fn, Finn et al 1998; G, Galvan et al 2014; Gr, Garris et al 1983; I, Ishikawa et al 1976; L, Lechan et al 1984; M, Min et al 2016; MR, Michael and Rees 1982; P, Pfaff et al 1976; Q, Quadri et al. 1977; SW, Shimo and Wichmann 2009; T, Thind et al 1993; V, Van Vugt et al 2006.

LIST OF JOURNAL ABBREVIATIONS

Am J Med Genet C Semin Med Genet ..... American Journal of Medical Genetics Part C: Seminars in Medical genetics

Annu Rev Neurosci..... Annual Review of Neuroscience

BMC Neurosci .....BMC Neuroscience

Brain Lang .....Brain and Language

Brain Res.....Brain Research

Brain Struct Funct .....Brain Structure and Function

Cell Metab.....Cell Metabolism

Cell Tissue Res .....Cell and Tissue Research

Clin Perinatol .....Clinics in Perinatology

Curr Opin Neurobiol .....Current Opinion in Neurobiology

Eur J Neurosci..... European Journal of Neuroscience

Front Neuroanat ..... Frontiers in Neuroanatomy

Front Neurol.....Frontiers in Neurology

IBRO Rep.....IBRO Reports

J Comp Neurol .....Journal of Comparative Neurology

J Endocr Soc .....Journal of the Endocrine Society

J Histochem Cytochem ..... Journal of Histochemistry & Cytochemistry

J Miscrosc ..... Journal of Microscopy

J Morphol..... Journal of Morphology

J Neurophysiol .....Journal of Neurophysiology

J Neurosci.....Journal of Neuroscience

Life Sci.....Life Sciences

Neurochem Res..... Neurochemical Research

Neurol Res .....Neurological Research

Neurosci Lett.....Neuroscience Letters

PLoS Biol.....PLOS Biology

Proc Natl Acad Sci USA..... Proceedings of the National Academy of Sciences of the United States of America

Sleep Med Rev.....Sleep Medicine Reviews

Trends Neurosci .....Trends in Neurosciences

REFERENCES

Abràmoff MD, Magalhães PJ, Ram SJ (2004) Image Processing with ImageJ. Biophotonics International 11(7):36–42

Andreu-Cervera A, Anselme I, Karam A, Laclef C, Catala M, Schneider-Maunoury S (2019) The Ciliopathy Gene Ftm/Rpgrip1l Controls Mouse Forebrain Patterning via Region-Specific Modulation of Hedgehog/Gli Signaling. J Neurosci 39 (13):2398-2415. doi:10.1523/JNEUROSCI.2199-18.2019

Bao AM, Swaab DF (2019) The human hypothalamus in mood disorders: The HPA axis in the center. IBRO Rep 6:45-53. doi:10.1016/j.ibror.2018.11.008

Barbas H (1986) Pattern in the laminar origin of corticocortical connections. J Comp Neurol 252:415–422. https://doi.org/10.1002/cne.902520310

Barbas H (1993) Organization of cortical afferent input to orbitofrontal areas in the rhesus monkey. Neuroscience 56:841-864

Barbas H (1995) Pattern in the cortical distribution of prefrontally directed neurons with divergent axons in the rhesus monkey. Cerebral Cortex **5**: 158-165

Barbas H (2000) Connections underlying the synthesis of cognition, memory, and emotion in primate prefrontal cortices. Brain Research Bulletin 52: 319-330

Barbas H (2007) Flow of information for emotions through temporal and orbitofrontal pathways. Journal of Anatomy 211 (2):237-249

Barbas H (2015) General cortical and special prefrontal connections: Principles from structure to function. Annu Rev Neurosci 38:269-289

Barbas H, García-Cabezas MA (2016) How the prefrontal executive got its stripes. Curr Opin Neurobiol 40:125-134. doi:10.1016/j.conb.2016.07.003

Barbas H, Gustafson EL, Greengard P (1993) Comparison of the immunocytochemical localization of DARPP-32 and I-1 in the amygdala and hippocampus of the rhesus monkey. J Comp Neurol 334 (1):1-18. doi:10.1002/cne.903340102

Barbas H, Pandya DN (1989) Architecture and intrinsic connections of the prefrontal cortex in the rhesus monkey. The Journal of Comparative Neurology 286:353–375. https://doi.org/10.1002/cne.902860306

Barbas H, Rempel-Clower N (1997) Cortical structure predicts the pattern of corticocortical connections. Cerebral Cortex 7:635-646

Barbas H, Saha S, Rempel-Clower N, Ghashghaei T (2003) Serial pathways from primate prefrontal cortex to autonomic areas may influence emotional expression. BMC Neurosci 4 (1):25

Barbas H, Medalla M, Alade O, Suski J, Zikopoulos B, Lera P (2005) Relationship of prefrontal connections to inhibitory systems in superior temporal areas in the rhesus monkey. Cerebral Cortex 15:1356 –1370

Barbas H, García-Cabezas MA, Zikopoulos B (2013). "Frontal-thalamic circuits associated with language." Brain Lang 126(1): 49-61.

Barbas H, Wang J, Joyce MKP, García-Cabezas MA (2018) Pathway mechanism for excitatory and inhibitory control in working memory. J Neurophysiol 120:2659-2678

Bleier R (1984) The Hypothalamus of the Rhesus Monkey: A Cytoarchitectonic Atlas. Univ. Wisconsin Press, Madison

Bozzelli PL, Alaiyed S, Kim E, Villapol S, Conant K (2018) Proteolytic Remodeling of Perineuronal Nets: Effects on Synaptic Plasticity and Neuronal Population Dynamics. Neural plasticity 2018:5735789. doi:10.1155/2018/5735789

Chen Z, Chen X, Liu M, Ma L, Yu S (2019) Volume of Hypothalamus as a Diagnostic Biomarker of Chronic Migraine. Front Neurol 10:606. doi:10.3389/fneur.2019.00606

Cowan WM, Gottlieb DI, Hendrickson AE, Price JL, Woolsey TA (1972) The autoradiographic demonstration of axonal connections in the central nervous system. Brain Res 37:21–51

De Luca C, Papa M (2016) Looking Inside the Matrix: Perineuronal Nets in Plasticity, Maladaptive Plasticity and Neurological Disorders. Neurochem Res 41 (7):1507-1515. doi:10.1007/s11064-016-1876-2

De Luca C, Papa M (2017) Matrix Metalloproteinases, Neural Extracellular Matrix, and Central Nervous System Pathology. Progress in molecular biology and translational science 148:167-202. doi:10.1016/bs.pmbts.2017.04.002

Dombrowski SM, Barbas H (1996) Differential expression of NADPH diaphorase in functionally distinct prefrontal cortices in the rhesus monkey. Neuroscience 72:49-62

Dombrowski SM, Hilgetag CC, Barbas H (2001) Quantitative architecture distinguishes prefrontal cortical systems in the rhesus monkey. Cerebral Cortex 11:975-988

Ferran JL, Puelles L, Rubenstein JL (2015) Molecular codes defining rostrocaudal domains in the embryonic mouse hypothalamus. Front Neuroanat 9:46. doi:10.3389/fnana.2015.00046

Fiala JC (2005) Reconstruct: a free editor for serial section microscopy. J Microsc 218 (Pt 1):52-61

Filby AB, Gross DS (1983) Distribution of immunoreactive somatostatin in the primate hypothalamus. Cell Tissue Res 233(1): 69-80

Finn PD, Cunningham MJ, Pau KY, Spies HG, Clifton DK, Steiner RA (1998) The stimulatory effect of leptin on the neuroendocrine reproductive axis of the monkey. Endocrinology 139(11): 4652-4662

Gallyas F (1979) Silver staining of myelin by means of physical development. Neurol Res 1:203-209

Galvan A, Hu X, Rommelfanger KS, Pare JF, Khan ZU, Smith Y, Wichmann T (2014) Localization and function of dopamine receptors in the subthalamic nucleus of normal and parkinsonian monkeys. J Neurophysiol 112(2): 467-479

García-Cabezas MA, John YJ, Barbas H, Zikopoulos B (2016) Distinction of Neurons, Glia and Endothelial Cells in the Cerebral Cortex: An Algorithm Based on Cytological Features. Front Neuroanat 10:107. doi.org/110.3389/fnana.2016.00107. doi:doi.org/10.3389/fnana.2016.00107

Garcia-Cabezas MA, Joyce MP, John Y, Zikopoulos B, Barbas H (2017) Mirror trends of plasticity and stability indicators in primate prefrontal cortex. Eur J Neurosci 46 (8):2392-2405

García-Cabezas MA, Martínez-Sánchez P, Sánchez-González MA, Garzón M, Cavada C (2009) Dopamine innervation in the thalamus: monkey versus rat. Cerebral Cortex 19 (2):424-434

Garcia-Cabezas MA, Zikopoulos B (2019) Evolution, development, and organization of the cortical connectome. PLoS Biol 17 (5):e3000259. doi:10.1371/journal.pbio.3000259

Garcia-Cabezas MA, Zikopoulos B, Barbas H (2019) The Structural Model: a theory linking connections, plasticity, pathology, development and evolution of the cerebral cortex. Brain Struct Funct 224 (3):985-1008. doi:10.1007/s00429-019-01841-9

Garris DR, Billiar RB, Takaoka Y, White R, Little B (1983) Autoradiographic localization of estradiol- and progesterone-concentrating neurons in the isolated rhesus monkey hypothalamus. Neurosci Lett 37(2): 149-154

Ghashghaei HT, Hilgetag CC, Barbas H (2007) Sequence of information processing for emotions based on the anatomic dialogue between prefrontal cortex and amygdala. NeuroImage 34 (3):905-923

Goldman-Rakic PS (1987a) Circuitry of primate prefrontal cortex and regulation of behavior by representational memory. In: Mountcastle V, Plum F (eds) Handbook of Physiology - The Nervous System, Higher Functions of the Brain, Vol. 5. American Physiological Society, Washington D.C., pp 373-417

Goldman-Rakic PS (1987b) Circuitry of the frontal association cortex and its relevance to dementia. Archives of gerontology and geriatrics 6 (3):299-309

Goldman-Rakic PS (1996) The prefrontal landscape: implications of functional architecture for understanding human mentation and the central executive. Philosophical Transactions of the Royal Society of London. Series B: Biological Sciences 351: 1445-1453

Grove KL, Chen P, Koegler FH, Schiffmaker A, Susan Smith M, Cameron JL (2003) Fasting activates neuropeptide Y neurons in the arcuate nucleus and the paraventricular nucleus in the rhesus macaque. Brain research Molecular brain research 113 (1-2):133-138. doi:10.1016/s0169-328x(03)00093-7

Hashimoto T, Elder CM, Okun MS, Patrick SK, Vitek JL (2003) Stimulation of the subthalamic nucleus changes the firing pattern of pallidal neurons. J Neurosci 23 (5):1916-1923

Haynes WI, Haber SN (2013) The organization of prefrontal-subthalamic inputs in primates provides an anatomical substrate for both functional specificity and integration: implications for Basal Ganglia models and deep brain stimulation. J Neurosci 33 (11):4804-4814. doi:10.1523/JNEUROSCI.4674-12.2013

Herrick CJ (1910) The morphology of the forebrain in amphibia and reptilia. Journal of Comparative Neurology and Psychology 20:413-547. doi:10.1002/cne.920200502

Hong M, Krauss RS (2018) Modeling the complex etiology of holoprosencephaly in mice. Am J Med Genet C Semin Med Genet 178 (2):140-150. doi:10.1002/ajmg.c.31611

Ishii M, Iadecola C (2015) Metabolic and Non-Cognitive Manifestations of Alzheimer's Disease: The Hypothalamus as Both Culprit and Target of Pathology. Cell Metab 22 (5):761-776. doi:10.1016/j.cmet.2015.08.016

Ishikawa M, Shimada S, Handa H, Tanaka C (1976) Distribution of catecholamine containing nerve endings in the hypothalamus of the rhesus monkey. No To Shinkei 28(11): 1235-1242

Jalalvand E, Robertson B, Tostivint H, Low P, Wallen P, Grillner S (2018) Cerebrospinal Fluid-Contacting Neurons Sense pH Changes and Motion in the Hypothalamus. J Neurosci 38 (35):7713-7724. doi:10.1523/JNEUROSCI.3359-17.2018

Johnson JD, Barnard DF, Kulp AC, Mehta DM (2019) Neuroendocrine Regulation of Brain Cytokines After Psychological Stress. J Endocr Soc 3 (7):1302-1320. doi:10.1210/js.2019-00053

Jones EG (2007) The Thalamus. Cambridge University Press, New York

Joyce MP, Barbas H (2018) Cortical connections position primate area 25 as a keystone for interoception, emotion, and memory. J Neurosci 38 (7):1677-1698. doi:10.1523/JNEUROSCI.2363-17.2017

Kandasamy M, Radhakrishnan RK, Poornimai Abirami GP, Roshan SA, Yesudhas A, Balamuthu K, Prahalathan C, Shanmugaapriya S, Moorthy A, Essa MM, Anusuyadevi M (2019) Possible Existence of the Hypothalamic-Pituitary-Hippocampal (HPH) Axis: A Reciprocal Relationship Between Hippocampal Specific Neuroestradiol Synthesis and Neuroblastosis in Ageing Brains with Special Reference to Menopause and Neurocognitive Disorders. Neurochem Res 44 (8):1781-1795. doi:10.1007/s11064-019-02833-1

Kuhlenbeck H (1973) The Central Nervous System of Vertebrates, Vol. 3/II: Overall Morphologic Pattern. S. Karger AG

Lechan RM, Lin HD, Ling N, Jackson IM, Jacobson S, Reichlin S (1984) Distribution of immunoreactive growth hormone releasing factor(1-44)NH2 in the tuberoinfundibular system of the rhesus monkey. Brain Res 309(1): 55-61

Louis ED, Ma K, Babij R, Cortes E, Liem RK, Vonsattel JP, Faust PL (2012) Neurofilament protein levels: quantitative analysis in essential tremor cerebellar cortex. Neurosci Lett 518 (1):49-54. doi:10.1016/j.neulet.2012.04.054

Medalla M, Barbas H (2006) Synaptic organization of prefrontal pathways associated with working memory. 10th ICCNS, Boston, MA

Mesulam MM, Hegarty E, Barbas H, Carson ECG, Mufson EJ (1980) Additional factors influencing sensitivity in the tetramethyl benzidine method for horseradish peroxidase. J Histochem Cytochem 28:1255–1259

Meyer D, Bonhoeffer T, Scheuss V (2014) Balance and Stability of Synaptic Structures during Synaptic Plasticity. Neuron 82:430–443. https://doi.org/10.1016/j.neuron.2014.02.031

Michael RP, Rees HD (1982) Autoradiographic localization of 3H-dihydrotestosterone in the preoptic area, hypothalamus, and amygdala of a male rhesus monkey. Life Sci 30(24): 2087-2093

Min HK, Ross EK, Lee KH, Dennis K, Han SR, Jeong JH, Marsh MP, Striemer B, Felmlee JP, Lujan JL, Goerss S, Duffy PS, Blaha C, Chang SY, Bennet KE (2014) Subthalamic nucleus deep brain stimulation induces motor network BOLD activation: use of a high precision MRI guided stereotactic system for nonhuman primates. Brain stimulation 7 (4):603-607. doi:10.1016/j.brs.2014.04.007

Min HK, Ross EK, Jo HJ, Cho S, Settell ML, Jeong JH, Duffy PS, Chang SY, Bennet KE, Blaha CD, Lee KH (2016) Dopamine release in the nonhuman primate caudate and putamen depends upon site of stimulation in the subthalamic nucleus. J Neurosci 36(22): 6022-6029

Mueller AL, Davis A, Sovich S, Carlson SS, Robinson FR (2016) Distribution of N-Acetylgalactosamine-Positive Perineuronal Nets in the Macaque Brain: Anatomy and Implications. Neural plasticity 2016:6021428. doi:10.1155/2016/6021428

Myers B, Mark Dolgas C, Kasckow J, Cullinan WE, Herman JP (2014) Central stress-integrative circuits: forebrain glutamatergic and GABAergic projections to the dorsomedial hypothalamus, medial preoptic area, and bed nucleus of the stria terminalis. Brain Struct Funct 219 (4):1287-1303. doi:10.1007/s00429-013-0566-y

Nauta WJH, Haymaker W (1969) Hypothalamic nuclei and fiber connections. In: Haymaker W, Anderson E, Nauta WJH (eds) The Hypothalamus. Thomas, Springfield, Illinois, pp 136-209

Nieuwenhuys R, Puelles L (2016) Towards a new neuromorphology. Springer International Publishing.

Pfaff DW, Gerlach JL, McEwen BS, Ferin M, Carmel P, Zimmerman EA (1976) Autoradiographic localization of hormone-concentrating cells in the brain of the female rhesus monkey. J Comp Neurol 170(3): 279-293

Puelles L (2011) Pallio-pallial tangential migrations and growth signaling: new scenario for cortical evolution? Brain, behavior and evolution 78 (1):108-127. doi:10.1159/000327905

Puelles L (2013) Chapter 10 - Plan of the Developing Vertebrate Nervous System. Patterning and cell Type Specification in the Developing CNS and PNS 1 (25)

Puelles L (2018) Developmental studies of avian brain organization. The International journal of developmental biology 62 (1-2-3):207-224. doi:10.1387/ijdb.170279LP

Puelles L (2019) Survey of Midbrain, Diencephalon, and Hypothalamus Neuroanatomic Terms Whose Prosomeric Definition Conflicts With Columnar Tradition. Front Neuroanat 13:20. doi:10.3389/fnana.2019.00020

Puelles L, Alonso A, Garcia-Calero E, Martinez-de-la-Torre M (2019a) Concentric ring topology of mammalian cortical sectors and relevance for patterning studies. J Comp Neurol. doi:10.1002/cne.24650

Puelles L, Domenech-Ratto G, Martinez-de-la-Torre M (1987) Location of the rostral end of the longitudinal brain axis: review of an old topic in the light of marking experiments on the closing rostral neuropore. J Morphol 194 (2):163-171. doi:10.1002/jmor.1051940205

Puelles L, Ferran JL (2012) Concept of neural genoarchitecture and its genomic fundament. Front Neuroanat 6:47. doi:10.3389/fnana.2012.00047

Puelles L, Martinez-de-la-Torre M, Bardet S, Rubenstein JLR (2012) Hypothalamus. In: The Mouse Nervous System. Elsevier, pp 221-312

Puelles L, Martínez de la Torre M, Martínez S, Watson C, Paxinos G (2019b) The Chick Brain in Stereotaxic Coordinates and Alternate Stains. 2nd edn. Academic Press - An imprint of Elsevier, San Diego, United States

Puelles L, Martínez Pérez S, Martínez de la Torre M (2008) Neuroanatomía. Editorial Medica Panamericana, Buenos Aires

Puelles L, Morales-Delgado N, Merchan P, Castro-Robles B, Martinez-de-la-Torre M, Diaz C, Ferran JL (2016) Radial and tangential migration of telencephalic somatostatin neurons originated from the mouse diagonal area. Brain Struct Funct 221 (6):3027-3065. doi:10.1007/s00429-015-1086-8

Puelles L, Rubenstein JL (2003) Forebrain gene expression domains and the evolving prosomeric model. Trends Neurosci 26 (9):469-476. doi:10.1016/S0166-2236(03)00234-0

Puelles L, Rubenstein JL (2015) A new scenario of hypothalamic organization: rationale of new hypotheses introduced in the updated prosomeric model. Front Neuroanat 9:27. doi:10.3389/fnana.2015.00027

Quadri SK, Norman RL, Spies HG (1977) Prolactin release following electrical stimulation of the brain in ovarectomized and ovariectomized estrogen-treated rhesus monkeys. Endocrinology 100(2): 325-330

Radad K, Moldzio R, Al-Shraim M, Kranner B, Krewenka C, Rausch WD (2017) Recent Advances on the Role of Neurogenesis in the Adult Brain: Therapeutic Potential in Parkinson's and Alzheimer's Diseases. CNS & neurological disorders drug targets 16 (7):740-748. doi:10.2174/1871527316666170623094728

Ramón y Cajal S (1904a) Textura del sistema nervioso del hombre y de los vertebrados. Tomo II, primera parte. Imprenta y Librería de Nicolás Moya, Madrid

Ramón y Cajal S (1904b) Textura del sistema nervioso del hombre y de los vertebrados. Tomo II, segunda parte. Imprenta y Librería de Nicolás Moya, Madrid

Rempel-Clower NL, Barbas H (1998) Topographic organization of connections between the hypothalamus and prefrontal cortex in the rhesus monkey. J Comp Neurol 398:393-419

Rollenhagen A, Ohana O, Sätzler K, et al (2018) Structural Properties of Synaptic Transmission and Temporal Dynamics at Excitatory Layer 5B Synapses in the Adult Rat Somatosensory Cortex. Frontiers in Synaptic Neuroscience 10: https://doi.org/10.3389/fnsyn.2018.00024

Rosene DL, Roy NJ, Davis BJ (1986) A cryoprotection method that facilitates cutting frozen sections of whole monkey brains from histological and histochemical processing without freezing artifact. J Histochem Cytochem 34:1301-1315

Rubenstein JL, Martinez S, Shimamura K, Puelles L (1994) The embryonic vertebrate forebrain: the prosomeric model. Science 266 (5185):578-580. doi:10.1126/science.7939711

Sánchez-González MA, García-Cabezas MA, Rico B, Cavada C (2005) The primate thalamus is a key target for brain dopamine. J Neurosci 25 (26):6076-6083

Santuy A, Rodríguez J-R, DeFelipe J, Merchán-Pérez A (2018) Study of the Size and Shape of Synapses in the Juvenile Rat Somatosensory Cortex with 3D Electron Microscopy. eneuro 5:ENEURO.0377-17.2017. https://doi.org/10.1523/ENEURO.0377-17.2017

Schwartz ML, Goldman-Rakic P (1990) Development and plasticity of the primate cerebral cortex. Clin Perinatol 17 (1):83-102

Shimo Y, Wichmann T (2009) Neuronal activity in the subthalamic nucleus modulates the release of dopamine in the monkey striatum. Eur J Neurosci 29(1): 104-113

Simon EM, Hevner R, Pinter JD, Clegg NJ, Miller VS, Kinsman SL, Hahn JS, Barkovich AJ (2000) Assessment of the deep gray nuclei in holoprosencephaly. AJNR American journal of neuroradiology 21 (10):1955-1961

Solomon BD, Pineda-Alvarez DE, Mercier S, Raam MS, Odent S, Muenke M (2010) Holoprosencephaly flashcards: A summary for the clinician. Am J Med Genet C Semin Med Genet 154C (1):3-7. doi:10.1002/ajmg.c.30245

Swanson LW (1992) Brain maps : structure of the rat brain. Elsevier, Amsterdam ; New York

Swanson LW (2003) Brain architecture: understanding the basic plan. Oxford University Press, Oxford ; New York

ten Donkelaar HJ, Lammens M, Cruysberg JRM, Ulzen KK-v, Hori A, Shiota K (2014) Development and Developmental Disorders of the Forebrain. In: Clinical Neuroembryology: Development and Developmental Disorders of the Human Central Nervous System. Springer Berlin Heidelberg, Berlin, Heidelberg, pp 421-521. doi:10.1007/978-3-642-54687-7_9

Thind KK, Boggan JE, Goldsmith PC (1993) Neuropeptide Y system of the female monkey hypothalamus: retrograde tracing and immunostaining. Neuroendocrinology 57(2): 289-298

van Eerdenburg FJ, Rakic P (1994) Early neurogenesis in the anterior hypothalamus of the rhesus monkey. Brain Research Developmental Brain Research 79:290-296

Van Erum J, Van Dam D, De Deyn PP (2018) Sleep and Alzheimer's disease: A pivotal role for the suprachiasmatic nucleus. Sleep Med Rev 40:17-27. doi:10.1016/j.smrv.2017.07.005

Van Vugt DA, Lujan ME, Froats M, Krzemien A, Couceyro PR, Reid RL (2006) Effect of fasting on cocaine-amphetamine-regulated transcript, neuropeptide Y, and leptin receptor expression in the non-human primate hypothalamus. Neuroendocrinology 84(2): 83-93

Whittier JR, Mettler FA (1949) Studies on the subthalamus of the rhesus monkey; hyperkinesia and other physiologic effects of subthalamic lesions; with special reference to the subthalamic nucleus of Luys. J Comp Neurol 90 (3):319-372

Williams RH, Jensen LT, Verkhratsky A, Fugger L, Burdakov D (2007) Control of hypothalamic orexin neurons by acid and CO2. Proc Natl Acad Sci USA 104 (25):10685-10690. doi:10.1073/pnas.0702676104

Xie Q, Chen X, Deng H, et al (2017) An automated pipeline for bouton, spine, and synapse detection of in vivo two-photon images. BioData Mining 10: https://doi.org/10.1186/s13040-017-0161-5

Zikopoulos B, Barbas H (2006) Prefrontal projections to the thalamic reticular nucleus form a unique circuit for attentional mechanisms. J Neurosci 26:7348-7361

Zikopoulos B, John YJ, García-Cabezas MA, Bunce JG, Barbas H (2016) The intercalated nuclear complex of the primate amygdala. Neuroscience 330:267-290. doi:http://dx.doi.org/10.1016/j.neuroscience.2016.05.052

CURRICULUM VITAE